# Faculty of Physics and Astronomy

## University of Heidelberg

**Diploma thesis**

in Physics

submitted by

Buth, Christian

born in Mönchengladbach

2002

# Non-Hermitian Perturbation Theory for the Electronic Decay of Excited and Ionized Molecules and Identification of the Electronic Decay Processes in the Auger Decay of Core-Ionized Xenon Fluorides

This diploma thesis has been carried out by Buth, Christian at the
*Physikalisch-Chemisches Institut*
under the supervision of
Prof. Cederbaum, Lorenz S.
and
Prof. Wehrse, Rainer
*Institut für Theoretische Astrophysik*

**Nicht-hermitesche Störungstheorie zur Beschreibung des elektronischen Zerfalls angeregter und ionisierter Moleküle und die Identifikation der elektronischen Zerfallsprozesse des Augerzerfalls core-ionisierter Xenonfluoride:** Resonanzen stellen ein fundamentales physikalisches Konzept dar. Trotz ihrer Bedeutung ist die Berechnung von Resonanzenernergieen keine Standardaufgabe. Der elektronische Zerfall eines angeregten Moleküls wird mit dem Ziel untersucht die beteiligten Zerfallsprozesse aufzuklären. Hierzu werden die Zerfallsbreiten mittels Wigner-Weisskopf Theorie und nicht-hermitescher, nicht-entarteter Rayleigh-Schrödinger Störungstheorie, mit komplexem absorbierenden Potential, berechnet. Um die Genauigkeit der vorigen beiden Zugänge zu verbessern wird eine allgemeine nicht-hermitesche Multireferenz Rayleigh-Schrödinger Störungstheorie abgeleitet und an einem Modellproblem getestet. Der Auger Zerfall eines Xe $4d$ Loches wird mit Elektronenpropagatormethoden in den Xenonfluoriden ($XeF_n,\ n = 2, 4, 6$) studiert. Die auftretenden Zerfallsprozesse können durch den Vergleich des Einfachionisierungsspektrums mit dem Doppelionisierungsspektrum identifiziert werden. Interatomare Zerfallsprozesse tragen entscheidend zur elektronischen Zerfallsbreite bei, wie anhand einer Beziehung zwischen Endzustandspopulation und Zerfallsbreite gezeigt wird. Dies steht im Widerspruch zu der herrschenden Meinung, dass eine reduzierte Valenzelektronendichte, wie sie am Xenon durch die Anwesenheit der Fluorliganden vorliegt, zwangsläufig zu einer niedrigeren elektronischen Zerfallsrate führt.

**Non-Hermitian Perturbation Theory for the Electronic Decay of Excited and Ionized Molecules and Identification of the Electronic Decay Processes in the Auger Decay of Core-Ionized Xenon Fluorides:** Resonances are a fundamental concept in physics, yet their calculation is by far not a matter of routine. The electronic decay of an excited molecule is investigated in terms of decay processes and the decay width is calculated in two ways with Wigner-Weisskopf theory and non-degenerate non-Hermitian Rayleigh-Schrödinger perturbation theory employing complex absorbing potentials. A general non-Hermitian multireference perturbation theory is devised, and tested on a model problem, to improve on the accuracy of the two former approaches. The molecular Auger decay of an initial Xe $4d$ core hole is studied in the xenon fluorides ($XeF_n,\ n = 2, 4, 6$) with electron propagator methods, and the electronic decay processes are identified by comparing the ionization spectra of the singly ionized molecule with its double ionization spectra. Electronic decay processes of interatomic character are found to have considerable impact on the electronic decay width in the xenon fluorides, due to a relation between the final state population and the decay width that is derived. The electron density in the valence shell of the xenon atom is low due to the fluorine atoms. The increase in decay width is, therefore, in contrast to the leading opinion that a low electron density on the atom that carries the initial core-hole, leads to a low decay width.

**Citation for this diploma thesis:**

Christian Buth, *Non-Hermitian Perturbation Theory for the Electronic Decay of Excited and Ionized Molecules and Identification of the Electronic Decay Processes in the Auger Decay of Core-Ionized Xenon Fluorides*, Diplomarbeit, Ruprecht-Karls Universität Heidelberg, Theoretische Chemie, Physikalisch-Chemisches Institut, Im Neuenheimer Feld 229, 69120 Heidelberg, Germany, 2002, `www.ub.uni-heidelberg.de/archiv`

**PACS numbers:** 31.15.-p, 31.15.Ar, 31.15.Md, 31.70.Hq, 33.15.Ry, 33.35.+r, 33.80.Eh

**Keywords:** Electronic Resonance, Decay Width, Decay Process, Excited State, Wigner-Weisskopf theory, Non-Hermitian, Perturbation theory, Complex Absorbing Potential, CAP, Multireference, Ionized Molecules, interatomic, Auger Decay, interatomic Coulombic Decay, ICD, Electron Transfer Mediated Decay, ETMD, Foreign Imaging, Xenon Fluorides, XeF2, XeF4, XeF6, Ab initio

**Schlagwörter (OSWD):** Resonanz, Störungstheorie, Ionisationsenergie, Molekülion, Ab-initio-Rechnung

**Freie Schlagwörter:** Elektronische Resonanz, Zerfallsbreite, Zerfallsprozess, Angeregter Zustand, Wigner-Weisskopf Theorie, Nichthermitesch, Komplexe Absorbierende Potentiale, CAP, Multireferenz, interatomar, Augerzerfall, ICD, ETMD, Xenon, Fluorid, Cluster, XeF2, XeF4, XeF6

**Contact:** `Christian.Buth@ePost.de`

**First edition:** 12.09.2002 (Two evaluation copies)
**Second edition:** 17.09.2002 (20 copies, electronic edition)

*Meinen lieben Eltern zur Freude.*

# Contents

# List of Figures

# List of Tables

# 1. Introduction

*Resonances* are a fundamental concept in physics which unifies the treatment of decaying states in the microscopic regime, namely resonances are studied in atomic, molecular, nuclear and particle physics. They are decaying states in contrast to bound states and arise frequently in scattering problems [1–4]. Resonances are described as discrete quantum states embedded in and interacting with a continuum of states. They possess a definite lifetime $\tau$. *Narrow resonances*, which are also termed *quasi-stationary*, are resonances with a long lifetime $\tau$. The decay of a resonance has deep physical consequences because it is an irreversible transition which introduces time asymmetry [5].

Resonances cannot be described in terms of bound state quantum mechanics because their wave functions are not part of the $\mathbb{L}^2$-Hilbert space as they do not fulfill the necessary boundary condition, they are not square-integrable. Nevertheless, they show properties similar to those of bound states, i.e. their wave function is highly localized in space and resembles the one of a bound state, except for its far asymptotic part. It is possible to assign a *complex* energy to resonances

$$E_{\mathrm{res}} = E_{\mathrm{R}} - \mathrm{i}\,\Gamma/2 \tag{1.1}$$

which is frequently called *Siegert energy* in the context of complex-energy poles of the $S$-matrix [1,6]. $E_{\mathrm{R}}$ is the energetic position of the resonance state and $\Gamma = \frac{\hbar}{\tau}$ its decay width.

*Electronic resonances* are resonances which decay by electron emission. They occur frequently in the scattering or photoionization experiments of atomic and molecular physics where a pronounced enhancement of the scattering cross-section is observed at the resonance energy. The non-Hermitian character of resonance states manifests in the context of electronic resonances in terms of the decay electron. This outgoing electron introduces remarkable difficulties as its wave function is not square-integrable.

The actual calculation of resonance energies is, despite of their importance, not a matter of routine. Generations of physicists have devised a variety of methods well-adapted to their specific problems [1]. Early attempts by Wigner and Weisskopf to calculate resonance energies are based on time-dependent perturbation theory [2,7]. With the help of this Wigner-Weisskopf theory the decay width of singly ionized molecules [8,9], section 6.3, and the decay width of excited molecules, section 3.1, can be calculated easily. The decay matrix elements of Wigner-Weisskopf theory can be pictured schematically [8, 9], section 3.1, in terms of many-body transitions, which provides a deeper understanding of the underlying physics.

In quantum chemistry the practical evaluation of the resulting expressions poses serious difficulties caused by the decay electron. Its continuum wave function must be represented in the finite $\mathbb{L}^2$ basis sets ubiquitous in the quantum chemistry of bound state problems

(section 2.1) with the help of *Stieltjes Chebyshev moment theory* ( [10, 11] and references therein).

Since then several other techniques have been devised to overcome the continuum problem in quantum chemistry, like Feshbach's projection operator formalism [1, 12, 13] or complex scaling [1, 14]. A recently devised method exploits the fact that the treatment of bound state problems in quantum chemistry is highly evolved (sections 2.1, 2.2 and chapter 5). There are professional *ab initio* software packages, like [15, 16], to calculate many properties of molecules with high accuracy. These programs exploit the localization of the electronic ground state wave functions by introducing finite basis sets in $\mathbb{L}^2$-*Hilbert space*.

The success of the former techniques raises the desire to harness these tools to calculate the Siegert energy (1.1) of resonances. At this point, the complex absorbing potential (CAP) [17] approach comes into play. An artificial potential is added to the Hamiltonian of the system to transform the calculation of a resonance state into a bound-state-like problem by absorbing the decay electron. Then a description of the resonance state in terms of localized $\mathbb{L}^2$-basis sets becomes feasible (section 2.3).

CAPs transform the time-dependent decay problem into a time-independent problem. Hence the analogue to the approach of Wigner and Weisskopf is a non-Hermitian non-degenerate Rayleigh-Schrödinger perturbation theory which is derived in section 3.2 and generalized to a multireference theory in section 3.3. In chapter 4, a model problem is used to test the non-Hermitian multireference Rayleigh-Schrödinger perturbation theory.

The Auger effect [18, 19] is caused by a special type of electronic resonance and has received a lot of attention since its discovery. Since then theorists have tried to calculate the Auger decay rate because the Auger effect can be used in many experimental situations. As soon as Auger transitions involving valence orbitals in molecules came into the focus of interest the question of the importance of interatomic transitions arose and is still not completely elucidated. Matthew and Komninos were the first to examine *interatomic Auger transition rates* [20]. They falsely concluded that these transitions have a small impact on the Auger rate, except in low energy Auger processes, due to too strong approximations [21]. In fact the effect of the chemical bond can be dramatic [22–24].

Auger decay is similar to the electronic decay of singly ionized *clusters* of (weakly) bound atoms or molecules. Clusters [25] have been receiving a lot of attention because they can be seen as a bridge between the individual monomer and solids formed by many monomers. The decay of singly ionized clusters of weakly bound atoms or molecules has been studied extensively. New electronic decay processes were discovered that involve neighboring atoms [8, 9, 26–29] (section 6.1).

In the weakly bound clusters studied, the electronic decay was energetically enabled by the neighboring atoms, due to a lowering of the double ionization threshold compared to the isolated monomer, caused by spatial separation of the two final state holes on two different monomers [8,9,26–29]. The ionization potentials were determined using *ab initio* electron propagator methods [30–33] (section 5.3) and hole-population analysis [34–36] (section 5.4) providing an exact identification of the decay mechanism. Furthermore, the lifetimes of these types of electronic resonances were calculated with the CAP-method. The electronic decay process turns out to be ultra fast, typical lifetimes are in the range 10–100 fs [37–39].

It has been tried to examine these theoretical predictions experimentally [40] with the help of *photoelectron spectroscopy* [18]. This is a common method, which is grounded on the *photoelectric effect* [18], to study the electronic structure of atoms, molecules, clusters and solids. The electronic decay processes in weakly bound clusters are hard to detect with photoelectron spectroscopy, because the decay electrons are ejected with low kinetic energy of around a few electronvolt [8,9]. The lower end of photoelectron spectra is usually ignored because the identification of the electrons originating from electronic decay is very difficult.

Photoelectron spectroscopy was also used to examine the Xe $4d$ lines in the xenon fluorides ($XeF_n$, $n = 2, 4, 6$) [41]. The data suggest that the line width increases with an increasing number of fluorine atoms (chapter 7). This observation raises the question whether the increase in line width may be caused by an increased electronic decay rate, or whether it is caused by, eg., vibrational broadening. If the increase in line width was caused by an increased electronic decay rate then the types of electronic decay processes, which are responsible, should be elucidated (chapter 7).

*Atomic units* are used throughout this diploma thesis, i.e. $\hbar$, the electron charge magnitude and the electron mass are set to one. The unit of length is the Bohr and the unit of energy is the Hartree. The conversion factors to *SI units* are $1\,\text{Bohr} = 52.917\,\text{pm}$ and $1\,\text{Hartree} = 27.211\,\text{eV}$ [42].

# Part I.

# Electronic Decay of Excited Molecular Systems

# 2. Electronic Structure Theory and Complex Absorbing Potentials

Nature distinguishes two sorts of elementary particles, *bosons* and *fermions*. It turns out that systems consisting of bosons are described by totally symmetric wave functions and systems consisting of fermions are represented by totally antisymmetric wave functions with respect to the interchange of particles.

In quantum chemistry one considers predominantly fermions due to the fermionic nature of electrons, the constituents of the atomic shells. Quantum mechanics is the theory to describe the microscopic world and *electronic structure theory* is the application of it to the electrons in atoms and molecules, i.e. (approximate) solutions to the many-body Schrödinger (or Dirac) equation are calculated to obtain the ground state electronic structure, excited, ionized and electron attachment states. The solution facilitates to calculate many properties of the atom, molecule or cluster [42].

In many cases, the coupled movement of the electrons and the nuclei in a molecular system can be neglected due to the fact that the movement of the electrons is much faster than the movement of the heavier nuclei. This leads to a separation of the total Hamiltonian and is called BORN-OPPENHEIMER approximation [42]. It will be assumed throughout. With the help of these adiabatic solutions to the problem non-Born-Oppenheimer effects, nevertheless, can be studied.

## 2.1. The Hartree-Fock Approximation

The electronic structure of a molecular system is approximately given by the solutions of the Schrödinger equation, employing the non-relativistic *electronic Hamiltonian*

$$\hat{H} = \sum_{i=1}^{N} \hat{h}_i + \sum_{i=1}^{N} \sum_{j=i+1}^{N} \frac{1}{r_{ij}} \tag{2.1}$$

with

$$\hat{h}_i = -\frac{1}{2}\Delta_i - \sum_{A=1}^{M} \frac{Z_A}{r_{iA}} \, .$$

$N$ denotes the number of electrons, $M$ is the number of nuclei, $Z_A$ stands for the charge of nucleus $A$, $r_{ij}$ is the distance between electron $i$ and electron $j$ and $r_{iA}$ is the distance between electron $i$ and nucleus $A$. $\hat{h}_i$ is called one-electron Hamiltonian. It is a one-electron operator because it involves only the coordinates of the electron $i$. Consequently, $r_{ij}^{-1}$ is called two-electron operator.

The task of this section is to find an approximate solution $\Phi(\vec{r}_1, \ldots, \vec{r}_N)$ to the ground state wave function of the $N$-electron system described by (2.1). $\vec{r}_i$: denotes the position of the $i$-th electron. *Ritz variational principle* [2, 42] helps to simplify this problem. It states that for an approximate ground state wave function

$$\frac{\langle \Phi(\vec{r}_1, \ldots, \vec{r}_N) \,|\, \hat{H} \,|\, \Phi(\vec{r}_1, \ldots, \vec{r}_N) \rangle}{\langle \Phi(\vec{r}_1, \ldots, \vec{r}_N) \,|\, \Phi(\vec{r}_1, \ldots, \vec{r}_N) \rangle} \geq \mathfrak{E}_0 \tag{2.2}$$

holds in Hilbert space, $\mathfrak{E}_0$ being the exact ground state energy. Therefore, this powerful principle provides a recipe to find an arbitrarily precise approximation to the ground state wave function of a molecular system: take trial functions and find the one with minimal energy, but the variational principle does not give any hint which trial functions to choose.

A product ansatz of $N$ *spin orbitals* $\chi_i,\ i = 1, \ldots, N$, i.e. one-electron wave functions with spin, for the ground state wave function, is a simple trial function assuming *non-interacting* particles but, as was stated in the introduction, electronic wave functions must be totally antisymmetric. This property can be incorporated into the product ansatz by forming a determinant of the spin orbitals, the *Slater determinant*

$$|\, \Phi(\vec{r}_1, \ldots, \vec{r}_N) \rangle = |\, \chi_1 \cdots \chi_N \,\rangle \,. \tag{2.3}$$

In (2.3) all permutations $\chi_i(\vec{r}_j)$ are formed [42].

The *Hartree-Fock approximation* [42–44] the applies the variational principle (2.2) to the ansatz (2.3). The problem turns out to be equivalent to the solution of an eigenvalue equation for the $i$-th electron

$$\hat{f}(i) \,|\, \chi_i(\vec{r}_i) \rangle = \varepsilon_i \,|\, \chi_i(\vec{r}_i) \rangle \qquad i = 1, \ldots, N \,. \tag{2.4}$$

with the *Fock operator* $\hat{f}(i) = \hat{h}(i) + \hat{v}^{(\mathrm{HF})}(i)$. The *Hartree-Fock potential* is given by

$$\hat{v}^{(\mathrm{HF})}(i) = \sum_{k=1}^{N} \int \mathrm{d}^3 r_j \; \chi_k^*(\vec{r}_j)\, r_{ij}^{-1} \,(\hat{\mathbb{1}} - \hat{P}_{ij})\, \chi_k(\vec{r}_j) \,. \tag{2.5}$$

This is the average potential experienced by electron $i$ due to the presence of the other electrons $j$. $\hat{P}_{ij}$ exchanges electrons $i$ and $j$ in the two spin orbitals written to its right. By comparing the Fock operator with (2.1) one sees that the two-electron operator $r_{ij}^{-1},\ i \neq j$ is replaced by a mean field in the Hartree-Fock method which is a considerable approximation to (2.1).

As $\hat{v}^{(\mathrm{HF})}(i)$ depends on the coordinates of all electrons one cannot solve (2.4) directly. Instead one has to determine the wave function iteratively by taking a trial one and then calculating the Hartree-Fock potential. Afterwards, a new trial wave function can be determined. Repeating this procedure results in a self consistent solution to arbitrary precision.

The Hilbert space, used so far, is the direct product space of spin and spatial Hilbert space. The spin can be integrated out and only the spatial part remains to be solved. There are two ways to derive spin-free equations to calculate the Hartree-Fock ground

state of a closed-shell ($\Longrightarrow N$ even) molecular system. The general spin orbital reads in PAULI's two-component spinor notation

$$\chi_i(\vec{r}) = \begin{cases} \phi_j^{\alpha}(\vec{r})\,\alpha(\omega) \\ \phi_j^{\beta}(\vec{r})\,\beta(\omega) \end{cases} \quad , \tag{2.6}$$

where $\alpha(\omega)$, $\beta(\omega)$ denote spin up and spin down, respectively, and $\phi_j^{\alpha}(\vec{r})$, $\phi_j^{\beta}(\vec{r})$ represent the corresponding spatial orbitals, i.e. the spatial one-electron wave function. One needs $N/2$ spatial orbitals to construct $N$ spin orbitals. If $\phi_j(\vec{r}) := \phi_j^{\alpha}(\vec{r}) = \phi_j^{\beta}(\vec{r})$ holds for all $j$ then the resulting spin-free Hartree-Fock equation reads [42]

$$f(\vec{r})\,\phi_j(\vec{r}) = \varepsilon_j\,\phi_j(\vec{r}) \qquad j = 1, \ldots, N/2\ . \tag{2.7}$$

This is called the *restricted Hartree-Fock case* [42, 43]. The *unrestricted Hartree-Fock case* [42, 44] assumes two different components in (2.6). Then two equations of the type (2.7) result, one for each component of the spinor.

To carry out Hartree-Fock calculations one expands the spatial orbitals in a basis of the spatial Hilbert space $|\,\varphi_\mu(\vec{r})\,\rangle$, $\mu = 1, \ldots, \infty$. As computer resources are finite the basis has to be truncated. This is an approximation and every effort has been made to develop suitable finite basis sets, especially those consisting of *Gaussian basis functions*, which are chosen owing to their simplicity and the quality of the results that can be obtained using them [42,45,46]. In molecular physics the expansion of the spatial orbitals in terms of linear combinations of a finite number of basis functions is frequently termed *linear combination of atomic orbitals (LCAO)* due to the relation of the basis sets to the electronic structure of the individual atoms in a molecular system. With $K$ basis functions, the expansion of the spatial orbitals reads, in the restricted Hartree-Fock case,

$$\phi_j(\vec{r}) = \sum_{\mu=1}^{K} C_{\mu j}\,\varphi_\mu(\vec{r}), \qquad j = 1 \ldots, K\ . \tag{2.8}$$

This expression can be used to transform (2.4) into the, so-called, *Roothaan equations* which can be written compactly as a matrix equation

$$\boldsymbol{FC} = \boldsymbol{SC\varepsilon} \tag{2.9}$$

$\boldsymbol{F}$ is the matrix representation of the Fock operator and $\boldsymbol{S}$ denotes the basis set *overlap matrix* $S_{\mu\nu} = \langle\,\varphi_\mu\,|\,\varphi_\nu\,\rangle$. In the unrestricted case, two equations of the type (2.8), (2.9), one for each spinor component, are needed. The solution of (2.9) is interpreted as follows: $\boldsymbol{\varepsilon} = \mathbf{diag}(\varepsilon_1, \ldots, \varepsilon_K)$ is the matrix of *orbital energies*. $\boldsymbol{C}$ are the expansion coefficients in (2.8). Via (2.6), (2.8) $2K$ spin molecular orbitals result, where the $N$ orbitals, lowest in energy, are occupied. The other are denoted *unoccupied (virtual) orbitals*.

Note that the mean field approximation in (2.4) modifies the problem appreciably. It does not account for the correlated movement of the electrons due to their mutual repulsion, therefore, it is a one-particle approximation (independent particle model). Several post Hartree-Fock methods have been developed and are studied to overcome this insufficiency. They take the result of a Hartree-Fock calculation and approximate the correlation

of the electrons. The energy difference between the ground state energies obtained using the independent particle model and a method that describes correlated electrons is termed *correlation energy*. One of the most prominent methods is presented in the ensuing section 2.2.

## 2.2. Configuration Interaction

*Configuration interaction (CI)* is a wide-spread method to tackle the many-body problem in quantum chemistry [42,47]. Its principle is very simple. The ground state of a Hartree-Fock calculation is used to generate *configuration state functions (CSF)* by forming all distinct occupations of the $2K$ molecular orbitals with $N$-electrons. These CSFs are used as a new basis set for succeeding computations, for example to calculate the *correlation energy*.

As the number of CSFs is $\binom{2K}{N}$ one usually truncates the expansion and uses only the ground state together with the singly (and doubly) excited CSFs to shorten computations. These two CI schemes are termed *singly excited CI (SCI)* and *singly and doubly excited CI (SDCI)*. The expansion still grows exponentially but in a less pronounced way because the number of $n$-tuply excited CSFs is $\binom{N}{n}\binom{2K-N}{n}$ [42].

The resulting CI-matrices are *sparse* and have following general form

$$\boldsymbol{H}^{(\mathrm{CI})} := \begin{pmatrix} \boldsymbol{H}_{00} & \mathbf{0} & \boldsymbol{H}_{0D} & \mathbf{0} & \mathbf{0} & \cdots \\ \mathbf{0} & \boldsymbol{H}_{SS} & \boldsymbol{H}_{SD} & \boldsymbol{H}_{ST} & \mathbf{0} & \cdots \\ \boldsymbol{H}_{D0} & \boldsymbol{H}_{DS} & \boldsymbol{H}_{DD} & \boldsymbol{H}_{DT} & \boldsymbol{H}_{DQ} & \cdots \\ \mathbf{0} & \boldsymbol{H}_{TS} & \boldsymbol{H}_{TD} & \boldsymbol{H}_{TT} & \boldsymbol{H}_{TQ} & \cdots \\ \mathbf{0} & \mathbf{0} & \boldsymbol{H}_{QD} & \boldsymbol{H}_{QT} & \boldsymbol{H}_{QQ} & \cdots \\ \vdots & \vdots & \vdots & \vdots & \vdots & \ddots \end{pmatrix} . \tag{2.10}$$

The CI-matrix is real-symmetric and is composed of block matrices which are abbreviated to $\boldsymbol{H}_{XY}$ where $X$ and $Y$ denote excitation classes: none (0), singly (S), doubly (D), triply (T), quadruply (Q). For example the Hartree-Fock ground state energy is the $1 \times 1$ matrix $\boldsymbol{H}_{00} := (\langle \Phi_0 | \hat{H} | \Phi_0 \rangle)$. There is no $\boldsymbol{H}_{0S}$ block due to *Brillouin's theorem* [42] which states that singly excited determinants do not couple to the Hartree-Fock ground state.

The CI problem is solved by diagonalizing (2.10) which gives the energies of the ground state and many excited states. This works in principle but the matrix (2.10) can be huge. Frequently, it is sufficient to calculate the eigenvalues of selected states only. Then the (real) analogue of the (approximate) diagonalization techniques of subsection 2.3.2 can be harnessed.

## 2.3. Complex Absorbing Potentials

The quantum chemistry of bound state problems is highly evolved. There are professional *ab initio* software packages to calculate many properties of atoms, molecules and clusters

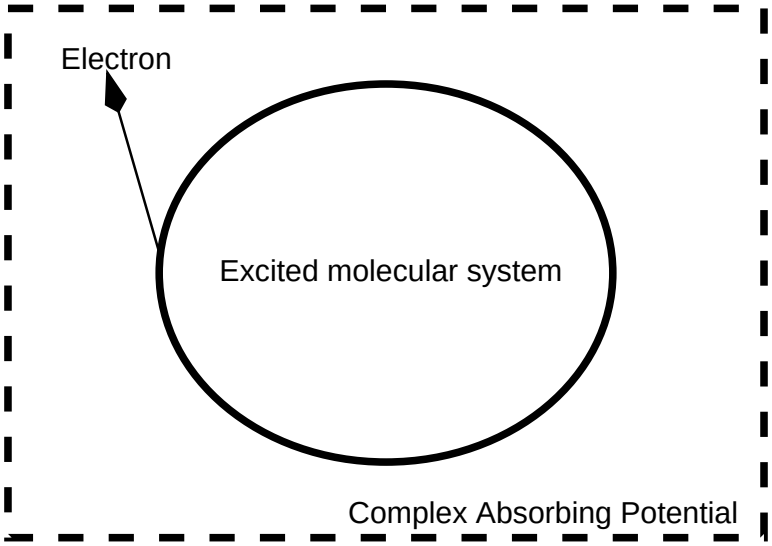


**Figure 2.1.:** A molecular system enclosed with a box complex absorbing potential (CAP). The emitted electron is absorbed by the CAP.

with high accuracy. These programs exploit the localization of the electronic ground state wave functions by introducing finite basis sets in $\mathbb{L}^2$-*Hilbert space*.

The success of these techniques raises the desire to harness them to calculate the Siegert energy (1.1) of resonances. This is where complex absorbing potentials [17] come into play. The artificial potential transforms the problem of computing a resonance state into a bound-state-like problem.

### 2.3.1. The Formalism

The idea is to enclose the molecular system with an appropriate potential, which enforces an absorbing boundary condition, as shown in figure 2.1. It absorbs the decay electron and consequently renders the former continuum wave function square-integrable [17, 37]. The Hamiltonian $\hat{H}$ of a molecular system reads with absorbing boundary condition

$$\hat{H}(\eta) = \hat{H} - \mathrm{i}\,\eta\,\hat{W}\ . \tag{2.11}$$

The artificial potential is called *complex absorbing potential (CAP)*. $\eta$ is a real positive parameter referred to as *CAP-strength parameter* and $\hat{W}$ is called *CAP-operator*.

A suitable $\hat{W}$ should be a local positive semidefinite one-particle operator. The exact prerequisites are derived in [17]. A fairly general flexible CAP is presented in [39]. See also equation (4.2) for a typical $\hat{W}$.

If a system is augmented by a CAP then one has to used a *complex symmetric bilinear form* instead of the *Hermitian scalar product* [17, 37]

$$(\varphi|\psi) := \int \varphi(\vec{r})\,\psi(\vec{r})\,\mathrm{d}^3 r\ . \tag{2.12}$$

As the basis functions, in quantum chemistry, are usually real this has little effect in practice.

Now, the problem of calculating the energy of a resonance is equivalent to solving a complex eigenvalue equation, the *CAP-Schrödinger equation* [17]

$$\hat{H}(\eta)\,|\,\Psi(\eta)\,) = E(\eta)\,|\,\Psi(\eta)\,) \ . \tag{2.13}$$

The solution of (2.13) can be obtained by introducing a square-integrable basis set to transform (2.13) into a matrix eigenvalue problem which can be diagonalized subsequently. As this is a complex symmetric eigenvalue problem it is not necessarily diagonalizable [10, 11].

If the basis set that is used to form the matrix representation of (2.13) is complete then the Siegert energy (1.1) of the resonance is simply $E_{\mathrm{res}} = \lim_{\eta\to 0} E(\eta)$. For a finite basis set, this is no longer the case and the condition

$$\left|\eta\frac{\mathrm{d}E}{\mathrm{d}\eta}\right| = \text{minimum} \ . \tag{2.14}$$

must be used instead [17, 37].

There are various advantages of complex absorbing potentials over other methods for calculating resonance energies like *complex scaling* [1, 14]. The method is *simple*, *reliable* and can be used for most systems examined in quantum chemistry. Furthermore CAPs are well suited to be *integrated* into existing quantum chemical software which opens the possibility to resort to the vast pool of excellent programs leaving a minimum amount of work to be done.

These features of the CAP-method are demonstrated by a couple of problems that were studied. In [48] the resonances of a long-range model potential are studied with the complex scaling and CAP-method. The representation of the CAP-operator in a Gaussian basis set, for a CAP calculation where the molecular system is described by CI (CAP/CI), is derived in [39] and a resonance of the neon dimer $Ne_2$ is investigated. Basis set effects due to energy selection in CAP/CI calculations are examined in [38]. Some resonances of the $(HF)_2^+$ dimer are studied in [37].

### 2.3.2. Calculation of Resonance Energies in Practice

The preceding subsection introduced a method to treat the continuum problem of decaying states. In quantum chemistry one has to face the many-body problem as well due to the interaction of the electrons in a molecular system. Configuration interaction was introduced in section 2.2 as a general means to tackle this issue.

The solution of the problem has to be optimized with respect to $\eta$, due to the condition (2.14), which can be achieved by diagonalizing a matrix representation of (2.13) in a range of values for $\eta$. Plotting the resulting spectra in one graph leads to an *$\eta$-trajectory* for each bound, resonance or *pseudocontinuum*[1] state of (2.11). Since the influence of the

[1] In a finite basis set it is of course not possible to represent the continuum of free-particle states. Instead, one obtains a discretized pseudocontinuum.

CAP vanishes for the first spectrum, due to $\eta = 0$ in (2.11), all $\eta$-trajectories start on the real axis. With an increasing value for $\eta$, the eigenvalues of resonance or pseudo-continuum states move into the lower complex plane. For a resonance state the solution which satisfies (2.14) best is chosen, the so-called *stabilization point* of the $\eta$-trajectory. Obviously the calculation of many complex spectra of (2.13), with the help of a CI-matrix representation, is very expensive even for small molecular systems. As all iterations are independent they can be computed in parallel. This can reduce the amount of *wall time*, i.e. the time that elapses in the real world, to calculate a resonance energy, considerably.

A complex version [49] of the *Davidson algorithm* [50] can be used to calculate the lowest eigenvalues $E(\eta)$ of a matrix representation of (2.13) for several $\eta$ values. The convergence of this method is sped up if the eigenvectors of one $\eta$-step are being used as start vectors in the succeeding $\eta$-step [49]. Unfortunately this removes the full parallelism[2] of the algorithm. Another approach, for selective computation of eigenvalues even amidst the spectrum, is the complex *Lanczos algorithm* [10, 11, 51]. Both approaches were used in several calculations before [39]. A major drawback of the complex versions of both algorithms is the ill-conditioned problem itself [51] which is not true for the real case.

An energy selection technique [52, 53] can be employed, to reduce the size of the CI-matrix of $\hat{H}(0)$. This reduced basis set is used in subsequent calculations [38] to form a matrix representation of $\hat{H}(\eta)$.

A related ansatz employs *parallel filter diagonalization (PFT)* [10, 11, 39, 54]. The eigenpairs, in selected spectral ranges[3] of $\boldsymbol{H}(0)$, can be calculated with the help of PFT in parallel. The resulting eigenvectors of a spectral range, which contains (a) resonance(s) of interest, are used to form a matrix representation of $\hat{H}(\eta)$. Then complex diagonalization algorithms can be applied to the small matrices for many values for $\eta$ with moderate computational effort. This method is called *subspace projection method* because the eigenvectors in the selected range form a subspace of $\hat{H}(0)$. This approach also is parallel and consequently CPU *and* wall time are reduced.

The procedure of the last paragraph bases on the fact that the dominant contributions to the description of the resonance state are made by the eigenvectors of $\hat{H}(0)$ which are close in energy to it [10, 11, 39, 54]. A drawback of the method is the use of the basis of the real Hamiltonian for $\eta > 0$ because the basis is not adapted to the modifications to the problem, introduced by the CAP. In addition the number of selected eigenvectors may be quite large to provide a suitable description of the system because some information is discarded by choosing only a subset of states. The projection step involves vector operations with the whole matrix which are costly.

The methods introduced in the preceding paragraphs are not satisfactory due to their high demand of computing power. In chapter 3 new approaches are introduced to speed up the computation of resonance energies.

[2] However, one can split the full set of values for $\eta$ into a couple of ranges of values for $\eta$ and compute these in parallel to reduce the amount of wall time needed.

[3] An overview of the spectrum of $\boldsymbol{H}(0)$ can be obtained, beforehand, by, eg., a few block Lanczos iterations, to make a suitable decision.

### 2.3.3. Suggestions for Improvements

The CAP-method, discussed in this section, reveals insufficiencies, apart from the performance: the way of computing resonances is not very convenient. One has to examine the complex eigenvalue spectra, obtained for a range of values for $\eta$, by hand to identify stabilization points of complex eigenvalues and run another computer program to analyze the $\eta$-trajectory of the interesting resonances, employing (2.14), see section 4.1.1. The results of the trajectory analysis have to be evaluated by hand, again, to find the optimal Siegert energy (1.1).

It would be desirable to have an algorithm to automatically perform the above mentioned steps. The algorithm should return the optimal Siegert energies (1.1) of all stabilization points observed in a plot of the complex eigenvalue spectra of a range of values for $\eta$. Such a method would render the calculation of resonance energies a routine problem nearly as simple as the calculation of a closed-shell ground state Hartree-Fock energy. Furthermore, one can think of an enhanced algorithm that is capable of optimizing $\eta$ in a cheaper way, i.e. an algorithm that needs a smaller set of values for $\eta$.

# 3. Application of Perturbation Theory to Electronically Decaying States

Approximation methods are a very important tool in quantum mechanics as only very few systems can be solved exactly. Perturbation theory is one of the most prominent [2]. On introductory level, perturbation theory comes in three flavors. The time-independent degenerate and non-degenerate *Rayleigh-Schrödinger perturbation theory* and the time-dependent *Dirac perturbation theory*.

In quantum chemistry, perturbation theory also is one of the dominant methods to obtain a variety of atomic and molecular properties. For example the Hartree-Fock ground state energy can be improved by applying simple time-independent non-degenerate perturbation theory to it. This is called *Møller-Plesset perturbation theory* [42,55,56] if the partition (5.5) is used. The second order scheme of this method is abbreviated to MP2. Using the partition (3.2) yields *Epstein-Nesbet perturbation theory* [55,57,58]. The treatment of electronic resonances with *complex absorbing potentials*, as presented in section 2.3, has so far not been subject to a perturbative solution.

This chapter discusses several approaches to treat resonances using perturbation theory. The first section introduces a time-dependent approach. The second and third section establish a non-Hermitian time-independent perturbation theory for resonances employing *complex absorbing potentials*.

## 3.1. Wigner-Weisskopf Theory

*Wigner-Weisskopf theory* [2,7] is the application of time-dependent perturbation theory to the decay of an electronic resonance to calculate its *Siegert energy* (1.1). The theory was applied in [8,9] to inner valence ionized clusters to study their electronic decay. The following treatment of excited states above the (auto)ionization threshold, i.e. electronic resonances, modifies the ideas developed in these publications by considering excited molecular systems.

Frequently, the single reference representation of the initial state used in this section is insufficient, especially in the inner valence, due to the breakdown of the single particle model and relaxation effects [59]. This insufficiency is overcome in section 3.3 using a multireference approach.

### 3.1.1. Formulation for Excited States

The orthonormal basis

$$\mathfrak{B} := \{ |\Phi_0\rangle, |\Phi_i^a\rangle, |\Phi_{ij}^{ab}\rangle, \ldots \mid 1 \leq i,j,\ldots \leq N < a,b,\ldots \leq K \} \tag{3.1}$$

**(1)** Difference of the excitation energies of the final and the initial state in terms of one-particle energies.

**(2)** Attraction between hole $i$ and excited electron $a$ in the initial state.

**(3)** Attraction among the holes and excited electrons in the final state.

**(4)** Repulsion among the holes and repulsion among the excited electrons in the final state.

**Table 3.1.:** Classification of the contributions to the energy difference between a singly excited initial state and a final state. Initial and final states are approximated in terms of excited Hartree-Fock determinants.

of the $n$-hole/$n$-particle excited determinants of the Hartree-Fock ground state is well suited to represent the problem. $N$ denotes the number of occupied spin orbitals in the Hartree-Fock ground state, i.e. the number of electrons, and $K$ the total number of spin orbitals in the specific discrete basis set. The basis becomes complete for $K \to \infty$.

The Hamiltonian $\hat{H}$ of the system is partitioned, according to EPSTEIN and NESBET [55, 57, 58], in an exact part and a perturbation

$$\begin{aligned} \hat{H} &= \hat{H}_0 + \hat{H}_1 \\ \hat{H}_0 &= \sum_{|\Phi_\mathrm{J}\rangle \in \mathfrak{B}} |\,\Phi_\mathrm{J}\,\rangle\,\langle\,\Phi_\mathrm{J}\,|\,\hat{H}\,|\,\Phi_\mathrm{J}\,\rangle\,\langle\,\Phi_\mathrm{J}\,| \\ \hat{H}_1 &= \sum_{\substack{|\Phi_\mathrm{J}\rangle, |\Phi_\mathrm{K}\rangle \in \mathfrak{B} \\ |\Phi_\mathrm{J}\rangle \neq |\Phi_\mathrm{K}\rangle}} |\,\Phi_\mathrm{J}\,\rangle\,\langle\,\Phi_\mathrm{J}\,|\,\hat{H}\,|\,\Phi_\mathrm{K}\,\rangle\,\langle\,\Phi_\mathrm{K}\,| \,. \end{aligned} \tag{3.2}$$

$|\,\Phi_\mathrm{I}\,\rangle := |\,\Phi_i^a\,\rangle$ is the initial state and $|\,\Phi_\mathrm{F}\,\rangle$ denotes a final state. In the framework of Wigner-Weisskopf theory, a resonance is characterized by a *complex energy* (1.1) [2, 8, 10, 11]

$$E_\mathrm{R} = \langle\,\Phi_\mathrm{I}\,|\,\hat{H}_0\,|\,\Phi_\mathrm{I}\,\rangle + \Delta_\mathrm{I} - \mathrm{i}\Gamma_\mathrm{I}/2 \,.$$

$\Gamma_\mathrm{I}$ denotes the decay width and $\Delta_\mathrm{I}$ denoting the energy shift. The decay width is

$$\Gamma_\mathrm{I} = 2\pi \sum_{F \neq I} |\,\langle\,\Phi_\mathrm{F}\,|\,\hat{H}\,|\,\Phi_\mathrm{I}\,\rangle\,|^2\, \delta(\langle\,\Phi_\mathrm{F}\,|\,\hat{H}\,|\,\Phi_\mathrm{F}\,\rangle - \langle\,\Phi_\mathrm{I}\,|\,\hat{H}\,|\,\Phi_\mathrm{I}\,\rangle) \tag{3.3}$$

in the first non-vanishing (second) order and the energy shift is

$$\Delta_\mathrm{I} = \langle\,\Phi_\mathrm{I}\,|\,\hat{H}_1\,|\,\Phi_\mathrm{I}\,\rangle + \mathrm{Pr} \sum_{F \neq I} \frac{|\,\langle\,\Phi_\mathrm{F}\,|\,\hat{H}\,|\,\Phi_\mathrm{I}\,\rangle\,|^2}{\langle\,\Phi_\mathrm{I}\,|\,\hat{H}\,|\,\Phi_\mathrm{I}\,\rangle - \langle\,\Phi_\mathrm{F}\,|\,\hat{H}\,|\,\Phi_\mathrm{F}\,\rangle} \,. \tag{3.4}$$

Note that the first order correction (the first term in (3.4)) vanishes due to the partition (3.2). The perturbation causes the electronic decay of the excited initial state. Equation (3.4) is what one expects from non-degenerate Rayleigh-Schrödinger perturbation theory. As one is interested in the electronic decay width of the initial state, the final states in (3.3), (3.4) are characterized by a continuum and some bound state indices. Hence the sum over final states $\sum_{F \neq I}$ contains, besides some sums over discrete orbital indices, $\sum_{\vec{k}}$ which can be rewritten as $\int \mathrm{d}E\, \varrho(E)$. $\varrho(E)$ denotes the density of final states that is the number of states in the interval $]\,E\,;E + \mathrm{d}E\,[$ [2].

### 3.1.2. Matrix Elements

Equation (3.3) contains three types of matrix elements

1. $\langle \Phi_\mathrm{F} | \hat{H} | \Phi_\mathrm{I} \rangle$ transition matrix element
2. $E_\mathrm{I} := \langle \Phi_\mathrm{I} | \hat{H} | \Phi_\mathrm{I} \rangle$ initial state energy matrix element
3. $E_\mathrm{F} := \langle \Phi_\mathrm{F} | \hat{H} | \Phi_\mathrm{F} \rangle$ final state energy matrix element

The *Slater-Condon rules*[1] are used to evaluate above matrix elements. The rules limit the classes of excited determinants which couple to $|\Phi_i^a\rangle$ in the transition matrix element. These classes are the singly $|\Phi_j^b\rangle$, doubly $|\Phi_{jl}^{bc}\rangle$ and triply $|\Phi_{jlm}^{bcd}\rangle$ excited determinants. The Hartree-Fock ground state does not couple to $|\Phi_i^a\rangle$ due to *Brillouin's theorem* [42]. The contribution of quadruply and higher excited determinants vanishes.

In the course of the following derivation two-electron integrals of spin orbitals of the type

$$\begin{aligned} V_{pq[rs]} &:= V_{pqrs} - V_{pqsr} \\ V_{pqrs} &:= \int\int \chi_p^\dagger(\vec{r}_1)\, \chi_r(\vec{r}_1)\, \frac{1}{|\vec{r}_1 - \vec{r}_2|}\, \chi_q^\dagger(\vec{r}_2)\, \chi_s(\vec{r}_2)\; \mathrm{d}^3 r_1\, \mathrm{d}^3 r_2 \; . \end{aligned} \tag{3.5}$$

occur which consist of a direct $V_{pqrs}$ and an exchange term $V_{pqsr}$ [42]. If these matrix elements (3.5) occur in transition amplitudes then $p, q$ denote final states, $r, s$ denote initial states. The matrix elements can be interpreted to stand for the two transitions $r \to p$ and $s \to q$. This interpretation is only valid if $p,\ q,\ r,\ s$ are interpreted as states in the one-particle picture.

#### Singly Excited Final State Determinants

Let $\Delta E := E_\mathrm{F} - E_\mathrm{I}$ and $b \equiv \vec{k}$. The final state index becomes $\vec{k}$ because one is only interested in the electronic decay width. Then the relevant matrix elements read

$$\begin{aligned} \langle \Phi_\mathrm{F} | \hat{H} | \Phi_\mathrm{I} \rangle &= \langle \Phi_j^{\vec{k}} | \hat{H} | \Phi_i^a \rangle = V_{\vec{k}i[ja]} \\ \Delta E &= \underbrace{\varepsilon_{\vec{k}} + \varepsilon_i - \varepsilon_j - \varepsilon_a}_{(1)} \underbrace{+ V_{ai[ai]}}_{(2)} \underbrace{- V_{\vec{k}j[\vec{k}j]}}_{(3)} \; . \end{aligned} \tag{3.6}$$

The contributions to $\Delta E$ can be classified, here and in the following, with the help of table 3.1. The transition matrix element is pictured schematically in figure 3.1. One obtains the partial decay width of this process by inserting (3.6) into (3.3)

$$\Gamma_\mathrm{singly} = 2\pi \sum_{\vec{k}} \sum_{j=1}^{N} |V_{\vec{k}i[ja]}|^2\, \delta(\Delta E) \; . \tag{3.7}$$

[1] Section 2.3 (pages 64–89) in [42], especially the expressions in Tables 2.3, 2.4 are frequently used. Furthermore, the results of exercise 3.1 on page 115 and equations (3.75), (3.76) are also employed.

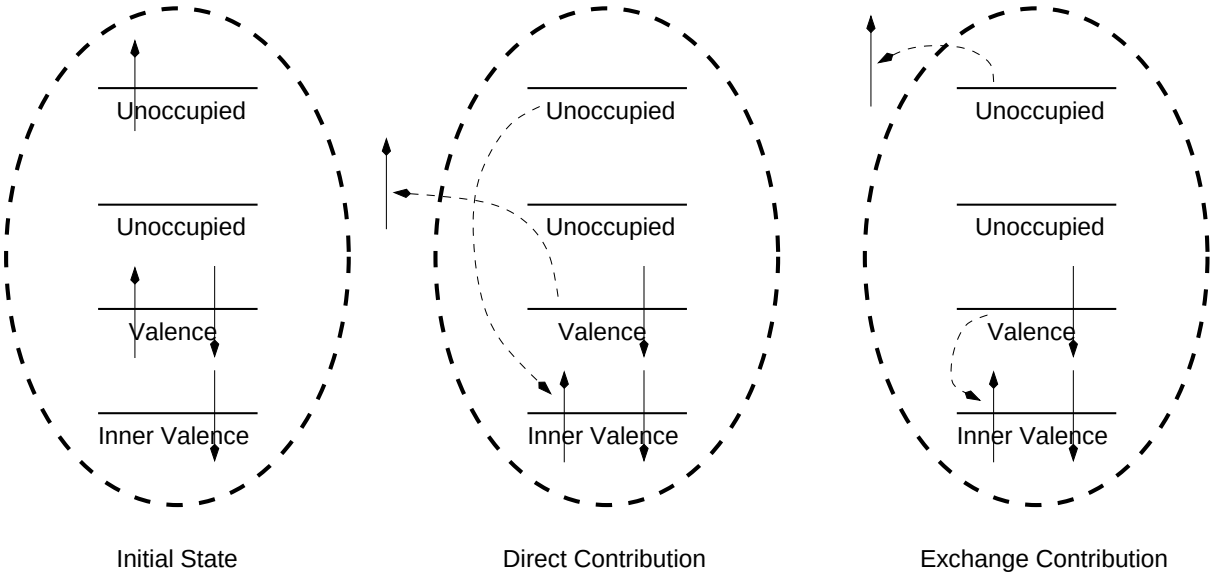


**Figure 3.1.:** Schematic representation of the decay of the singly excited initial state $|\Phi_i^a\rangle$ into the singly excited final state $|\Phi_j^{\vec{k}}\rangle$. The process is pictured in terms of Hartree-Fock orbitals.

### Doubly Excited Final State Determinants

The doubly excited determinants $|\Phi_{jl}^{bc}\rangle$ contribute if $i \in \{j,l\}$ or $a \in \{b,c\}$. One final state index becomes $\vec{k}$ because one is only interested in electronic decay. There are three cases to distinguish:

**Case 1:** Four combinations $i \in \{j,l\}$ and $a \in \{b,c\}$. The other final state becomes $\vec{k}$.

**Case 2:** Four combinations $i \in \{j,l\}$ and $\vec{k} \in \{b,c\}$.

**Case 3:** Two combinations $a \in \{b,c\}$. The other final state becomes $\vec{k}$.

Each case corresponds to a distinct group of matrix elements. Within a group the matrix elements are identical, apart from their sign, because the matrix element $\langle \Phi_i^a | \hat{H} | \Phi_{jl}^{bc} \rangle$ changes its sign under interchange of $j \leftrightarrow l$ or $b \leftrightarrow c$. Hence each group is represented by a single schematic representation similar to figure 3.1 (for the singly excited final states). $\langle \Phi_{jl}^{bc} | \hat{H} | \Phi_{jl}^{bc} \rangle$, $\langle \Phi_i^a | \hat{H} | \Phi_i^a \rangle$ are invariant under this interchange. As one can transform any choice of $i \in \{j,l\}$ or $a, \vec{k} \in \{b,c\}$ in a group to another, the combinations are non-physical and the multiplicities must not be accounted for in the partial decay widths which correspond to the groups. Hence one can choose arbitrarily which indices are taken.

**Case 1** The matrix elements read, setting $l \equiv i,\ b \equiv \vec{k},\ c \equiv a$

$$\begin{aligned} \langle \Phi_{\mathrm{F}} | \hat{H} | \Phi_{\mathrm{I}} \rangle &= \langle \Phi_{ji}^{\vec{k}a} | \hat{H} | \Phi_i^a \rangle = V_{\vec{k}a[ja]} - V_{\vec{k}i[ji]} \\ \Delta E &= \underbrace{\varepsilon_{\vec{k}} - \varepsilon_j}_{(1)} \underbrace{- V_{i\vec{k}[i\vec{k}]} - V_{ja[ja]} - V_{j\vec{k}[j\vec{k}]}}_{(3)} \underbrace{+ V_{ij[ij]} + V_{a\vec{k}[a\vec{k}]}}_{(4)} . \end{aligned}$$

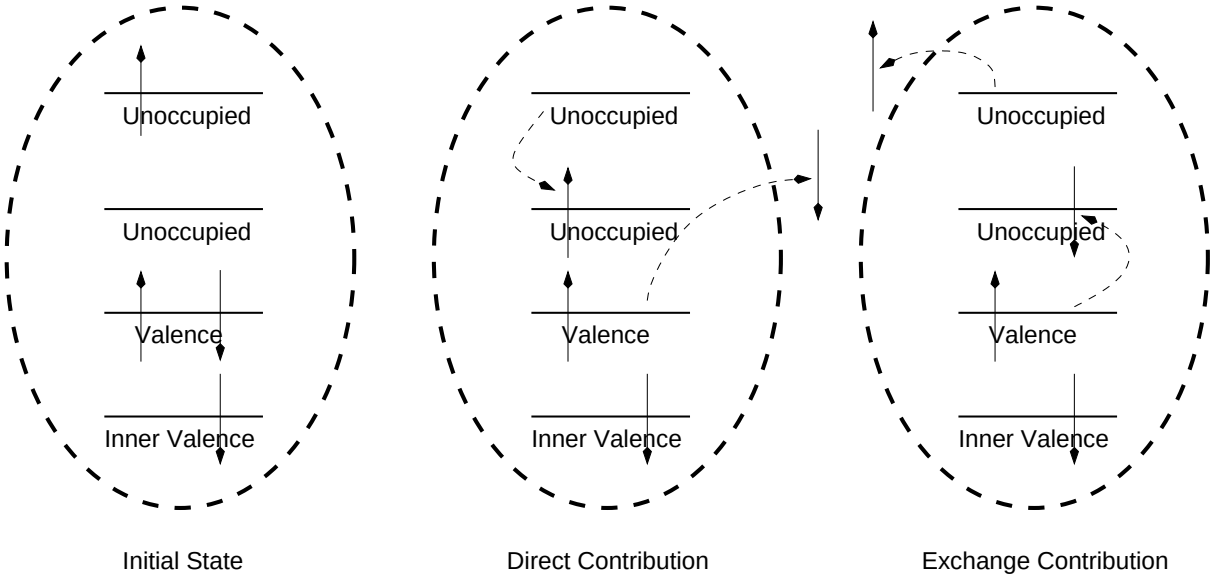


**Figure 3.2.:** Schematic representation of the decay of the singly excited initial state $|\,\Phi_i^a\,\rangle$ into the doubly excited final state $|\,\Phi_{ji}^{\vec{k}b}\,\rangle$. The process is pictured in terms of Hartree-Fock orbitals.

The transition matrix element is not intuitively clear. It arises from the coupling of the determinants. This shows that the excited determinants are not physical states. In addition the decay process cannot be visualized in a single picture – instead it is the difference between "two pictures". The partial decay width (3.3) of this process is

$$\Gamma_{\text{doubly},1} = 2\pi \sum_{\vec{k}} \sum_{\substack{j=1 \\ j\neq i}}^{N} |V_{\vec{k}a[ja]} - V_{\vec{k}i[ji]}|^2 \, \delta(\Delta E) \; . \tag{3.8}$$

**Case 2** The matrix elements read, setting $l \equiv i,\ c \equiv \vec{k},\ b \neq a$

$$\begin{aligned} \langle\,\Phi_{\mathrm{F}}\,|\,\hat{H}\,|\,\Phi_{\mathrm{I}}\,\rangle &= \langle\,\Phi_{ji}^{\vec{k}b}\,|\,\hat{H}\,|\,\Phi_i^a\,\rangle = V_{\vec{k}b[ja]} \\ \Delta E &= \underbrace{\varepsilon_b + \varepsilon_{\vec{k}} - \varepsilon_a - \varepsilon_j}_{(1)} \underbrace{+ V_{ia[ia]}}_{(2)} \\ &\quad \underbrace{- V_{i\vec{k}[i\vec{k}]} - V_{ib[ib]} - V_{j\vec{k}[j\vec{k}]} - V_{jb[jb]}}_{(3)} \underbrace{+ V_{ij[ij]} + V_{b\vec{k}[b\vec{k}]}}_{(4)} \end{aligned}$$

The transition matrix element is pictured in figure 3.2. The partial decay width (3.3) of this process is

$$\Gamma_{\text{doubly},2} = 2\pi \sum_{\vec{k}} \sum_{\substack{b=N+1 \\ b\neq a}}^{K} \sum_{\substack{j=1 \\ j\neq i}}^{N} |V_{b\vec{k}[aj]}|^2 \, \delta(\Delta E). \tag{3.9}$$

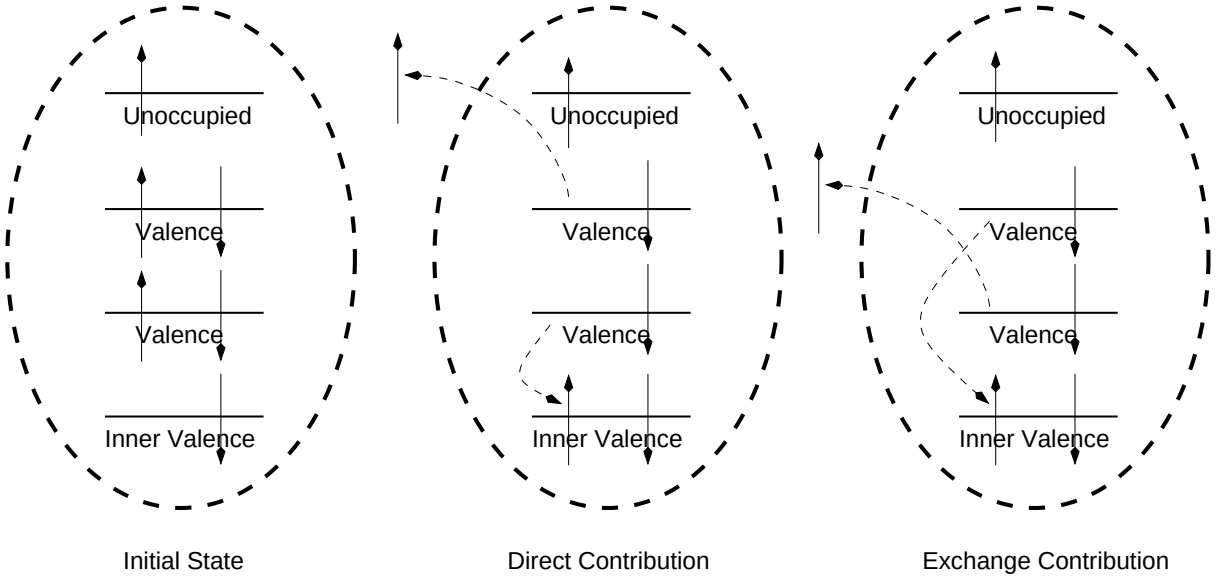


**Figure 3.3.:** Schematic representation of the decay of the singly excited initial state $|\,\Phi_i^a\,\rangle$ into the doubly excited final state $|\,\Phi_{jl}^{\vec{k}a}\,\rangle$. The process is pictured in terms of Hartree-Fock orbitals.

**Case 3** The matrix elements read, setting $b \equiv \vec{k},\ c \equiv a,\ j,l \neq i$

$$\begin{aligned}\langle\,\Phi_{\mathrm{F}}\,|\,\hat{H}\,|\,\Phi_{\mathrm{I}}\,\rangle &= \langle\,\Phi_{jl}^{\vec{k}a}\,|\,\hat{H}\,|\,\Phi_i^a\,\rangle = -V_{i\vec{k}[lj]} \\ \Delta E &= \underbrace{\varepsilon_{\vec{k}} + \varepsilon_i - \varepsilon_j - \varepsilon_l}_{(1)} \underbrace{+ V_{ia[ia]}}_{(2)} \\ &\quad \underbrace{- V_{l\vec{k}[l\vec{k}]} - V_{j\vec{k}[j\vec{k}]} - V_{ja[ja]} - V_{la[la]}}_{(3)} \underbrace{+ V_{jl[jl]} + V_{a\vec{k}[a\vec{k}]}}_{(4)}\end{aligned}$$

The transition matrix elements is pictured in figure 3.3. The partial decay width (3.3) of this process is

$$\Gamma_{\mathrm{doubly,3}} = 2\pi \sum_{\vec{k}} \sum_{\substack{j,l=1 \\ j,l\neq i \\ j<l}}^{N} |V_{i\vec{k}[lj]}|^2\, \delta(\Delta E). \tag{3.10}$$

### Triply Excited Final State Determinants

The triply excited determinants $\Phi_{jlm}^{cbd}$ contribute if $i \in \{j,l,m\}$ and $a \in \{b,c,d\}$. There are three possibilities to choose $i \in \{j,l,m\}$. Furthermore there are $\binom{3}{2}\,2! = 6$ possibilities to set $\{a,\vec{k}\} \subseteq \{b,c,d\}$ giving 18 combinations in total whose matrix elements may differ only by sign. These combinations are again non-physical (see the discussion in the previous subsubsection). $\vec{k}$ is required to be included in the final states because one is interested in electronic decay processes. The matrix elements read, setting $m \equiv i,\ c \equiv \vec{k},\ d \equiv a$

$$\langle\,\Phi_{\mathrm{F}}\,|\,\hat{H}\,|\,\Phi_{\mathrm{I}}\,\rangle = \langle\,\Phi_{jli}^{\vec{k}ba}\,|\,\hat{H}\,|\,\Phi_i^a\,\rangle = V_{\vec{k}b[jl]}$$

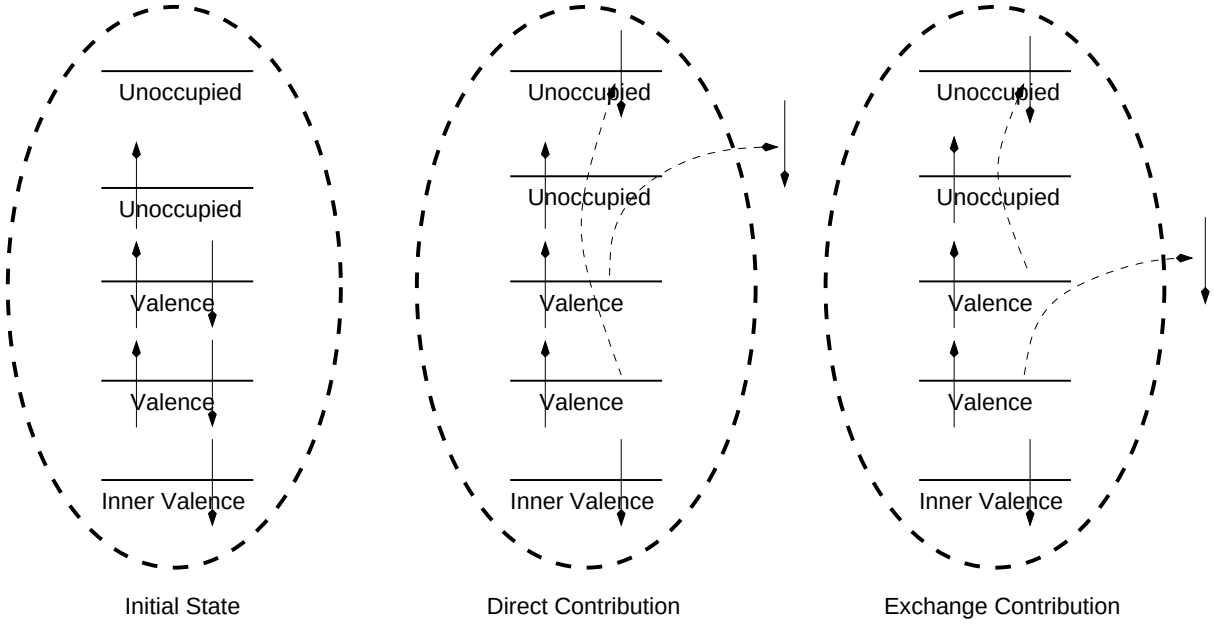


**Figure 3.4.:** Schematic representation of the decay of the singly excited initial state $|\,\Phi_i^a\,\rangle$ into the triply excited final state $|\,\Phi_{jli}^{\vec{k}ba}\,\rangle$. The process is pictured in terms of Hartree-Fock orbitals.

$$\begin{aligned}\Delta E \;=\; & \underbrace{\varepsilon_{\vec{k}} + \varepsilon_b - \varepsilon_j - \varepsilon_l}_{(1)} \\ & \underbrace{- V_{i\vec{k}[i\vec{k}]} - V_{j\vec{k}[j\vec{k}]} - V_{l\vec{k}[l\vec{k}]} - V_{ib[ib]} - V_{jb[jb]} - V_{lb[lb]} - V_{ja[ja]} - V_{la[la]}}_{(3)} \\ & \underbrace{+ V_{ij[ij]} + V_{il[il]} + V_{jl[jl]} + V_{a\vec{k}[a\vec{k}]} + V_{b\vec{k}[b\vec{k}]} + V_{ab[ab]}}_{(4)}\end{aligned}$$

The transition matrix elements is pictured in figure 3.4. The partial decay width (3.3) of this process is

$$\Gamma_{\text{triply}} = 2\pi \sum_{\vec{k}} \sum_{\substack{b=N+1 \\ b\neq a}}^{K} \sum_{\substack{j,l=1 \\ j,l\neq i \\ j<l}}^{N} |V_{b\vec{k}[jl]}|^2 \, \delta(\Delta E). \tag{3.11}$$

From a physical point of view the process does not look reasonable because neither the initial hole nor the initial particle state is involved. This fact reminds us of the non-physical nature of the determinants.

### 3.1.3. The Decay Width

Collecting all *partial decay widths* (3.7), (3.8), (3.9), (3.10), (3.11) from the preceding subsection results in the total electronic decay width accurate up to second order in perturbation theory

$$\Gamma_{\text{I}} = \Gamma_{\text{singly}} + \Gamma_{\text{doubly},1} + \Gamma_{\text{doubly},2} + \Gamma_{\text{doubly},3} + \Gamma_{\text{triply}}.$$

The accuracy of this formula also depends on the quality of the description of the initial and final states which may be less accurate than second order. All equations in this section are given in terms of spin orbitals. A spin-free version can be derived easily by integrating out the spin in the final equations (3.7), (3.8), (3.9), (3.10), (3.11) [42]

Till now the continuum index $\vec{k}$ has been treated like an ordinary bound state index. This way of proceeding is questionable because continuum wave functions are $\delta$-function normalized. Hence they are not square integrable. Therefore, they are not a member of the $N$-electron Hilbert space spanned by (3.1). A standard technique to overcome this problem is *Stieltjes Chebyshev moment theory*. For details see section 2.4 in [10, 11] and references therein.

## 3.2. Single Reference Perturbation Theory

In the preceding section 3.1 time-dependent perturbation theory is applied to describe the decay of a singly excited state, using a single reference to represent the initial state. This section will tackle the same question with a different approach.

In section 2.3 complex absorbing potentials are introduced to transform the time-dependent decay problem into a time-independent problem. Hence augmenting a molecular system by a CAP, renders the decay problem describable by a simple non-Hermitian non-degenerate Rayleigh-Schrödinger approach.

If a single reference is used to describe the initial state [2]. (Near) degeneracies of the chosen reference with other states are very unpleasant because the non-degenerate Rayleigh-Schrödinger approach is not defined, then. This problem may not occur if a CAP is present because the degeneracy may be removed. Nevertheless one should seek a more robust multireference approach in the case of degeneracies. This is done in the ensuing section 3.3.

The reason for presenting a single reference approach, in spite of its inherent insufficiencies, is the fact that it represents the formal equivalent to the time-dependent theory derived before. Hence this section demonstrates how CAPs transform the electronic decay problem.

### 3.2.1. Formulation

The particle-hole basis set (3.1) is used here, too, with the Hermitian kets $|\cdot\rangle$ replaced by their non-Hermitian pendant $|\cdot)$ which changes only the notation because the basis set (3.1) is assumed to be real. There are two common ways of partitioning the Hamiltonian. The *Epstein-Nesbet partition* [55, 57, 58] (3.2) is augmented by adding the diagonal and the off-diagonal part of $\hat{W}$

$$\begin{aligned} \hat{W}_0 &= \sum_{|\Phi_J)\in\mathfrak{B}} |\Phi_J)\,(\Phi_J|\,\hat{W}\,|\Phi_J)\,(\Phi_J| \qquad (3.12)\\ \hat{W}_1 &= \sum_{\substack{|\Phi_J),|\Phi_K)\in\mathfrak{B}\\ J\neq K}} |\Phi_J)\,(\Phi_J|\,\hat{W}\,|\Phi_K)\,(\Phi_K| \end{aligned}$$

to $\hat{H}_0$ and $\hat{H}_1$ respectively

$$\begin{aligned} \hat{H}(\eta) &= \hat{H}_0(\eta) + \hat{H}_1(\eta) \\ \hat{H}_0(\eta) &= \hat{H}_0 - \mathrm{i}\eta\hat{W}_0 \\ \hat{H}_1(\eta) &= \hat{H}_1 - \mathrm{i}\eta\hat{W}_1 \,. \end{aligned} \tag{3.13}$$

Furthermore there is the *Møller-Plesset partition* [42,55,56] of the real Hamiltonian (5.5) that is also frequently used. As the CAP is considered a perturbation to the real system one may write

$$\begin{aligned} \hat{H}^{(\mathrm{MP})}(\eta) &= \hat{H}_0^{(\mathrm{MP})}(\eta) + \hat{H}_1^{(\mathrm{MP})}(\eta) \\ \hat{H}_0^{(\mathrm{MP})}(\eta) &= \hat{H}_0^{(\mathrm{MP})} \\ \hat{H}_1^{(\mathrm{MP})}(\eta) &= \hat{H}_1^{(\mathrm{MP})} - \mathrm{i}\eta\hat{W} \,. \end{aligned}$$

This way of adding a CAP to the system may give better results compared to the partition (3.1), (3.12) because the matrix representation of $\hat{W}$ in the basis (3.1) is not supposed to be diagonal dominant, i.e. its diagonal cannot be thought of to be a zeroth order contribution. The perturbation $\hat{H}_1(\eta)$ of both partitions of the CAP-Hamiltonian depends on $\eta$. Therefore one can expect perturbation theory to converge only for small $\eta$. The Møller-Plesset partition is not considered any further.

The CAP-Hamiltonian in Epstein-Nesbet partition (3.13) is used for a simple time-independent *Rayleigh-Schrödinger perturbation theory* [2,3] using one reference $|\,\Phi_\mathrm{I}\,)$ which is termed the "initial state". This term originates from the time-dependent picture. In this context $|\,\Phi_\mathrm{I}\,)$ denotes a state whose Siegert energy (1.1) is calculated. For convenience and to emphasize the analogy to the time-dependent case, the terminology of section 3.1 is used throughout.

The CAP-Schrödinger equation for the unperturbed part of (3.13) is

$$\hat{H}_0(\eta)\,|\,\Phi_\mathrm{J}\,) = E_\mathrm{J}^{(0)}(\eta)\,|\,\Phi_\mathrm{J}\,)\,,$$

for an arbitrary $|\,\Phi_\mathrm{J}\,) \in \mathfrak{B}$. Now the well-known derivation of the Rayleigh-Schrödinger perturbation series [2, 3] can be transferred to the non-Hermitian case. Up to second order, the energy of the initial state is given by

$$E_\mathrm{I}^{(0)}(\eta) = (\,\Phi_\mathrm{I}\,|\,\hat{H}_0(\eta)\,|\,\Phi_\mathrm{I}\,) \tag{3.14a}$$

$$E_\mathrm{I}^{(1)}(\eta) = (\,\Phi_\mathrm{I}\,|\,\hat{H}_1(\eta)\,|\,\Phi_\mathrm{I}\,) \tag{3.14b}$$

$$E_\mathrm{I}^{(2)}(\eta) = \sum_{\substack{|\Phi_\mathrm{F})\in\mathfrak{B} \\ F\neq I}} \frac{(\,\Phi_\mathrm{I}\,|\,\hat{H}_1(\eta)\,|\,\Phi_\mathrm{F}\,)^2}{E_\mathrm{I}^{(0)}(\eta) - E_\mathrm{F}^{(0)}(\eta)} \,. \tag{3.14c}$$

In (3.14c) $E_\mathrm{F}^{(0)}(\eta)$ denotes the analogue to (3.14a) $E_\mathrm{F}^{(0)}(\eta) = (\,\Phi_\mathrm{F}\,|\,\hat{H}_0(\eta)\,|\,\Phi_\mathrm{F}\,)$ for an arbitrary state $|\,\Phi_\mathrm{F}\,) \in \mathfrak{B}$, $F \neq I$. The first order correction (3.14b) vanishes due to the partition (3.2), (3.12).

Equation (3.14c) may not be defined if $|\,\Phi_\mathrm{I}\,)$ and $|\,\Phi_\mathrm{F}\,)$ are degenerate because the imaginary parts in the denominator, originating from the CAP, may also cancel. This

is not a problem for the calculation of the decay width in section 3.1. Inspecting (3.4) shows that the degeneracy problem in the single reference perturbation theory, derived here, occurs due to the fact that the full Siegert energy (1.1) is calculated.

To study the real and imaginary parts of the energy correction (3.14c), an abbreviated notation is introduced

$$\begin{aligned} H_{\mathrm{IF}} &:= (\Phi_{\mathrm{I}}\,|\,\hat{H}\,|\,\Phi_{\mathrm{F}}) \\ \Delta H &:= (\Phi_{\mathrm{I}}\,|\,\hat{H}\,|\,\Phi_{\mathrm{I}}) - (\Phi_{\mathrm{F}}\,|\,\hat{H}\,|\,\Phi_{\mathrm{F}}) \\ W_{\mathrm{IF}} &:= (\Phi_{\mathrm{I}}\,|\,\hat{W}\,|\,\Phi_{\mathrm{F}}) \\ \Delta W &:= (\Phi_{\mathrm{I}}\,|\,\hat{W}\,|\,\Phi_{\mathrm{I}}) - (\Phi_{\mathrm{F}}\,|\,\hat{W}\,|\,\Phi_{\mathrm{F}})\ . \end{aligned}$$

The matrix elements in (3.14c) can now be split into contributions of $\hat{H}$ and contributions of $\hat{W}$ because

$$(\Phi_{\mathrm{J}}\,|\,\hat{H}(\eta)\,|\,\Phi_{\mathrm{K}}) = (\Phi_{\mathrm{J}}\,|\,\hat{H}\,|\,\Phi_{\mathrm{K}}) - \mathrm{i}\eta\,(\Phi_{\mathrm{J}}\,|\,\hat{W}\,|\,\Phi_{\mathrm{K}}) \tag{3.15}$$

holds for arbitrary $J, K$. This yields for the summand in (3.14c)

$$P_2(F) := \frac{(H_{\mathrm{IF}} - \mathrm{i}\eta W_{\mathrm{IF}})^2}{\Delta H - \mathrm{i}\eta\Delta W} = \frac{(H_{\mathrm{IF}} - \mathrm{i}\eta W_{\mathrm{IF}})^2\,(\Delta H + \mathrm{i}\eta\Delta W)}{(\Delta H)^2 + (\eta\Delta W)^2}$$

$$\mathrm{Re}\,P_2(F) = \frac{H_{\mathrm{IF}}^2\,\Delta H - \eta^2\,\Delta H\,W_{\mathrm{IF}}^2 + 2\,\eta^2\,\Delta W\,W_{\mathrm{IF}}\,H_{\mathrm{IF}}}{(\Delta H)^2 + (\eta\Delta W)^2} \tag{3.16a}$$

$$\mathrm{Im}\,P_2(F) = \frac{\eta\,H_{\mathrm{IF}}^2\,\Delta W - 2\,\eta\,H_{\mathrm{IF}}\,W_{\mathrm{IF}}\,\Delta H - \eta^3\,\Delta W\,W_{\mathrm{IF}}^2}{(\Delta H)^2 + (\eta\Delta W)^2}\ . \tag{3.16b}$$

In a complete basis, $\eta \to 0$ yields the exact Siegert energy (1.1) [17]. In this case, the real part (3.16a) reduces to

$$\lim_{\eta\to 0} \mathrm{Re}\,P_2(F) = \frac{H_{\mathrm{IF}}^2}{\Delta H},$$

which is the simple Rayleigh-Schrödinger result for a non-degenerate state. Dirac's $\delta$-function possesses following representation

$$\delta(x) = \lim_{\varepsilon\to 0}\delta_\varepsilon(x) = \lim_{\varepsilon\to 0}\frac{1}{\pi}\frac{\varepsilon}{x^2+\varepsilon^2},$$

which can be used to transform (3.16b) to

$$\mathrm{Im}\,P_2(F) = -\pi\,H_{\mathrm{IF}}^2\,\delta_\varepsilon(\Delta H) + \frac{2\,\pi\,H_{\mathrm{IF}}\,W_{\mathrm{IF}}\,\Delta H}{\Delta W}\,\delta_\varepsilon(\Delta H) + \pi\,\eta^2\,W_{\mathrm{IF}}^2\,\delta_\varepsilon(\Delta H)$$

with $\varepsilon := -\eta\,\Delta W$. Using $\eta \to 0 \Longrightarrow \varepsilon \to 0$, the last two terms vanish. They are an artificial contribution introduced by the CAP. For finite $\eta$, a suitable projection operator (3.19) can be used, as shown below, then $W_{\mathrm{IF}}$ and the last two terms vanish. Hence the imaginary part assumes the form

$$\mathrm{Im}\,P_2(F) = -\pi\,H_{\mathrm{IF}}^2\,\delta_\varepsilon(\Delta H) \tag{3.17}$$

which is identical to (3.3) due to (1.1) in the limit $\eta \to 0$.

### 3.2.2. Matrix Elements

The initial state is chosen to be $|\Phi_\mathrm{I}) := |\Phi_i^a)$ following the arguments in section 3.1. The initial and final state energy matrix elements and the transition matrix elements of subsection 3.1.2 occur in the equations (3.14) because (3.15) holds and the Hermitian scalar product does not differ from the complex symmetric bilinear (2.12) form, in the case of real determinants. Hence the formulae of subsection 3.1.2 for the matrix elements can be applied here as well. Solely the matrix elements of $\hat{W}$ have to be calculated.

$\hat{W}$ denotes a one-particle operator, according to section 2.3.1. Hence all matrix elements between determinants, which differ by more than one spin orbital, vanish due to the Slater-Condon rules (footnote 1 on page 17). The coupling of $|\Phi_i^a)$, $|\Phi_j^k)$, $|\Phi_{ji}^{ka})$, $|\Phi_{ji}^{bk})$, $|\Phi_{jl}^{ka})$, $|\Phi_{jli}^{\vec{k}ba})$ to itself is needed for the initial and final state energy matrix elements. Note that the continuum index $\vec{k}$ is replaced by a discrete index $k$ due to the CAP. Furthermore the coupling of $|\Phi_i^a)$ to determinants, differing only by one spin orbital, is needed for the transition matrix elements. These are $|\Phi_0)$, $|\Phi_j^a)$, $|\Phi_i^b)$, $|\Phi_{ji}^{ka})$.

#### Coupling to Itself

The initial state energy matrix element is

$$(\Phi_i^a|\hat{W}|\Phi_i^a) = \sum_{\substack{l=1\\l\neq i}}^{N} (\chi_l|\hat{W}|\chi_l) + (\chi_a|\hat{W}|\chi_a) \ . \tag{3.18}$$

The electrons in the initial state spin orbitals are influenced by the CAP by $(\chi_l|\hat{W}(l)|\chi_l)$. This is not desired because a non-physical perturbation of the initial state is introduced in this way. Therefore, a *projection operator*

$$\hat{\mathfrak{P}} = \sum_{\substack{l=N+1\\l\neq a}}^{K} |\chi_l)(\chi_l| \tag{3.19}$$

is introduced to project $\hat{W}$ on unoccupied initial state orbitals (without the initial hole). Replacing $\hat{W}$ by $\hat{W}_\mathfrak{P} = \hat{\mathfrak{P}}\hat{W}\hat{\mathfrak{P}}$ yields for equation (3.18) $(\Phi_i^a|\hat{W}_\mathfrak{P}|\Phi_i^a) = 0$. The final state energy matrix elements are on the analogy of equation (3.18)

$$\begin{aligned}
(\Phi_j^k|\hat{W}_\mathfrak{P}|\Phi_j^k) &= (\chi_k|\hat{W}|\chi_k)\\
(\Phi_{ji}^{ka}|\hat{W}_\mathfrak{P}|\Phi_{ji}^{ka}) &= (\chi_k|\hat{W}|\chi_k)\\
(\Phi_{ji}^{kb}|\hat{W}_\mathfrak{P}|\Phi_{ji}^{kb}) &= (\chi_b|\hat{W}|\chi_b) + (\chi_k|\hat{W}|\chi_k)\\
(\Phi_{jl}^{ka}|\hat{W}_\mathfrak{P}|\Phi_{jl}^{ka}) &= (\chi_k|\hat{W}|\chi_k)\\
(\Phi_{jli}^{kba}|\hat{W}_\mathfrak{P}|\Phi_{jli}^{kba}) &= (\chi_b|\hat{W}|\chi_b) + (\chi_k|\hat{W}|\chi_k) \ .
\end{aligned} \tag{3.20}$$

The matrix elements (3.20) cause a non-physical perturbation of the excited electrons and the absorption of the "outgoing" electron. The effect of the CAP on the excited electrons can be reduced by choosing an appropriate $\hat{W}$.

#### Coupling to Other Determinants

The transition matrix elements of the CAP-operator are

$$\begin{aligned}(\Phi_i^a\,|\,\hat{W}\,|\,\Phi_0\,) &= (\chi_a\,|\,\hat{W}\,|\,\chi_i\,)\\ (\Phi_i^a\,|\,\hat{W}\,|\,\Phi_j^a\,) &= -(\chi_j\,|\,\hat{W}\,|\,\chi_i\,)\\ (\Phi_i^a\,|\,\hat{W}\,|\,\Phi_i^b\,) &= (\chi_a\,|\,\hat{W}\,|\,\chi_b\,)\\ (\Phi_i^a\,|\,\hat{W}\,|\,\Phi_{ji}^{ka}\,) &= (\chi_j\,|\,\hat{W}\,|\,\chi_k\,)\end{aligned}$$

The minus sign is caused by the maximum coincidence enforced by exchanging the $i$-th and the $j$-th spin orbital in one of the determinants [42]. The transition $\hat{W} \to \hat{W}_{\mathfrak{P}}$ (3.19) makes all transition matrix elements of the CAP-operator vanish. Hence the CAP does not cause artificial transitions and (3.17) holds for $\eta > 0$. The influence of the CAP is restricted to (3.20).

## 3.3. Multireference Perturbation Theory

The degenerate time-independent perturbation theory is, in fact, a special multireference approach as the subspace of degenerate states, belonging to a certain energy eigenvalue, is taken. Then the subspace is diagonalized to decouple the states and to yield corrections to the energy in first and to the wave function in zeroth order. After this non-degenerate perturbation theory can be applied to each linear combination of the initial states, if the degeneracy is resolved in the new basis, to obtain higher order corrections [2,3].

A general multireference approach can be devised analogously. An arbitrary set of initial states can be taken. Then one can proceed as described in the previous paragraph. This is, essentially, what is done in this section.

### 3.3.1. The Effective Eigenvalue Problem

#### Partition of the Hamiltonian

The CAP-Schrödinger equation (2.13)

$$\hat{H}(\eta)|\Psi_j(\eta)) = E_j(\eta)|\Psi_j(\eta)) \tag{3.21}$$

shall be solved for several complex eigenvalues, the resonance states of interest, using perturbation theory. An orthonormal (configuration interaction) basis set $|\Phi_j)$, $j = 1,\ldots,K$ (see section 2.2) is used to form a complex symmetric matrix representation of (3.21). The Hamiltonian reads in this basis

$$\hat{H}(\eta) \approx \sum_{i,j=1}^{K} |\Phi_i)\,(\Phi_i|\hat{H}(\eta)|\Phi_j)\,(\Phi_j|.$$

The approximation becomes exact for $K \to \infty$.

Out of the basis, a set of $n$ configurations is selected as *references* $|\Phi_j)$, $j = 1, \ldots, n$ which approximate[2] $n$ physical states $|\Psi_j(\eta))$, $j = 1, \ldots, n$. For ease of notation, the references are denoted with the first $n$ numbers. For the case of a singly excited resonance state, discussed in the preceding sections 3.1, 3.2, the most important configurations are the singly excited *particle-hole configurations*, which are close to the resonance energy, because they have usually a big overlap with the eigenvector of the resonance. In fact most configurations which are close to the resonance energy are important. See [52, 53] and references therein, for techniques to select the essential configurations.

Next a *reference space* or *model space* and its *complement space* is formed with the help of *projection operators* [10, 11, 39]

$$\hat{\mathfrak{P}} = \sum_{j=1}^{n} |\Phi_j)(\Phi_j| \qquad \hat{\mathfrak{Q}} = \hat{\mathbb{1}} - \hat{\mathfrak{P}} = \sum_{j=n+1}^{K} |\Phi_j)(\Phi_j| \tag{3.22}$$

obeying

$$\hat{\mathfrak{P}}^2 = \hat{\mathfrak{P}}, \qquad \hat{\mathfrak{Q}}^2 = \hat{\mathfrak{Q}}, \qquad \hat{\mathfrak{P}}^{\mathrm{T}} = \hat{\mathfrak{P}}, \qquad \hat{\mathfrak{Q}}^{\mathrm{T}} = \hat{\mathfrak{Q}}, \qquad \hat{\mathfrak{P}} + \hat{\mathfrak{Q}} = \hat{\mathbb{1}}, \qquad \hat{\mathfrak{P}}\,\hat{\mathfrak{Q}} = 0\ . \tag{3.23}$$

Applying (3.22) to (3.21) yields

$$\hat{\mathfrak{P}}\hat{H}(\eta)\hat{\mathfrak{P}}\,|\Psi_j(\eta)) + \hat{\mathfrak{P}}\hat{H}(\eta)\hat{\mathfrak{Q}}\,|\Psi_j(\eta)) = E_j(\eta)\,\hat{\mathfrak{P}}|\Psi_j(\eta)) \tag{3.24a}$$

$$\hat{\mathfrak{Q}}\hat{H}(\eta)\hat{\mathfrak{P}}\,|\Psi_j(\eta)) + \hat{\mathfrak{Q}}\hat{H}(\eta)\hat{\mathfrak{Q}}\,|\Psi_j(\eta)) = E_j(\eta)\,\hat{\mathfrak{Q}}|\Psi_j(\eta))\ . \tag{3.24b}$$

Adding (3.24a) to (3.24b) gives

$$\hat{H}(\eta) = \hat{\mathfrak{P}}\hat{H}(\eta)\hat{\mathfrak{P}} + \hat{\mathfrak{P}}\hat{H}(\eta)\hat{\mathfrak{Q}} + \hat{\mathfrak{Q}}\hat{H}(\eta)\hat{\mathfrak{P}} + \hat{\mathfrak{Q}}\hat{H}(\eta)\hat{\mathfrak{Q}}\ . \tag{3.25}$$

The matrix representation of (3.25) reads

$$\boldsymbol{H}(\eta) = \left(\begin{array}{c|c} \mathfrak{P}\boldsymbol{H}(\eta)\mathfrak{P} & \mathfrak{P}\boldsymbol{H}(\eta)\mathfrak{Q} \\ \hline \mathfrak{Q}\boldsymbol{H}(\eta)\mathfrak{P} & \mathfrak{Q}\boldsymbol{H}(\eta)\mathfrak{Q} \end{array}\right) \tag{3.26}$$

in the basis set $|\Phi_j)$, $j = 1, \ldots, K$. One notices that the matrix representation of eg. $\hat{\mathfrak{P}}\hat{H}(\eta)\hat{\mathfrak{P}}$ is a $K \times K$ matrix $\mathfrak{P}\boldsymbol{H}(\eta)\mathfrak{P}$ with a non-zero upper $n \times n$ matrix. For notational brevity, the $K \times K$ matrix $\mathfrak{P}\boldsymbol{H}(\eta)\mathfrak{P}$ is identified with the smaller non-zero $n \times n$ matrix. The same applies to the other blocks of (3.26).

### The Effective Hamiltonian

Equation (3.24b) is solved for $\hat{\mathfrak{Q}}|\Psi_j(\eta))$, with the help of (3.23) which yields

$$\hat{\mathfrak{Q}}|\Psi_j(\eta)) = [E_j(\eta)\,\hat{\mathbb{1}} - \hat{\mathfrak{Q}}\hat{H}(\eta)\hat{\mathfrak{Q}}]^{-1}\,\hat{\mathfrak{Q}}\hat{H}(\eta)\hat{\mathfrak{P}}|\Psi_j(\eta))\ . \tag{3.27}$$

[2] The approximation of the physical states needs only to be good for the desired resonance states, thus the number of references is usually larger than the actual number of states of interest.

The operator $\hat{G}(\eta) := [E_j(\eta)\,\hat{\mathbb{1}} - \hat{\mathfrak{Q}}\hat{H}(\eta)\hat{\mathfrak{Q}}]^{-1}$ has poles at the eigenvalues of $\hat{\mathfrak{Q}}\hat{H}(\eta)\hat{\mathfrak{Q}}$. It is the *Green's function* [42] of the complement space. To avoid singularities, the complement space must not contain states which are degenerate with a reference state.

Near degeneracies are also a problem because $\hat{G}(\eta)$ is nearly singular in this case the perturbation series does not converge and instabilities in numerical calculations arise. The problem is overcome by enlarging the reference space to include the problematic states. Such nearly degenerate states are called *intruder states* [60] if they couple only weakly[3] to the reference states.

Inserting equation (3.27) into (3.24a), multiplying with $(\Psi_i(\eta)|\hat{\mathfrak{P}}$, results in

$$E_j(\eta)\,(\Psi_i(\eta)|\hat{\mathfrak{P}}|\Psi_j(\eta)) = (\Psi_i(\eta)|\hat{H}_{\text{eff}}(\eta)|\Psi_j(\eta)) \tag{3.28a}$$

$$\hat{H}_{\text{eff}}(\eta) = \hat{\mathfrak{P}}\hat{H}(\eta)\hat{\mathfrak{P}} + \hat{\mathfrak{P}}\hat{H}(\eta)\hat{\mathfrak{Q}}\,[E_j(\eta)\,\hat{\mathbb{1}} - \hat{\mathfrak{Q}}\hat{H}(\eta)\hat{\mathfrak{Q}}]^{-1}\,\hat{\mathfrak{Q}}\hat{H}(\eta)\hat{\mathfrak{P}} \tag{3.28b}$$

for the *exact* eigenvalues $E_j(\eta)$ of the states $|\Psi_j(\eta))$, $j = 1, \ldots, n$. The wave functions $\hat{\mathfrak{P}}|\Psi_j(\eta))$ are assumed to be neither orthogonal nor normalized. Equation (3.28) is no simplification but a convenient reformulation of the original problem (3.21).

#### The Wave Function

The perturbation expansion of the wave function can be obtained using

$$|\Psi_j(\eta)) = \hat{\mathfrak{P}}|\Psi_j(\eta)) + \hat{\mathfrak{Q}}|\Psi_j(\eta))\,.$$

Inserting equation (3.27) yields

$$|\Psi_j(\eta)) = \hat{\mathfrak{P}}|\Psi_j(\eta)) + [E_j(\eta)\,\hat{\mathbb{1}} - \hat{\mathfrak{Q}}\hat{H}(\eta)\hat{\mathfrak{Q}}]^{-1}\,\hat{\mathfrak{Q}}\hat{H}(\eta)\hat{\mathfrak{P}}\,|\Psi_j(\eta))\,. \tag{3.29}$$

This is an expansion of the $j$-th state $|\Psi_j(\eta))$ in terms of its projection onto the reference space $\hat{\mathfrak{P}}|\Psi_j(\eta))$ and corrections to the projected state in the complement space that derive from $\hat{\mathfrak{P}}|\Psi_j(\eta))$.

### 3.3.2. The Expansion in a Series

#### Diagonalization of the Hamiltonian in the Reference space

The matrix representation of the Hamiltonian in the reference space $\mathfrak{P}\boldsymbol{H}(\eta)\mathfrak{P}$ in (3.26) can be diagonalized to decouple the reference configurations, to improve the single reference approximation and to remove degeneracies. The diagonalization of $\mathfrak{P}\boldsymbol{H}(\eta)\mathfrak{P}$ is similar to the projection method discussed in subsection 2.3.2. The intent of this section is to go beyond the simple projection method and to account for the neglected configurations with the help of perturbation theory.

[3] If a state couples strongly to a reference state it is essential for the description of the perturbed state and is put in the reference space.

The diagonalization of $\mathfrak{P}\boldsymbol{H}(\eta)\mathfrak{P}$ means a change to the new, orthonormal, basis[4]

$$|\varphi_j(\eta)) := \begin{cases} \sum_{k=1}^{n} Q_{kj}\,|\Phi_k) & ;\, j \in \{1,\ldots,n\} \\ |\Phi_j) & ;\, j \in \{n+1,\ldots,K\} \end{cases} . \tag{3.30}$$

The new basis coincides with the old outside the reference space. Changing the basis in equation (3.28a) gives

$$\begin{aligned} & E_j(\eta) \sum_{k,l,p=1}^{n} (\Psi_i(\eta)|\varphi_k(\eta))\,(\varphi_k(\eta)|\Phi_p)\,(\Phi_p|\varphi_l(\eta))\,(\varphi_l(\eta)|\Psi_j(\eta)) \qquad (3.31) \\ = & \sum_{k,l,p,q=1}^{n} (\Psi_i(\eta)|\varphi_k(\eta))\,(\varphi_k(\eta)|\Phi_p)\,(\Phi_p|\hat{H}_{\text{eff}}(\eta)|\Phi_q)\,(\Phi_q|\varphi_l(\eta))\,(\varphi_l(\eta)|\Psi_j(\eta)) . \end{aligned}$$

This equation describes a general change of basis. To diagonalize $\mathfrak{P}\boldsymbol{H}(\eta)\mathfrak{P}$ in (3.26) one has to choose a suitable $Q_{pq} := (\Phi_p|\varphi_q(\eta))$, $p,q = 1,\ldots,n$, in other words, one has to solve the *complex symmetric eigenvalue problem*

$$\boldsymbol{Q}^{\mathrm{T}}\mathfrak{P}\boldsymbol{H}(\eta)\mathfrak{P}\boldsymbol{Q} = \mathbf{diag}(E_1^{(0)}(\eta),\ldots,E_n^{(0)}(\eta)) =: \boldsymbol{E}^{(0)}(\eta) .$$

This eigenvalue problem is not *a priori* soluble, in contrast to the real symmetric problem [10, 11]. If it is soluble then this can be achieved by a *complex orthogonal transformation* $\boldsymbol{Q}$, obeying $\boldsymbol{Q}\boldsymbol{Q}^{\mathrm{T}} = \boldsymbol{Q}^{\mathrm{T}}\boldsymbol{Q} = \mathbb{1}$.

The effective eigenvalue problem (3.31) reads in matrix notation, with (3.28b)

$$\begin{aligned} E_j(\eta)\,\vec{\Psi}_i{}^{\mathrm{T}}(\eta)\vec{\Psi}_j(\eta) &= \vec{\Psi}_i{}^{\mathrm{T}}(\eta)\,\boldsymbol{H}_{\text{eff}}(\eta)\,\vec{\Psi}_j(\eta) \\ \boldsymbol{H}_{\text{eff}}(\eta) &= \boldsymbol{E}^{(0)}(\eta) + \boldsymbol{Q}^{\mathrm{T}}\,\mathfrak{P}\boldsymbol{H}(\eta)\mathfrak{Q}\,\boldsymbol{G}(\eta)\,\mathfrak{Q}\boldsymbol{H}(\eta)\mathfrak{P}\,\boldsymbol{Q} \end{aligned} \tag{3.32}$$

setting $(\vec{\Psi}_j(\eta))_k := (\varphi_k(\eta)|\Psi_j(\eta))$ and $(H_{\text{eff}})_{kl} := (\varphi_k(\eta)|\hat{H}_{\text{eff}}(\eta)|\varphi_l(\eta))$ for $k,l = 1,\ldots,n$.

The change of basis becomes more obvious if its effect on the full Hamiltonian matrix (3.26) is analyzed. The transformation reads

$$\check{\boldsymbol{H}}(\eta) := \check{\boldsymbol{Q}}^{\mathrm{T}}\boldsymbol{H}(\eta)\check{\boldsymbol{Q}}, \qquad \check{\boldsymbol{Q}} := \left(\begin{array}{c|c} \boldsymbol{Q} & \boldsymbol{0} \\ \hline \boldsymbol{0} & \mathbb{1} \end{array}\right) \tag{3.33}$$

which yields

$$\check{\boldsymbol{H}}(\eta) = \left(\begin{array}{c|c} \boldsymbol{E}^{(0)}(\eta) & \boldsymbol{Q}^{\mathrm{T}}\,\mathfrak{P}\boldsymbol{H}(\eta)\mathfrak{Q} \\ \hline \mathfrak{Q}\boldsymbol{H}(\eta)\mathfrak{P}\,\boldsymbol{Q} & \mathfrak{Q}\boldsymbol{H}(\eta)\mathfrak{Q} \end{array}\right) . \tag{3.34}$$

[4] The normalization of the basis functions of the diagonalized matrix representation of the Hamiltonian in the reference space is *intermediate normalization* (see equation (3.53)) which is applied frequently in perturbation theory [42, 55].

### The Expansion in a Series

To be able to apply perturbation theory the Hamiltonian matrix (3.34) is decomposed in a diagonal and an off-diagonal part. This is the so-called Epstein-Nesbet partition [55,57,58]

$$\check{\boldsymbol{H}}(\eta) = \boldsymbol{H}_{\mathrm{D}}(\eta) + \lambda\, \boldsymbol{H}_{\mathrm{N}}(\eta)$$

setting

$$\boldsymbol{H}_{\mathrm{D}}(\eta) := \mathbf{diag}(\check{\boldsymbol{H}}(\eta)), \qquad \boldsymbol{H}_{\mathrm{N}}(\eta) := \left(\begin{array}{cccc|cccc} 0 & 0 & \cdots & 0 & * & * & \cdots & * \\ 0 & \ddots & \ddots & \vdots & * & \ddots & \ddots & \vdots \\ \vdots & \ddots & \ddots & 0 & \vdots & \ddots & \ddots & * \\ 0 & \cdots & 0 & 0 & * & \cdots & * & * \\ \hline * & * & \cdots & * & 0 & * & \cdots & * \\ * & \ddots & \ddots & \vdots & * & \ddots & \ddots & \vdots \\ \vdots & \ddots & \ddots & * & \vdots & \ddots & \ddots & * \\ * & \cdots & * & * & * & \cdots & * & 0 \end{array}\right). \tag{3.35}$$

Examining the matrix (3.34) in the light of (3.35), one sees that the effective eigenvalue problem (3.32) acquires the form

$$E_j(\eta)\, \vec{\Psi}_i{}^{\mathrm{T}}(\eta)\vec{\Psi}_j(\eta) = \vec{\Psi}_i{}^{\mathrm{T}}(\eta)\, \boldsymbol{H}_{\mathrm{eff}}(\eta)\, \vec{\Psi}_j(\eta) \tag{3.36a}$$

$$\boldsymbol{H}_{\mathrm{eff}}(\eta) = \boldsymbol{E}^{(0)}(\eta) + \lambda^2\, \boldsymbol{Q}^{\mathrm{T}}\, \mathfrak{P}\boldsymbol{H}(\eta)\mathfrak{Q}\, \boldsymbol{G}(\eta)\, \mathfrak{Q}\boldsymbol{H}(\eta)\mathfrak{P}\, \boldsymbol{Q} \tag{3.36b}$$

in the basis set (3.30).

Setting $\boldsymbol{H}_{\mathrm{D}}^{\mathfrak{Q}\mathfrak{Q}}(\eta) := (\mathfrak{Q}\boldsymbol{H}(\eta)\mathfrak{Q})_{\mathrm{diagonal}}$ and $\boldsymbol{H}_{\mathrm{N}}^{\mathfrak{Q}\mathfrak{Q}}(\eta) := (\mathfrak{Q}\boldsymbol{H}(\eta)\mathfrak{Q})_{\mathrm{off-diagonal}}$ to define

$$\boldsymbol{G}(\eta) = [E_j(\eta)\, \mathbb{1} - \boldsymbol{H}_{\mathrm{D}}^{\mathfrak{Q}\mathfrak{Q}}(\eta) - \lambda \boldsymbol{H}_{\mathrm{N}}^{\mathfrak{Q}\mathfrak{Q}}(\eta)]^{-1}, \tag{3.37}$$

$\boldsymbol{G}(\eta)$ is a $(K-n)\times(K-n)$ matrix. Inserting $E_j^{(0)}(\eta) - E_j^{(0)}(\eta) = 0$ in equation (3.37) results in

$$\boldsymbol{G}(\eta) = [\boldsymbol{\chi}(\eta)^{-1}\, (\mathbb{1} + \boldsymbol{\chi}(\eta)\, ((E_j(\eta) - E_j^{(0)}(\eta))\, \mathbb{1} - \lambda\, \boldsymbol{H}_{\mathrm{N}}^{\mathfrak{Q}\mathfrak{Q}}(\eta)))]^{-1}, \tag{3.38}$$

upon setting $\boldsymbol{\chi}(\eta) := [E_j^{(0)}(\eta)\, \mathbb{1} - \boldsymbol{H}_{\mathrm{D}}^{\mathfrak{Q}\mathfrak{Q}}(\eta)]^{-1}$. Provided that $\|\boldsymbol{\chi}(\eta)\, ((E_j(\eta) - E_j^{(0)}(\eta))\, \mathbb{1} - \lambda\, \boldsymbol{H}_{\mathrm{N}}^{\mathfrak{Q}\mathfrak{Q}}(\eta))\| < 1$ holds one can expand (3.38) in a geometric series (Lemma 2.3.3 in [61] which also holds for complex matrices)

$$\boldsymbol{G}(\eta) = \Big[\sum_{k=0}^{\infty}(-1)^k\, (\boldsymbol{\chi}(\eta)\, ((E_j(\eta) - E_j^{(0)}(\eta))\, \mathbb{1} - \lambda\, \boldsymbol{H}_{\mathrm{N}}^{\mathfrak{Q}\mathfrak{Q}}(\eta)))^k\Big]\, \boldsymbol{\chi}(\eta)\,. \tag{3.39}$$

One sees that the convergence of the perturbation series of the resonance energy that results from (3.36) follows from the convergence of the series of the Green's function (3.39).

### 3.3.3. Approximation of the Eigenvalues

#### Truncation of the Series

With

$$E_j(\eta) = E_j^{(0)}(\eta) + \lambda\, E_j^{(1)}(\eta) + \lambda^2\, E_j^{(2)}(\eta) + \lambda^3\, E_j^{(3)}(\eta) + \lambda^4\, E_j^{(4)}(\eta) + O(\lambda^5) \tag{3.40}$$

the expansion of (3.39)

$$\boldsymbol{G}(\eta) = \boldsymbol{G}^{(0)}(\eta) + \lambda\, \boldsymbol{G}^{(1)}(\eta) + \lambda^2\, \boldsymbol{G}^{(2)}(\eta) + O(\lambda^3) \tag{3.41}$$

can be done yielding

$$\begin{aligned}
\boldsymbol{G}^{(0)}(\eta) &= \boldsymbol{\chi}(\eta) \\
\boldsymbol{G}^{(1)}(\eta) &= -E_j^{(1)}(\eta)\, \boldsymbol{\chi}(\eta)^2 + \boldsymbol{\chi}(\eta)\, \boldsymbol{H}_{\mathrm{N}}^{\Omega\Omega}(\eta)\, \boldsymbol{\chi}(\eta) \\
\boldsymbol{G}^{(2)}(\eta) &= -E_j^{(2)}(\eta)\, \boldsymbol{\chi}(\eta)^2 + E_j^{(1)}(\eta)^2\, \boldsymbol{\chi}(\eta)^3 \\
&\quad - E_j^{(1)}(\eta)\, \boldsymbol{\chi}(\eta)^2 \boldsymbol{H}_{\mathrm{N}}^{\Omega\Omega}(\eta)\, \boldsymbol{\chi}(\eta) \\
&\quad - E_j^{(1)}(\eta)\, \boldsymbol{\chi}(\eta)\, \boldsymbol{H}_{\mathrm{N}}^{\Omega\Omega}(\eta)\, \boldsymbol{\chi}(\eta)^2 \\
&\quad + \boldsymbol{\chi}(\eta)\, \boldsymbol{H}_{\mathrm{N}}^{\Omega\Omega}(\eta)\, \boldsymbol{\chi}(\eta)\, \boldsymbol{H}_{\mathrm{N}}^{\Omega\Omega}(\eta)\, \boldsymbol{\chi}(\eta)
\end{aligned} \tag{3.42}$$

after expanding the geometric series (3.39) up to $k = 2$ and sorting for orders in $\lambda$.

With the help of (3.36b), the perturbation series for $\boldsymbol{G}(\eta)$ leads to a perturbation series of the effective Hamiltonian

$$\boldsymbol{H}_{\mathrm{eff}}(\eta) = \boldsymbol{H}_{\mathrm{eff}}^{(0)}(\eta) + \lambda\, \boldsymbol{H}_{\mathrm{eff}}^{(1)}(\eta) + \lambda^2\, \boldsymbol{H}_{\mathrm{eff}}^{(2)}(\eta) + \lambda^3\, \boldsymbol{H}_{\mathrm{eff}}^{(3)}(\eta) + \lambda^4\, \boldsymbol{H}_{\mathrm{eff}}^{(4)}(\eta) + O(\lambda^5)\ . \tag{3.43}$$

Inspecting (3.36b), one sets $\boldsymbol{H}_{\mathrm{eff}}^{(0)}(\eta) := \boldsymbol{E}^{(0)}(\eta)$. If $\mathfrak{P}\boldsymbol{H}(\eta)\mathfrak{P}$ was not diagonalized then $\boldsymbol{H}_{\mathrm{eff}}^{(1)}(\eta)$ would become the off-diagonal part of $\mathfrak{P}\boldsymbol{H}(\eta)\mathfrak{P}$ due to the partition (3.35), therefore, $\boldsymbol{H}_{\mathrm{eff}}^{(1)}(\eta) := \boldsymbol{0}$.

The effective eigenvalue problem (3.36) can be solved by expanding the exact wave function $\vec{\Psi}_j(\eta)$ in a series

$$\vec{\Psi}_j(\eta) = \vec{\Psi}_j^{(0)}(\eta) + \lambda\, \vec{\Psi}_j^{(1)}(\eta) + \lambda^2\, \vec{\Psi}_j^{(2)}(\eta) + \lambda^3\, \vec{\Psi}_j^{(3)}(\eta) + \lambda^4\, \vec{\Psi}_j^{(4)}(\eta) + O(\lambda^5)\ . \tag{3.44}$$

Inspecting (3.36a), one sets $(\vec{\Psi}_j^{(0)}(\eta))_k := (\varphi_k(\eta)|\varphi_j(\eta)) = \delta_{kj}$ for $k = 1, \ldots, n$.

A series expansion for the energy is obtained by inserting (3.40), (3.43), (3.44) into

$$\boldsymbol{H}_{\mathrm{eff}}(\eta)\, \vec{\Psi}_j(\eta) = E_j(\eta)\, \vec{\Psi}_j(\eta)\ .$$

which derives from (3.36a). This yields

$$\begin{aligned}
&\boldsymbol{H}_{\mathrm{eff}}^{(0)}(\eta)\, \vec{\Psi}_j^{(0)}(\eta) + \lambda\, \boldsymbol{H}_{\mathrm{eff}}^{(0)}(\eta)\, \vec{\Psi}_j^{(1)}(\eta) \\
&+ \lambda^2\, [\boldsymbol{H}_{\mathrm{eff}}^{(0)}(\eta)\, \vec{\Psi}_j^{(2)}(\eta) + \boldsymbol{H}_{\mathrm{eff}}^{(1)}(\eta)\, \vec{\Psi}_j^{(1)}(\eta) + \boldsymbol{H}_{\mathrm{eff}}^{(2)}(\eta)\, \vec{\Psi}_j^{(0)}(\eta)] \\
&+ \lambda^3\, [\boldsymbol{H}_{\mathrm{eff}}^{(0)}(\eta)\, \vec{\Psi}_j^{(3)}(\eta) + \boldsymbol{H}_{\mathrm{eff}}^{(1)}(\eta)\, \vec{\Psi}_j^{(2)}(\eta) + \boldsymbol{H}_{\mathrm{eff}}^{(2)}(\eta)\, \vec{\Psi}_j^{(1)}(\eta) + \boldsymbol{H}_{\mathrm{eff}}^{(3)}(\eta)\, \vec{\Psi}_j^{(0)}(\eta)]
\end{aligned}$$

$$
\begin{aligned}
&+ \lambda^4 \left[ \boldsymbol{H}_{\text{eff}}^{(0)}(\eta)\, \vec{\Psi}_j^{(4)}(\eta) + \boldsymbol{H}_{\text{eff}}^{(1)}(\eta)\, \vec{\Psi}_j^{(3)}(\eta) + \boldsymbol{H}_{\text{eff}}^{(2)}(\eta)\, \vec{\Psi}_j^{(2)}(\eta) \right. \\
&\qquad \left. + \boldsymbol{H}_{\text{eff}}^{(3)}(\eta)\, \vec{\Psi}_j^{(1)}(\eta) + \boldsymbol{H}_{\text{eff}}^{(4)}(\eta)\, \vec{\Psi}_j^{(0)}(\eta) \right] \qquad (3.45) \\
= \;& E_j^{(0)}(\eta)\, \vec{\Psi}_j^{(0)}(\eta) + \lambda \left[ E_j^{(1)}(\eta)\, \vec{\Psi}_j^{(0)}(\eta) + E_j^{(0)}(\eta)\, \vec{\Psi}_j^{(1)}(\eta) \right] \\
&+ \lambda^2 \left[ E_j^{(0)}(\eta)\, \vec{\Psi}_j^{(2)}(\eta) + E_j^{(1)}(\eta)\, \vec{\Psi}_j^{(1)}(\eta) + E_j^{(2)}(\eta)\, \vec{\Psi}_j^{(0)}(\eta) \right] \\
&+ \lambda^3 \left[ E_j^{(0)}(\eta)\, \vec{\Psi}_j^{(3)}(\eta) + E_j^{(1)}(\eta)\, \vec{\Psi}_j^{(2)}(\eta) + E_j^{(2)}(\eta)\, \vec{\Psi}_j^{(1)}(\eta) + E_j^{(3)}(\eta)\, \vec{\Psi}_j^{(0)}(\eta) \right] \\
&+ \lambda^4 \left[ E_j^{(0)}(\eta)\, \vec{\Psi}_j^{(4)}(\eta) + E_j^{(1)}(\eta)\, \vec{\Psi}_j^{(3)}(\eta) + E_j^{(2)}(\eta)\, \vec{\Psi}_j^{(2)}(\eta) \right. \\
&\qquad \left. + E_j^{(3)}(\eta)\, \vec{\Psi}_j^{(1)}(\eta) + E_j^{(4)}(\eta)\, \vec{\Psi}_j^{(0)}(\eta) \right] .
\end{aligned}
$$

Multiplying from left with $\vec{\Psi}_j^{(0)\mathrm{T}}(\eta)$ yields

$$
E_j^{(k)}(\eta) = \vec{\Psi}_j^{(0)\mathrm{T}}(\eta) \boldsymbol{H}_{\text{eff}}^{(k)}(\eta)\, \vec{\Psi}_j^{(0)}(\eta) \qquad \text{for } k = 0, 2, 3 \qquad (3.46)
$$

due to

$$
\vec{\Psi}_j^{(0)\mathrm{T}}(\eta) \vec{\Psi}_j^{(1)}(\eta) = \vec{\Psi}_j^{(0)\mathrm{T}}(\eta) \vec{\Psi}_j^{(2)}(\eta) = \ldots = 0 \; .
$$

$E_j^{(1)}(\eta)$ and $\vec{\Psi}_j^{(1)}(\eta)$ vanish. The fourth order correction to the energy can be obtained by multiplying (3.45) from left with $\vec{\Psi}_j^{(0)\mathrm{T}}(\eta)$

$$
E_j^{(4)}(\eta) = \vec{\Psi}_j^{(0)\mathrm{T}}(\eta) \boldsymbol{H}_{\text{eff}}^{(2)}(\eta)\, \vec{\Psi}_j^{(2)}(\eta) + \vec{\Psi}_j^{(0)\mathrm{T}}(\eta) \boldsymbol{H}_{\text{eff}}^{(4)}(\eta)\, \vec{\Psi}_j^{(0)}(\eta) \; . \qquad (3.47)
$$

The second order correction to the wave function $\vec{\Psi}_j^{(2)}(\eta)$ is needed in (3.47). It is determined with the help of

$$
\vec{\Psi}_j^{(2)}(\eta) = \sum_{\substack{k=1 \\ k \neq j}}^{n} \vec{\Psi}_k^{(0)\mathrm{T}}(\eta) \vec{\Psi}_j^{(2)}(\eta)\; \vec{\Psi}_k^{(0)}(\eta) \qquad (3.48)
$$

because the reference space is, trivially, complete.

The expansion coefficients $\vec{\Psi}_k^{(0)\mathrm{T}}(\eta) \vec{\Psi}_j^{(2)}(\eta)$ are obtained from (3.49) by multiplying the second order equation from left with $\vec{\Psi}_k^{(0)\mathrm{T}}(\eta)$

$$
\begin{aligned}
&\vec{\Psi}_k^{(0)\mathrm{T}}(\eta) \boldsymbol{H}_{\text{eff}}^{(0)}(\eta)\, \vec{\Psi}_j^{(2)}(\eta) + \vec{\Psi}_k^{(0)\mathrm{T}}(\eta) \boldsymbol{H}_{\text{eff}}^{(2)}(\eta)\, \vec{\Psi}_j^{(0)}(\eta) \\
= \;& E_j^{(0)}(\eta)\, \vec{\Psi}_k^{(0)\mathrm{T}}(\eta) \vec{\Psi}_j^{(2)}(\eta) + E_j^{(2)}(\eta)\, \vec{\Psi}_k^{(0)\mathrm{T}}(\eta) \vec{\Psi}_j^{(0)}(\eta)
\end{aligned} \; . \qquad (3.49)
$$

The last term in (3.49) vanishes due to $k \neq j$. The second order correction to the wave function reads with the help of (3.48), (3.49), (3.46)

$$
\vec{\Psi}_j^{(2)}(\eta) = \sum_{\substack{k=1 \\ k \neq j}}^{n} \frac{\vec{\Psi}_k^{(0)\mathrm{T}}(\eta) \boldsymbol{H}_{\text{eff}}^{(2)}(\eta)\, \vec{\Psi}_j^{(0)}(\eta)}{E_j^{(0)}(\eta) - E_k^{(0)}(\eta)}\; \vec{\Psi}_k^{(0)}(\eta) \qquad (3.50)
$$

The energy corrections, up to fourth order, can be written in terms of the matrix elements (3.34) by inserting the definitions of the projection operators (3.23). The final

equation reads

$$
\begin{aligned}
E_j(\eta) \;=\; & E_j^{(0)}(\eta) + \lambda^2 \sum_{k=n+1}^{K} \frac{\check{H}_{jk}^2}{E_j^{(0)}(\eta) - \check{H}_{kk}} \\
& + \lambda^3 \sum_{\substack{k,l=n+1 \\ k\neq l}}^{K} \frac{\check{H}_{jk}\,\check{H}_{kl}\,\check{H}_{lj}}{(E_j^{(0)}(\eta) - \check{H}_{kk})\,(E_j^{(0)}(\eta) - \check{H}_{ll})} \\
& + \lambda^4 \Bigg[ \sum_{\substack{k=1 \\ k\neq j}}^{n} \sum_{l=n+1}^{K} \frac{\check{H}_{kl}^2\,\check{H}_{lj}^2}{(E_j^{(0)}(\eta) - E_k^{(0)}(\eta))\,(E_j^{(0)}(\eta) - \check{H}_{ll})^2} \\
& \quad + \sum_{\substack{k,l,m=n+1 \\ k,m\neq l}}^{K} \frac{\check{H}_{jk}\,\check{H}_{kl}\,\check{H}_{lm}\,\check{H}_{mj}}{(E_j^{(0)}(\eta) - \check{H}_{kk})\,(E_j^{(0)}(\eta) - \check{H}_{ll})\,(E_j^{(0)}(\eta) - \check{H}_{mm})} \\
& \quad - E_j^{(2)}(\eta) \sum_{k=n+1}^{K} \frac{\check{H}_{jk}\,\check{H}_{kj}}{(E_j^{(0)}(\eta) - \check{H}_{kk})^2} \Bigg] + O(\lambda^5)\;.
\end{aligned}
\tag{3.51}
$$

For notational brevity, the $\eta$ dependence is not explicitly stated for the matrix elements of the Hamiltonian (3.34).

Let us have a closer look at (3.51). The zeroth order energy $E_j^{(0)}(\eta)$ is the energy obtained by diagonalizing the matrix representation of the Hamiltonian in the reference space. The first order correction vanishes due to $\lambda^2$ in equation (3.36) which originates from the partition (3.35). The second and higher order corrections represent the effect of the configurations in the complement space. In fourth order, corrections within the reference space are also needed.

Chen *et al.* have independently derived a formally similar theory in [55] (equation (25)) using a direct Taylor series expansion of the secular equation for the energy of bound states of a molecular system. They explicitly state the perturbation expansion for the real energy up to third order. Chen *et al.* further observe that this kind of multireference approach reduces to single reference Epstein-Nesbet perturbation theory if only one reference is used. The non-Hermitian multireference perturbation theory of this section also reduces to the non-Hermitian single reference theory as can be seen by comparing (3.53) with (3.14), noticing that the first order correction (3.14b) vanishes.

### The Wave Function

A perturbation expansion of the wave function $\vec{\Psi}_j(\eta)$ can be obtained from (3.29). This equation reads

$$
\vec{\Psi}_j(\eta) = \boldsymbol{\mathfrak{P}}\,\vec{\Psi}_j(\eta) + \lambda\,\boldsymbol{G}(\eta)\,\boldsymbol{\mathfrak{Q}}\boldsymbol{H}(\eta)\boldsymbol{\mathfrak{P}}\,\boldsymbol{Q}\,\vec{\Psi}_j(\eta) \tag{3.52}
$$

using the partition (3.35). Inserting (3.41), (3.42) and (3.50) into (3.52) yields

$$\begin{aligned}\vec{\Psi}_j(\eta) &= \vec{\Psi}_j^{(0)}(\eta) + \lambda \sum_{k=n+1}^{K} \frac{\check{H}_{kj}}{E_j^{(0)}(\eta) - \check{H}_{kk}}\, \vec{\Psi}_k^{(0)}(\eta) \\ &\quad + \lambda^2 \Bigg[ \sum_{\substack{k=1 \\ k\neq j}}^{n} \sum_{l=n+1}^{K} \frac{\check{H}_{kl}\,\check{H}_{lj}}{(E_j^{(0)}(\eta) - E_k^{(0)}(\eta))\,(E_j^{(0)}(\eta) - \check{H}_{ll})}\, \vec{\Psi}_k^{(0)}(\eta) \\ &\qquad + \sum_{\substack{k,l=n+1 \\ k\neq l}}^{K} \frac{\check{H}_{kl}\,\check{H}_{lj}}{(E_j^{(0)}(\eta) - \check{H}_{kk})\,(E_j^{(0)}(\eta) - \check{H}_{ll})}\, \vec{\Psi}_k^{(0)}(\eta) \Bigg] \\ &\quad + O(\lambda^3)\,. \end{aligned} \tag{3.53}$$

Again the $\eta$ dependence is not explicitly stated for the matrix elements of the Hamiltonian. The corrections to the wave function (3.53) are not explicitly given in [55].

There are two sorts of corrections to $\vec{\Psi}_j^{(0)}(\eta)$. Firstly, there are corrections to the wave function in the reference space. These corrections account for the fact that $\mathfrak{P}\vec{\Psi}_j^{(0)}(\eta)$ is not equal to $\mathfrak{P}\vec{\Psi}_j(\eta)$. Secondly, there are corrections to $\vec{\Psi}_j^{(0)}(\eta)$ which occur solely in the complement space and consequently do not change the projection onto the reference space. Nevertheless, these corrections are essential for the energy corrections of the second and higher order, see (3.36b).

# 4. Application of Non-Hermitian Multireference Perturbation Theory

## 4.1. The Model Problem

### 4.1.1. The Setting

A model problem is introduced in this section which serves to illustrate the multireference perturbation theory, derived in section 3.3. See section 3.1 of [10, 11] for more details concerning the model. The $s$-wave scattering of electrons at the spherically symmetric one-particle potential (figure 4.1)

$$\hat{V}(r) = \begin{cases} -V_0 & ; 0 \leq r < a \\ V_0 & ; a \leq r < 2a \\ 0 & ; r \geq 2a \end{cases}$$

is studied.

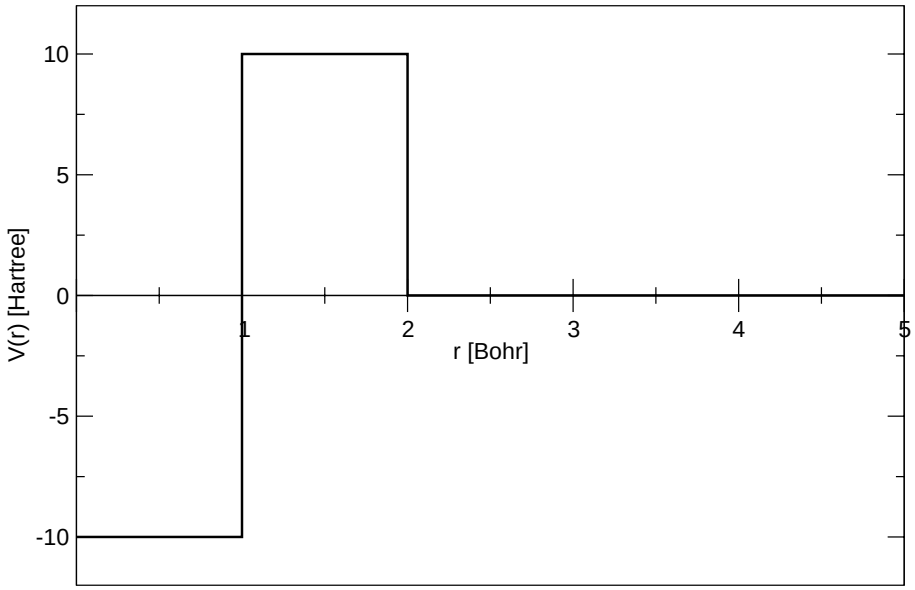


**Figure 4.1.:** The radial part of a spherically symmetric one-particle potential for testing the non-Hermitian multireference perturbation theory of section 3.3.

The solution of the scattering problem is essentially given by the radial part of the

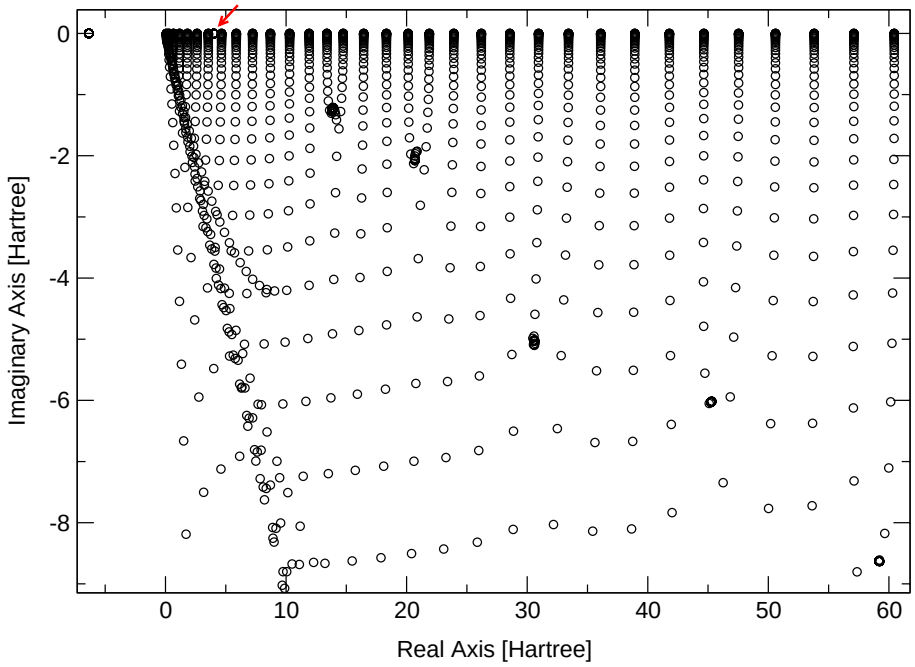


**Figure 4.2.:** (Color) Complex spectra of the CAP-Hamiltonian (4.3) for a range of values for $\eta$. The red arrow points at the $\eta$-trajectory of the first resonance state. The matrix representation of the CAP-Hamiltonian is diagonalized fully for $\eta = 0, \ldots, 72.6850$ (70 iterations: $\eta_{i+1} = 1.2\,\eta_i + 0.00005,\ \eta_1 = 0$).

wave function which can be obtained using the one-dimensional Hamiltonian [10, 11]

$$\hat{H}(r) = -\frac{1}{2}\left(\frac{\partial^2}{\partial r^2} + \frac{2}{r}\frac{\partial}{\partial r}\right) + \hat{V}(r), \tag{4.1}$$

because the case of $s$-wave scattering implies $Y_{00}(\vartheta, \varphi) = 1$ [10, 11]. There exists a quasi-analytic solution, giving $-6.353803650$ Hartree for the only bound state and $4.001414397 - 0.003616371\,\mathrm{i}$ Hartree for the first resonance, assuming $V_0 = 10$ Hartree, $a = 1$ Bohr.

The energy of the first resonance is calculated using the CAP-method of section 2.3, employing the *CAP-operator*

$$\hat{W}(r) := \begin{cases} (r-c)^2 & ;\, r \geq c \\ 0 & ;\, 0 \leq r < c \end{cases} . \tag{4.2}$$

The parameter $c$ determines a sphere around the origin ($r = 0$) where the CAP does not absorb the wave function. If $c$ is too large, with respect to a chosen finite basis set, the basis is not suited to represent the wave function.

Conversely, if $c$ is too small the damping of the wave function is too large and the result is not satisfactory. $c = 2a = 2$ Bohr is a good choice [10, 11] to calculate the Siegert energy (1.1) of the first resonance of the model problem. The CAP-Hamiltonian of the model problem is given by (2.11), (4.1), (4.2)

$$\hat{H}(\eta) = \hat{H} - \mathrm{i}\,\eta\,\hat{W} . \tag{4.3}$$

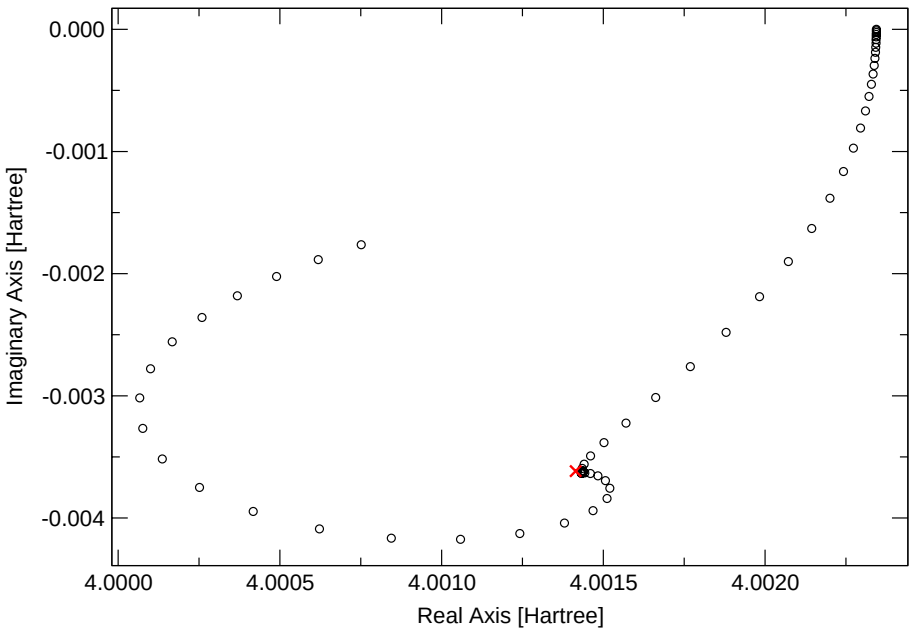


**Figure 4.3.:** (Color) The $\eta$-trajectory of the first resonance of the model problem. The red cross represents the exact Siegert energy of the first resonance. Magnification of figure 4.2 by 2000.

The matrix representation of this equations is constructed using a basis of particle-in-a-box functions ($k = 1, \ldots, N$)

$$\phi_k(r) = \begin{cases} \sqrt{\frac{2}{L}} \sin\left(\frac{k\pi r}{L}\right) & ; 0 \leq r < L \\ 0 & ; r \geq L \end{cases} . \tag{4.4}$$

The spatial extension $L = 10\,\text{Bohr}$ is assumed throughout. $L$ is sufficiently large because the CAP starts to absorb at $c = 2\,\text{Bohr}$.

### 4.1.2. Full Diagonalization of the Matrix Representation of the CAP-Hamiltonian

The calculations of this section were performed using a FORTRAN 95 [62] program, written by Robin Santra. I reworked the code to include the perturbation theory of section 3.3. The implementation is similar to that described in section 4.2. The main difference is that all operations are carried out in main storage because the involved matrices are kept small.

In this subsection the program is used to study the full spectra of the matrix representation of the CAP-Hamiltonian. The program constructs the complex symmetric matrix representation of (4.3) with the help of the basis (4.4). Afterwards, it diagonalizes the matrix representation with the LAPACK routine `zgeev` [63] to obtain its complex eigenvalue spectrum, see section 2.3.2.

Several complex spectra are calculated in a range of values for $\eta$, starting with $\eta = 0$. Each bound, resonance or pseudocontinuum state of (4.3) is represented by an $\eta$-trajectory.

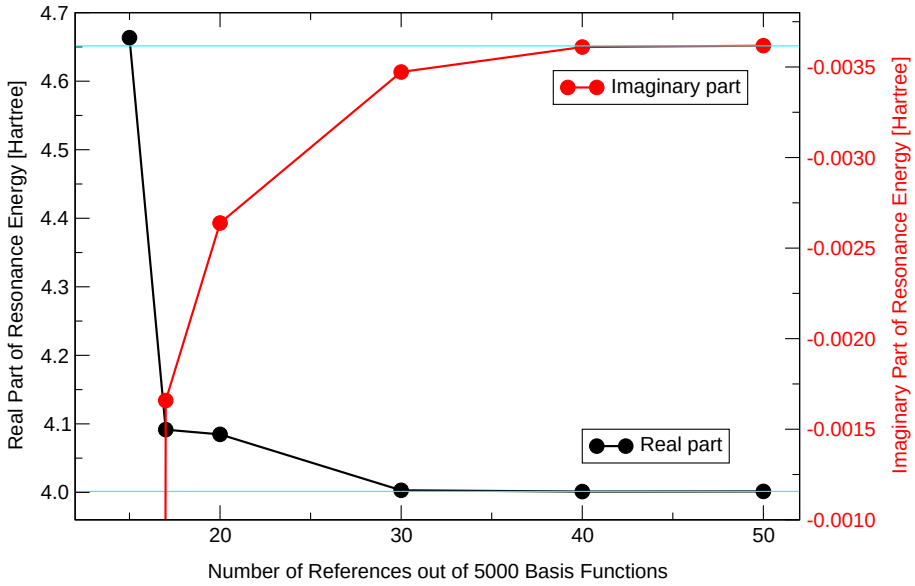


**Figure 4.4.:** (Color) The energy of the first resonance of the model problem for an increasing number of references. The resonance energy is obtained by applying non-Hermitian multireference perturbation theory, up to second order. The horizontal lines are the exact values for the real and the imaginary part of the energy of the first resonance.

Figure 4.2 shows an overview of many complex spectra of $\hat{H}(\eta)$ for varying CAP-strength $\eta$. At about $-6$ Hartree one can find the trajectory of the bound state clearly separated from all other trajectories.

At about 4 Hartree there is a "circle" between two quasi-continuum states, marked by the red arrow. This is not a single circle but the $\eta$-trajectory of the first resonance state of the model problem. The "circle" is shown, magnified by 2000, in figure 4.3. The stabilization point of the resonance is clearly visible. It is the point where the effect of the finite basis set and the effect due to the perturbation of the CAP-operator balance. According to [17] this is the Siegert energy (1.1) of the resonance. There are more resonance states visible in the spectrum 4.2. Their signature is a more or less extended blob of accumulated circles.

### 4.1.3. Advantages of Perturbation Theory

Comparing different methods fairly is *not* very easy and usually one does wrong to all due to the fact that one has to select a set of *observables* to compare the methods. As each algorithm produces its own set of observables, in most cases distinct from the sets produced by the others, the selection of a common subset neglects certain features unique to each algorithm. The common subset is usually optimized to the strengths of the "new" method.

The candidates to compare here are the multireference perturbation theory (MRPT) of section 3.3 versus the diagonalization of the CAP-Hamiltonian in the reference space only with respect to the accuracy of the energy eigenvalue of the first resonance state of

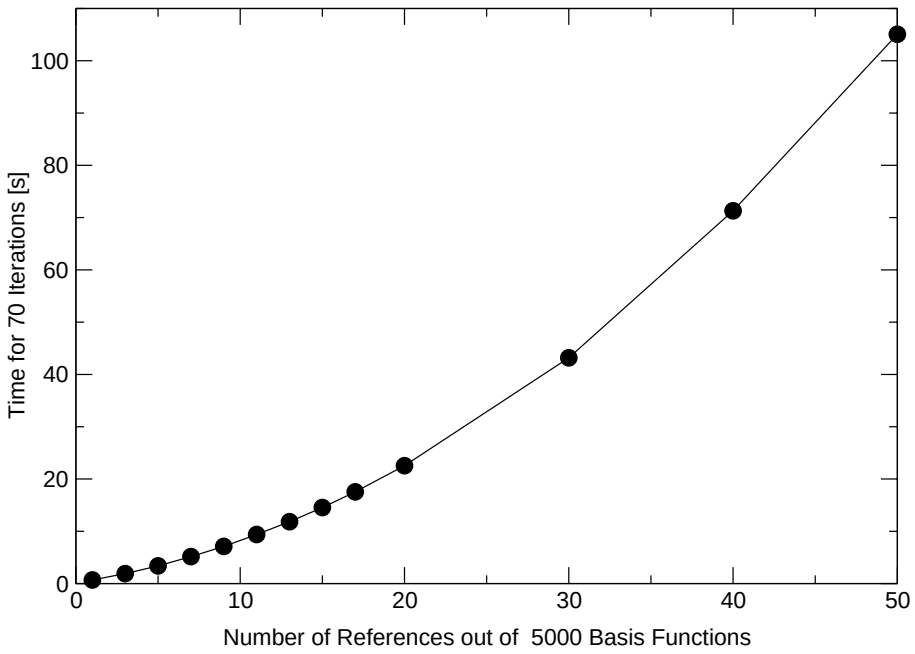


**Figure 4.5.:** Timing of non-Hermitian multireference perturbation theory for an increasing reference space. Each point corresponds to the time needed for 70 iterations with varying $\eta$. The time for the construction of the basis (see text) is not included.

the model problem.

The full diagonalization of the matrix representation is not considered to be a candidate for a comparison because it calculates the whole spectrum of $\hat{H}(\eta)$, in the matrix representation employed[1], usually containing the energies of many resonances. Perturbation theory and the diagonalization of the CAP-Hamiltonian in the reference space calculate only the energies of selected resonances.

Timing was done using a fixed basis set of 5000 functions, increasing the size of the reference space employed. The amount of time needed to apply the multireference perturbation theory to this problem is shown in figure 4.5 for an increasing number of references. The amount of time needed to carry out a full diagonalization is $\approx 20\,\mathrm{d}$.

This comparison of MRPT with full diagonalization is unfair because the latter yields the whole spectrum of the CAP-Hamiltonian matrix in the chosen basis but here one is only interested in the Siegert energy (1.1) of the first resonance. So the time needed for a selective calculation of this eigenvalue by the methods introduced in section 2.3.2 would be more appropriate to compare with MRPT. To implement these kinds of algorithms would have caused considerable work which is surely not sensible for such a simple model problem. Since the selective determination of eigenvalues involves matrix times vector products, they are slower than MRPT for large basis sets because the second order scheme of MRPT used here, only requires to evaluate the coupling blocks of the matrix.

Some remarks have to be made on the construction of the basis set used in the MRPT

[1] This is not necessarily a large section of the spectrum of $\hat{H}(\eta)$.

computations of this subsection. A matrix representation of the real Hamiltonian for a potential well depth of $V_0 = 20\,\text{Hartree}$, see figure 4.1, is formed using the basis (4.4). To construct an adapted basis to the problem the matrix representation is diagonalized. Then the matrices of the real and imaginary parts for $V_0 = 10\,\text{Hartree}$ are formed and projected onto the formerly calculated new basis set. This procedure mimics the diagonal dominance of CI-matrices. The sparsity of CI-matrices (2.10) cannot be achieved by this construction. The old and the new basis exhibit another drawback. The distortion of states with high energy by the model potential is small and the matrix of the real part is nearly diagonal in both basis sets for these states because particle-in-a-box functions (4.4) are then a very good approximation. This is not the case for CI-matrices.

The particle-in-a-box functions (4.4) are not good references because their overall shape differs a lot from the shape of the wave function of a resonance (figure 3.4 in [10,11]). Hence the overlap between a reference, of an energy close to the real part of the energy of a resonance, and the resonance itself is small and the description is insufficient. The diagonal dominance[2] of the matrix representation of the problem in the new basis assures the quality of the references. As this construction is very costly the amount of time used to calculate this basis set is subtracted from the total time needed to carry out the MRPT computations.

Figure 4.4 shows the convergence of the real and the imaginary part separately, for the first resonance with an increasing reference space. The horizontal lines denote the exact values of subsection 4.1.1. The real part converges slightly faster than the imaginary part due to the better adaption of the basis to the former. This should also be observed in the case of CI-matrices. The time needed to apply MRPT for 70 values for $\eta$ is shown in figure 4.5 for an increasing reference space.

A different way of looking at the convergence of MRPT is to keep the reference space size constant for an increasing size of the basis set but in practice one is more interested in increasing the reference space. In *multireference configuration interaction (MRCI)* programs the basis increases with the size of the reference space, too. This is not accounted for here.

To show the advantage of using perturbation theory, in contrast to takeing only the energy of the first resonance in the diagonalized reference space, is shown in figure 4.6 for a number of different reference space sizes. Obviously the results are less satisfactory compared to figure 4.4. Using 40 references, MRPT yields $-0.003610\,\text{i}$ for the imaginary part of the energy of the first resonance. In the reference space, the imaginary part is $-0.003474\,\text{i}$. Compared to the exact value $-0.003616371\,\text{i}$, MRPT yields more accurate results for a given reference space size than the simple diagonalization of the CAP-Hamiltonian in the reference space.

## 4.2. Configuration Interaction

The theory of section 3.3 can be used to study resonances in atoms, molecules or clusters using the configuration interaction method of section 2.2. The following paragraphs de-

[2]The matrix representation in the new basis is in fact not diagonally dominant due to a few diagonal elements which are small, in the presented calculations here.

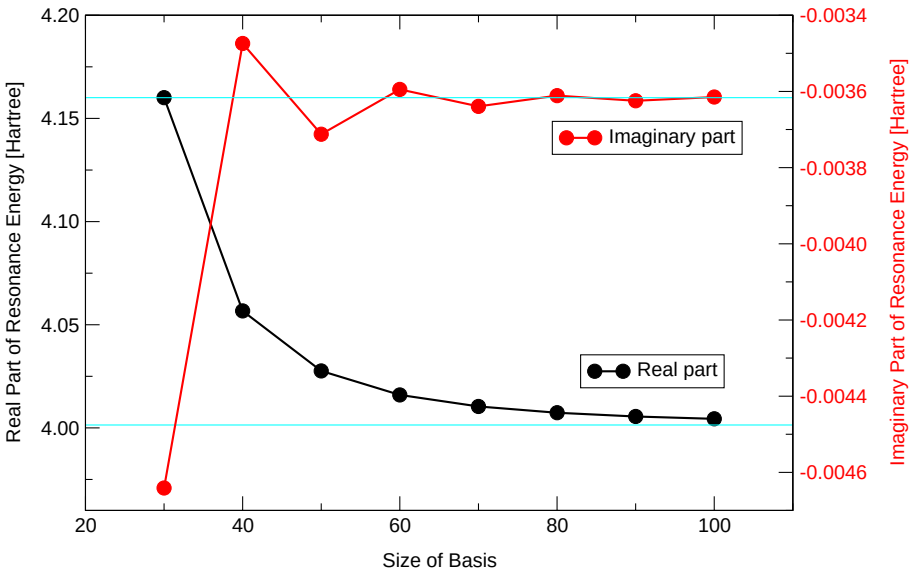


**Figure 4.6.:** (Color) The energy of the first resonance of the model problem in the reference space with an increasing number of references. The resonance energy is obtained by diagonalizing the reference space for varying $\eta$. The values differ from those in figure 4.4 by the perturbative corrections. The horizontal lines are the exact values for the real and the imaginary part of the energy of the first resonance.

scribe a computer program which implements MRPT for SDCI-matrices. In future, it is planed to use the program to study some electronic resonances in molecules.

The *ab initio* program package MOLCAS [15] is used to carry out the ground state Hartree-Fock calculation described in section 2.1. The matrix representation of the CAP-operator $\hat{W}$ in the SDCI basis is generated by a module which bases on the DIESEL MRCI package [64–66]. It is saved on mass storage. This matrix is not as large as the (SD)CI-matrix (2.10) because $\hat{W}$ is a one-particle operator. Hence only few matrix elements are non-zero.

Another module for DIESEL MRCI was written by me to carry out the perturbation theory. The program reads in the matrix representation of $\hat{W}$ and uses DIESEL'S matrix generator to calculate the diagonal, the reference space matrix $\mathfrak{P}\boldsymbol{H}\mathfrak{P}$ and the coupling block $\mathfrak{P}\boldsymbol{H}\mathfrak{Q}$ of the (real) SDCI-matrix. The coupling block is saved on mass storage. After this initialization phase the program commences.

For a set of values for $\eta$, MRPT is applied. For each $\eta$, the diagonal of $\boldsymbol{H}(\eta)$ is computed. Afterwards $\mathfrak{P}\boldsymbol{H}\mathfrak{P}$ is obtained and combined with $\mathfrak{P}\boldsymbol{W}\mathfrak{P}$ to give $\mathfrak{P}\boldsymbol{H}(\eta)\mathfrak{P}$ which is diagonalized using the LAPACK routine `zgeev` [63]. Now $\mathfrak{P}\boldsymbol{H}\mathfrak{Q}$ is read in column-wise and combined on the fly with a column of $\mathfrak{P}\boldsymbol{W}\mathfrak{Q}$ to give a column of $\mathfrak{P}\boldsymbol{H}(\eta)\mathfrak{Q}$. The column is then transformed according to (3.30) using the eigenvector matrix of the reference space. Now, the second order correction to the energy (3.51) can be calculated.

# Part II.

# Electronic Decay of Ionized Molecular Systems

# 5. Calculation of Ionization Spectra with Many-body Green's Functions

This chapter serves as an introduction to *Green's function methods* to calculate the ionization potentials of atoms, molecules or clusters. Only *vertical* ionization potentials are calculated here, i.e. the geometry of the molecular system is the same in the initial and the final state of the ionization process [42]. Although ionization potentials are brought into focus, many other properties of molecular systems can be calculated with Green's functions [31,67,68].

The aim is to introduce the *algebraic diagrammatic construction scheme* (ADC) which transforms the calculation of the many-body Green's function into a Hermitian eigenvalue problem. The problem is simplified by perturbation theory. The results of the ADC method are frequently impressive because the ADC equations contain, besides the diagrams up to the order in perturbation theory chosen, infinite sums of diagrams that derive from those.

In this chapter the formalism of *second quantization* is used to describe the creation and annihilation of (quasi)particles. $\hat{c}_p$ denotes an annihilator, $\hat{c}_p \,|\, \chi_p \,\rangle = |\, 0 \,\rangle$, and $\hat{c}_p^\dagger$ denotes a creator, $\hat{c}_p^\dagger \,|\, 0 \,\rangle = |\, \chi_p \,\rangle$ of electrons in spin orbitals. $|\, 0 \,\rangle$ represents the vacuum state [42,68]. The fermion field is quantized by the anticommutation relations

$$\{\hat{c}_p, \hat{c}_q\} = 0, \qquad \{\hat{c}_p^\dagger, \hat{c}_q^\dagger\} = 0, \qquad \{\hat{c}_p, \hat{c}_q^\dagger\} = \delta_{pq} \; .$$

## 5.1. Many-body Green's Functions

The *one-particle Green's function* (*particle propagator*) reads [30,48,67–69] in the *Heisenberg picture*

$$G_{pq}(t,t') = (-\mathrm{i}) \, \langle \, \Psi_0^N \,|\, \hat{T}[\hat{c}_p(t) \, \hat{c}_q^\dagger(t')] \,|\, \Psi_0^N \, \rangle \; , \tag{5.1}$$

with *Wick's time-ordering operator* $\hat{T}$. $|\, \Psi_0^N \,\rangle$ is the exact (closed-shell) ground state of the considered $N$-particle system. The *two-particle Green's function* is defined analogously [32,48,67,68]

$$G_{rs;r's'}(t_1,t_2;t_1't_2') = (-\mathrm{i})^2 \, \langle \, \Psi_0^N \,|\, \hat{T}[\hat{c}_r(t_1) \, \hat{c}_s(t_2) \, \hat{c}_{s'}^\dagger(t_2') \, \hat{c}_{r'}^\dagger(t_1')] \,|\, \Psi_0^N \, \rangle \; . \tag{5.2}$$

The *particle-particle propagator* follows from (5.2) by equating time arguments

$$\mathbf{\Pi}(t,t') = \lim_{\substack{t_1,t_2 \to t \\ t_1',t_2' \to t'}} \mathrm{i} \, \boldsymbol{G}(t_1,t_2;t_1',t_2') \; .$$

The Fourier transformation of the particle and the particle-particle propagator yields their *spectral representations*. This representation in energy space reveals valuable information about the energetics within a molecule. The spectral representation of the particle propagator (5.1) is

$$\begin{aligned} G_{pq}(\omega) &= \sum_n \frac{\langle \Psi_0^N \,|\, \hat{c}_p \,|\, \Psi_n^{N+1} \rangle \langle \Psi_n^{N+1} \,|\, \hat{c}_q^\dagger \,|\, \Psi_0^N \rangle}{\omega + E_0^N - E_n^{N+1} + \mathrm{i}\eta} \\ &\quad + \sum_m \frac{\langle \Psi_0^N \,|\, \hat{c}_q^\dagger \,|\, \Psi_m^{N-1} \rangle \langle \Psi_m^{N-1} \,|\, \hat{c}_p \,|\, \Psi_0^N \rangle}{\omega + E_m^{N-1} - E_0^N - \mathrm{i}\eta} \end{aligned} \tag{5.3}$$

and the spectral representation of the particle-particle propagator is

$$\begin{aligned} \Pi_{rs,r's'}(\omega) &= \sum_n \frac{\langle \Psi_0^N \,|\, \hat{c}_r \hat{c}_s \,|\, \Psi_n^{N+2} \rangle \langle \Psi_n^{N+2} \,|\, \hat{c}_{s'}^\dagger \hat{c}_{r'}^\dagger \,|\, \Psi_0^N \rangle}{\omega + E_0^N - E_n^{N+2} + \mathrm{i}\eta} \\ &\quad - \sum_m \frac{\langle \Psi_0^N \,|\, \hat{c}_s^\dagger \hat{c}_r^\dagger \,|\, \Psi_m^{N-2} \rangle \langle \Psi_m^{N-2} \,|\, \hat{c}_{r'} \hat{c}_{s'} \,|\, \Psi_0^N \rangle}{\omega + E_0^{N-2} - E_m^N - \mathrm{i}\eta} \\ &= \Pi^{\mathrm{I}}_{rs,r's'}(\omega) - \Pi^{\mathrm{II}}_{rs,r's'}(\omega) \,. \end{aligned} \tag{5.4}$$

The propagators (5.3), (5.4) are both sums of two parts. The physical meaning of the parts is revealed by the negative of the *pole positions* $I_n^{N-1} = E_n^{N-1} - E_0^N$, $A_m^{N-1} = E_m^{N+1} - E_0^N$ of (5.3) and $I_n^{N-2} = E_n^{N-2} - E_0^N$, $A_m^{N-2} = E_m^{N+2} - E_0^N$ of (5.4). Obviously the *ionization potentials* are given by $I_n^{N-1}$, $I_n^{N-2}$ and the *electron affinities* by $A_n^{N-1}$, $A_n^{N-2}$.

The so-called *pole strengths* $x_p^{(m)} = \langle \Psi_m^{N-1} \,|\, \hat{c}_p \,|\, \Psi_0^N \rangle$ and $y_p^{(n)} = \langle \Psi_n^{N+1} \,|\, \hat{c}_p^\dagger \,|\, \Psi_0^N \rangle$ for the particle propagator are related to the *spectral intensities* of ionization and electron affinity. Likewise the pole strengths $x_{rs}^{(m)} = \langle \Psi_m^{N-2} \,|\, \hat{c}_r \hat{c}_s \,|\, \Psi_0^N \rangle$ and $y_{rs}^{(n)} = \langle \Psi_0^{N+2} \,|\, \hat{c}_s^\dagger \hat{c}_r^\dagger \,|\, \Psi_n^N \rangle$ for the particle-particle propagator are related to the spectral intensities of double ionization and double electron affinity.

## 5.2. Diagrammatic Perturbation Expansion of the Propagators

The Green's function method is a formulation of the many-body problem but no simplification [67, 68]. Therefore, perturbation theory is applied to reduce the problem. The Møller-Plesset partition [42, 55, 56] of the many-body Hamiltonian is used

$$\begin{aligned} \hat{H} &= \hat{H}_0 + \hat{H}_1 \\ \hat{H}_0 &= \sum_{i=1}^{K} \varepsilon_i \, \hat{c}_i^\dagger \, \hat{c}_i \\ \hat{H}_1 &= -\sum_{i,j=1}^{K} V_{ij}^{(\mathrm{HF})} \, \hat{c}_i^\dagger \, \hat{c}_j + \tfrac{1}{2} \sum_{i,j,k,l=1}^{K} V_{ijkl} \, \hat{c}_i^\dagger \, \hat{c}_j^\dagger \, \hat{c}_l \, \hat{c}_k \,. \end{aligned} \tag{5.5}$$

The terms in (5.5) result from a Hartree-Fock calculation, described in section 2.1; In detail $\varepsilon_i$ denote orbital energies, $V_{ijkl}$ are the two-electron integrals of (3.5). The Hartree-Fock potential (2.5) reads in terms of spin orbitals $V_{ij}^{(\mathrm{HF})} = \sum_{k=1}^{N} V_{ik[jk]}$.

This partition is particularly well suited for an expansion of the propagators in a perturbation series which possesses a diagrammatic representation in the famous *Feynman diagrams* [67,68]. The rules for drawing and evaluating these kinds of diagrams provide a simple way to calculate the $n$-th order contribution to the perturbation series.

An algebraic derivation of the $n$-th order contribution with the help of *Wick's theorem* [67,68] is cumbersome and lengthy. In addition the Feynman diagrams provide a pictorial representation of the underlying physics that helps to understand more deeply the effect of the interaction.

To evaluate a $n$-th order Feynman diagram one has to consider $n!$ time orderings. Each of these orderings can be pictured by a *Goldstone diagram* [67,68]. Collecting the contributions of all Goldstone diagrams up to a certain order yields the desired perturbation series up to that order.

The process described in the preceding paragraphs is well known and has been applied frequently in *many-body quantum mechanics* and *quantum field theory* [67,68].

## 5.3. Algebraic Diagrammatic Construction

### 5.3.1. General Formulation

*Algebraic diagrammatic construction* (ADC) fuses the ease of diagrammatic evaluation of many-body perturbation theory with the perturbation expansion of a Hermitian eigenvalue problem, via the so-called *general algebraic form (ADC form)*. As is shown in the following subsections explicitly, both parts of the spectral representations of a propagator can be cast into this form. The ADC theory, presented in this subsection, is taken from [30,32,70].

The ADC form of one part of a propagator reads $\mathbf{\Pi}(\omega)$

$$\mathbf{\Pi}(\omega) = \boldsymbol{f}^\dagger \left(\omega \, \mathbb{1} - \boldsymbol{K} - \boldsymbol{C}\right)^{-1} \boldsymbol{f} \; . \tag{5.6}$$

In this equation $\boldsymbol{f}$ stands for the matrix of *modified (effective) transition amplitudes*. $\boldsymbol{K}$ is a diagonal Hermitian matrix. The Hermitian matrix $\boldsymbol{C}$ is referred to as *effective interaction matrix*.

Solving equation (5.6) leads to a Hermitian eigenvalue problem because the matrix inversion therein can be carried out by solving

$$(\boldsymbol{K} + \boldsymbol{C})\boldsymbol{Y} = \boldsymbol{Y}\mathbf{\Omega}, \quad \boldsymbol{Y}^\dagger \boldsymbol{Y} = \mathbb{1} \; . \tag{5.7}$$

$\mathbf{\Omega}$ is the diagonal matrix of eigenvalues, which are the poles of the propagator, and $\boldsymbol{Y}$ denotes the eigenvector matrix.

The perturbation expansion of the Hermitian eigenvalue problem is obtained from equation (5.6) as follows

$$\begin{aligned} \mathbf{\Pi}(\omega) &= \boldsymbol{f}^\dagger \left[\mathbb{1} - (\omega \, \mathbb{1} - \boldsymbol{K})^{-1} \boldsymbol{C}\right]^{-1} (\omega \, \mathbb{1} - \boldsymbol{K})^{-1} \boldsymbol{f} \\ &= \boldsymbol{f}^\dagger \sum_{n=0}^{\infty} [(\omega \, \mathbb{1} - \boldsymbol{K})^{-1} \boldsymbol{C}]^n \, (\omega \, \mathbb{1} - \boldsymbol{K})^{-1} \boldsymbol{f}. \end{aligned} \tag{5.8}$$

The idea behind this form is the fact that the ubiquitous geometric series that also played the prominent role in the multireference perturbation theory presented in section 3.3, reproduces the general structure of the algebraic terms of the individual diagrams. The issue of convergence of the series is addressed in section 3.3.

Inserting expansions for $\boldsymbol{f}$ and $\boldsymbol{C}$

$$\begin{aligned} \boldsymbol{f} &= \boldsymbol{f}^{(0)} + \boldsymbol{f}^{(1)} + \boldsymbol{f}^{(2)} + \dots \\ \boldsymbol{C} &= \boldsymbol{C}^{(1)} + \boldsymbol{C}^{(2)} + \dots \end{aligned} \tag{5.9}$$

in equation (5.8) yields

$$\begin{aligned} \boldsymbol{\Pi}(\omega) &= \boldsymbol{f}^{(0)\dagger} \left(\omega \, \mathbb{1} - \boldsymbol{K}\right)^{-1} \boldsymbol{f}^{(0)} \\ &\quad + \boldsymbol{f}^{(0)\dagger} \left(\omega \, \mathbb{1} - \boldsymbol{K}\right)^{-1} \boldsymbol{C}^{(1)} \left(\omega \, \mathbb{1} - \boldsymbol{K}\right)^{-1} \boldsymbol{f}^{(0)} \\ &\quad + \boldsymbol{f}^{(1)\dagger} \left(\omega \, \mathbb{1} - \boldsymbol{K}\right)^{-1} \boldsymbol{f}^{(0)} \\ &\quad + \boldsymbol{f}^{(0)\dagger} \left(\omega \, \mathbb{1} - \boldsymbol{K}\right)^{-1} \boldsymbol{f}^{(1)} + \dots \end{aligned} \tag{5.10}$$

a perturbation series for $\boldsymbol{\Pi}(\omega)$. Note that the expansion for the effective interaction matrix (5.9) starts in first order because the unperturbed part is put in $\boldsymbol{K}$.

Comparing the algebraic expressions for the diagrams with the expansion (5.9) one can assign terms to $\boldsymbol{f}^{(n)}$, $\boldsymbol{K}$ and $\boldsymbol{C}^{(n)}$. Having found these expressions up to order $n$ one can insert these $n$-th order approximations into equation (5.6) to obtain the ADC($n$) equation. Carrying out the matrix inversion (5.7) yields an approximation for $\boldsymbol{\Pi}(\omega)$ which contains infinite summations of all the diagrams which derive from the first $n$ orders of the expansion (5.11).

### 5.3.2. ADC for the Particle Propagator

There is the *Dyson equation* [30, 31, 48] for the particle propagator (5.3)

$$\boldsymbol{G}(\omega) = \boldsymbol{G}^0(\omega) + \boldsymbol{G}^0(\omega)\boldsymbol{\Sigma}(\omega)\boldsymbol{G}(\omega), \tag{5.11}$$

where $\boldsymbol{G}^0(\omega)$ is the *free Green's function* and $\boldsymbol{\Sigma}(\omega)$ denotes the *self-energy*. The self-energy can be decomposed in a *static self-energy part* ($\omega$ independent) and a *dynamic self-energy part* ($\omega$ dependent)

$$\boldsymbol{\Sigma}(\omega) = \boldsymbol{\Sigma}(\infty) + \boldsymbol{M}(\omega) \, .$$

Unfortunately, these parts cannot be calculated independently of each other. The dynamic self-energy part $\boldsymbol{M}(\omega)$ is represented in terms of the *2ph propagator* which possesses a spectral representation

$$\begin{aligned} M_{pq}(\omega) &= \sum_{n \in \{N+1\}} \frac{m_p^{(n)} m_q^{(n)*}}{\omega - \omega_n + \mathrm{i}\eta} + \sum_{n \in \{N-1\}} \frac{m_p^{(n)} m_q^{(n)*}}{\omega - \omega_n - \mathrm{i}\eta} \\ &= M_{pq}^{\mathrm{I}}(\omega) + M_{pq}^{\mathrm{II}}(\omega) \, . \end{aligned}$$

Inspecting $\boldsymbol{M}^{\mathrm{I}}(\omega)$, one notices that it can be cast into the general algebraic form (5.6) reading here

$$\boldsymbol{M}^{\mathrm{I}}_{pq}(\omega) = (\vec{U}^{\mathrm{I}}_p)^\dagger \, (\omega \, \mathbb{1} - \boldsymbol{K}^{\mathrm{I}} - \boldsymbol{C}^{\mathrm{I}})^{-1} \, \vec{U}^{\mathrm{I}}_q \, . \tag{5.12}$$

A similar equation holds for the second part $\boldsymbol{M}^{\mathrm{II}}(\omega)$ of the dynamic self-energy. Noticing that the series expansion of $\vec{U}^{\mathrm{I,II}}_q$ starts in first order one can proceed according to section 5.3.1. Having obtained $\boldsymbol{M}^{\mathrm{I,II}}(\omega)$ one can solve the Dyson equation (5.11) provided that the static self-energy part $\boldsymbol{\Sigma}(\infty)$ is approximated sufficiently accurate by applying the inversion method to the matrices $\boldsymbol{K}^{\mathrm{I,II}} + \boldsymbol{C}^{\mathrm{I,II}}$ in (5.12) [31].

The individual steps of solving the general algebraic form (5.6) and Dyson equation (5.11) can be combined. Then the following diagonalization problem

$$\boldsymbol{B}\boldsymbol{X} = \boldsymbol{X}\boldsymbol{E}, \qquad \boldsymbol{X}^\dagger\boldsymbol{X} = \mathbb{1}$$

$$\boldsymbol{B} = \begin{pmatrix} \boldsymbol{\varepsilon} + \boldsymbol{\Sigma}(\infty) & (\boldsymbol{U}^{\mathrm{I}})^\dagger & (\boldsymbol{U}^{\mathrm{II}})^\dagger \\ \boldsymbol{U}^{\mathrm{I}} & \boldsymbol{K}^{\mathrm{I}} + \boldsymbol{C}^{\mathrm{I}} & 0 \\ \boldsymbol{U}^{\mathrm{II}} & 0 & \boldsymbol{K}^{\mathrm{II}} + \boldsymbol{C}^{\mathrm{II}} \end{pmatrix} \tag{5.13}$$

has to be solved. The explicit construction of the ADC scheme up to fourth order is done in [30]. The ADC form sums infinitely many diagrams before its results are put in the Dyson equation to sum more diagrams.

The block of electron affinities $\boldsymbol{K}^{\mathrm{II}} + \boldsymbol{C}^{\mathrm{II}}$ is much larger than the block of ionization potentials $\boldsymbol{K}^{\mathrm{I}} + \boldsymbol{C}^{\mathrm{I}}$. If one is only interested in the ionization potentials, one can approximate the block of electron affinities by replacing it with the result of a few block Lanczos iterations [48, 71]. The matrix (5.13) can also be reduced for the calculation of core-level ionization potentials, if the *core-valence separation approximation* is applied [72].

A major drawback of the calculation of ionization potentials, as sketched in this subsection, is the fact that the Dyson equation couples ionization potentials and electron affinities. So a lot of computational effort can be saved, if it is not used. Then the electron affinities are left out completely [73] and the resulting method is similar to that described in the ensuing subsection 5.3.3. A Dyson equation exists only for the particle propagator [74] so the derivation presented here is not applicable to the particle-particle propagator.

### 5.3.3. ADC for the Particle-Particle Propagator

The treatment of the double ionization and the double attachment part in (5.4) is alike and the following derivation concentrates on the double ionization part $\boldsymbol{\Pi}^{\mathrm{II}}(\omega)$ which can be represented by

$$\boldsymbol{\Pi}^{\mathrm{II}}(\omega) = \boldsymbol{X}^\dagger(\omega \, \mathbb{1} - \boldsymbol{\Omega})^{-1}\boldsymbol{X} \, . \tag{5.14}$$

$X_{m,rs} = x^{(m)}_{rs}$ is the matrix of spectral intensities, $\Omega_m$ is the diagonal matrix of the negative of the double ionization energies.

The central point to note is that (5.14) is equivalent to the general algebraic form (5.6) with the help of (5.7) and $\boldsymbol{X} = \boldsymbol{Y}^\dagger\boldsymbol{f}$. $\boldsymbol{Y}$ is a unitary transformation to transform between

both representations. Hence the ADC procedure of subsection 5.3.1 can be applied, since the diagrammatic equations of the perturbation expansion of the particle-particle propagator fit well in the structure of (5.11). Therefore, (5.14) can be calculated in the ADC formalism. The explicit construction of the ADC scheme up to third order is done in [32, 33].

### 5.3.4. Other ADC Schemes and the Properties of ADC

Excitation spectra of molecules can be calculated with the *polarization propagator* [67, 68, 70, 75, 76] which, too, results from the two-particle Green's function (5.2). The pole positions of its spectral representation are the excitation energies of a molecular system. An ADC scheme, similar to those presented in the preceding subsections 5.3.2, 5.3.3 for ionization spectra, can be derived [70, 75, 76].

Another possibility is the calculation of triple ionization potentials by using the *three-particle propagator* [77].

The ADC scheme for singly ionized molecules has been combined with the CAP-method of section 2.3 to treat electronic resonances [10, 11, 78].

Algebraic propagator methods possess very nice properties. In [79–81] the method is interpreted in terms of *intermediate state representations* (ISR). The ISR approach replaces the creation and annihilation operators on the Hartree-Fock ground state with pendants on a correlated (physical) ground state. This reformulation of ADC can be used to compare it to various other wide-spread *ab initio* methods under the objective of *separability* and *compactness*.

If an *ab initio* method is separable it is *size-consistent*. The separability of the algebraic propagator approach is shown in [82]. The compactness property addresses the size of the basis needed to describe each order in perturbation theory. It could be shown that ADC is compact [79, 80].

Aside from the theoretical advantages of the formulation of ADC with the help of intermediate state representations, it is applied to examine, eg., core-level ionization of molecular systems [83].

## 5.4. Population Analysis for Ionization Spectra

Population analysis is a tool to reveal the distribution of (a) final state hole(s) in a molecular system after ionization. This can provide further insight into the physics of the decay as can be seen in chapter 6.

The population analysis for singly ionized molecules is developed in detail in [34, 48]. For doubly ionized molecules this is done in [35, 36]. Both schemes derive from the Mulliken style population analysis [42, 84] for Hartree-Fock orbitals and suffer from the same deficiencies, the basis set dependence of the results.

### 5.4.1. Singly Ionized Molecules

The density $\Delta(\vec{r})$ of an electron vacancy (hole-density) in $\vec{r}$ can be measured with the help of the number operator $\hat{\varrho}(\vec{r}) = \hat{\psi}^\dagger(\vec{r})\hat{\psi}(\vec{r})$

$$\Delta(\vec{r}) = -\langle \Psi_n^{N-1} | \hat{\varrho}(\vec{r}) | \Psi_n^{N-1} \rangle + \langle \Psi_0^N | \hat{\varrho}(\vec{r}) | \Psi_0^N \rangle . \tag{5.15}$$

in the sudden approximation [85]. This hole-density describes the fraction of an electron charge that is missing in the given state $|\Psi_n^{N-1}\rangle$ at $\vec{r}$ compared with the correlated ground state $|\Psi_0^N\rangle$. The number operator $\hat{\varrho}(\vec{r})$ can be expanded in terms of one-particle functions using

$$\hat{\psi}(\vec{r}) = \sum_{p=1}^{K} \chi_p(\vec{r})\, \hat{c}_p$$

for the field operator [68]. This yields

$$\Delta(\vec{r}) = \sum_{p,q=1}^{K} \chi_p^*(\vec{r})\, \chi_q(\vec{r}) \underbrace{[-\langle \Psi_n^{N-1} | \hat{c}_p^\dagger\, \hat{c}_q | \Psi_n^{N-1} \rangle + \langle \Psi_0^N | \hat{c}_p^\dagger\, \hat{c}_q | \Psi_0^N \rangle]}_{\Delta_{pq}}. \tag{5.16}$$

The matrix $\Delta_{pq}$ is termed *hole-density matrix*. The actual shape of the one-particle orbitals $\chi_p(\vec{r})$ is not included just their effective occupation.

The correlated ground state $|\Psi_0^N\rangle$, in the ISR formulation of ADC of subsection 5.3.4, is now approximated by the uncorrelated Hartree-Fock ground state $|\Phi_0^N\rangle$. With the expansion of the ionized state in terms of ionized determinants derived from the Hartree-Fock ground state of the neutral system

$$|\Psi_n^{N-1}\rangle = \sum_{i=1}^{N} x_i \underbrace{\hat{c}_i\, |\Phi_0\rangle}_{1h\ \text{config}} + \sum_{r=N+1}^{K} \sum_{\substack{i,j=1 \\ i>j}}^{N} x_{rij} \underbrace{\hat{c}_r^\dagger\, \hat{c}_i\, \hat{c}_j\ |\Phi_0\rangle}_{2h1p\ \text{config}} + \ldots \tag{5.17}$$

one can evaluate the hole-density matrix $\mathbf{\Delta}$ in terms of Hartree-Fock orbitals. The expansion coefficients $x_i$ and $x_{rij}$ are elements of an ADC(3) eigenvector describing the $n$-th cationic state. Since ADC(3) contains only $1h$ and $2h1p$ configurations higher excited configurations are dropped.

Inserting (5.17) into (5.16) one can work out the hole-density matrix $\Delta_{pq}$ for spin orbitals. After integrating out the spin, the spatial orbitals can be expanded in terms of their localized atomic basis functions $\varphi_\mu$ which are regrouped according, eg., to their atomic origins $A, B, \ldots$, in a MULLIKEN-like manner [84]

$$\Delta = \sum_{A,B} \sum_{p,q=1}^{K} \Delta_{pq} \sum_{\substack{\mu \in A \\ \nu \in B}} C_{\mu p}^*\, C_{\nu q}\, \varphi_\mu^*\, \varphi_\nu \ .$$

In this equation $C_{\mu p}$ are the Hartree-Fock expansion coefficients of the spatial molecular orbitals in terms of atomic basis function. For a single hole $\int \Delta \, \mathrm{d}^3 r = \sum_{A,B} Q_{AB} = 1$ holds.

This defines the hole-population matrix $\boldsymbol{Q}$

$$Q_{AB} = \sum_{p,q=1}^{K} \Delta_{pq} \sum_{\substack{\mu \in A \\ \nu \in B}} C^*_{\mu p}\, S_{\mu\nu}\, C_{\nu q} \ . \tag{5.18}$$

where $S_{\mu\nu}$ denotes the overlap matrix between atomic basis functions. (5.18) provides a quantitative partition of the spatial distribution of a single electron vacancy. The off-diagonal elements of $\boldsymbol{Q}$ quantify the degree of overlap between the individual sets of basis functions.

Frequently the ADC matrices (5.13) of the ADC(3) scheme are big and cannot be diagonalized fully. Then the expansion (5.17) has to be reduced to the first term ($1h$ population analysis) because not all eigenvectors are available.

### 5.4.2. Doubly Ionized Molecules

One would suspect that two-hole population analysis follows the same line of derivation presented in the preceding subsection 5.4.1 by replacing the singly ionized wave function $|\,\Psi_n^{N-1}\rangle$ by a doubly ionized one $|\,\Psi_n^{N-2}\rangle$ in equation (5.15). This can in fact be done, but the two-hole population analysis, used together with the two-particle ADC(2) program, is done in another way: the contribution of the $2h$ configurations to the total $2h$ pole strength is taken.

The analogue of the expansion of the singly ionized wave function (5.17) in the Hartree-Fock approximation reads for a doubly ionized molecule

$$|\,\Psi_n^{N-2}\rangle = \sum_{ij} (\vec{X}_n)_{ij} \underbrace{\hat{c}_i \hat{c}_j\, |\,\Phi_0\,\rangle}_{2h \text{ config}} + \ldots , \tag{5.19}$$

where $\vec{X}_n$ is the $2h$ part of the ADC eigenvector of the $n$-th dicationic state. The two-hole population analysis examines only the $2h$ components because in most cases the two-particle ADC(2) matrices cannot be diagonalized fully. Therefore not all eigenvectors for the $3h1p$ part are available.

The two-hole configurations can be either singlet or triplet states which do not couple. A spin adapted $2h$ configuration in molecular orbital basis $|\,ij^{(s,t)}\rangle$ can be expanded in $2h$ configurations built in the atomic orbital basis $|\,pq^{(s,t)}\rangle$

$$|\,ij^{(s,t)}\rangle = \sum_{pq} U^{(s,t)}_{pq,ij}\ |\,pq^{(s,t)}\rangle\,. \tag{5.20}$$

The superscripts $s$ and $t$ denote singlet or triplet spin multiplicity, respectively, and $ij$ and $pq$ are hole indices.

The expansion coefficients $U^{(s,t)}_{pq,ij}$ can be worked out in terms of the Hartree-Fock eigenvector matrix $\boldsymbol{C}$. The overlap matrix over the $2h$ functions in atomic orbital basis $O^{(s,t)}_{pq,rs} = \langle\, pq^{(s,t)} \,|\, rs^{(s,t)}\rangle$ is expressed in terms of the basis set overlap matrix $\boldsymbol{S}$. The orthonormality for the molecular orbitals thus reads $\boldsymbol{U}^\dagger \boldsymbol{O} \boldsymbol{U} = \mathbb{1}$.

For a specific state $|\Psi_n^{N-2}\rangle$ the spin multiplicity is fixed. The equations are invariant with respect to spin. Therefore the spin indices can be dropped. With the equations (5.19) and (5.20) one can express the $n$-th dicationic state in terms of the $2h$ functions in atomic orbital basis

$$|\Psi_n^{N-2}\rangle = \sum_{ij}(\vec{X}_n)_{ij}\,|ij\rangle + \ldots = \sum_{pq}\sum_{ij} U_{pq,ij}\,(\vec{X}_n)_{ij}\,|pq\rangle + \ldots\ . \tag{5.21}$$

This gives new expansion coefficients $\vec{Y}_n := \boldsymbol{U}\vec{X}_n$. Using this new vector to transform the total $2h$ weight (ADC pole strength) gives

$$\vec{X}_n^\dagger \vec{X}_n = \vec{Y}_n^\dagger \boldsymbol{O} \vec{Y}_n = \sum_{pq} Q_{pq,n} \tag{5.22}$$

with the $2h$ population matrix

$$Q_{pq,n} = Y_{pq,n}\sum_{rs}\boldsymbol{O}_{pq,rs}Y_{rs,n}\ .$$

Now sets of atomic basis functions $A$, $B$ can be formed to get population numbers

$$Q_{AB,n} = \sum_{\substack{p\in A\\ q\in B}} Q_{pq,n}\ .$$

# 6. Electronic Decay Processes and Widths in Singly Ionized Clusters

*Clusters* are (weakly) bound systems of several atoms or molecules [25] which have been receiving a lot of attention because clusters can be seen as a bridge between an individual monomer and solids formed by many monomers. This chapter investigates decay processes and decay phenomena of atoms or molecules following the ionization out of the core or inner valence shells.

All decays presented here are electronic decays, i.e. an electron is emitted after the initial first ionization. For sure, there is always the possibility of a decay by *photon emission* or *dissociation*, but lifetime calculations show that the electronic decay is very fast and consequently dominates [10, 11] in the calculation of lifetimes.

## 6.1. Decay Processes

This section summarizes the possible decay channels after one single inner valence or core ionization. The processes leading to these decay channels can be generalized to higher ionized monomers or clusters [28].

### 6.1.1. Intra-atomic Decay

*Intra-atomic decay* is the most prominent electronic decay process of core ionized molecules because it is equivalent to the well known *Auger decay* [19] in single atoms. In atoms this mechanism is well understood [18]: the initial core hole is filled by a valence electron and the excess energy is transferred to a second valence electron which is emitted subsequently (figure 6.1).

In molecules or clusters intra-atomic decay is not the only decay process. Other processes can occur which involve neighbor atoms or neighbor molecules. If intra-atomic decay is energetically forbidden, the latter processes are dominant and are described in the following subsections.

### 6.1.2. Interatomic and Intermolecular Coulombic Decay

In clusters of atoms or molecules there are other electronic decay processes. If one removes an *inner valence* electron from an isolated monomer, in general, it cannot decay by electron emission because it is below the double ionization threshold. The situation changes if the monomer is part of a cluster: then an electron of a neighboring monomer may be emitted due to double ionization channels which are not present in the single monomer.

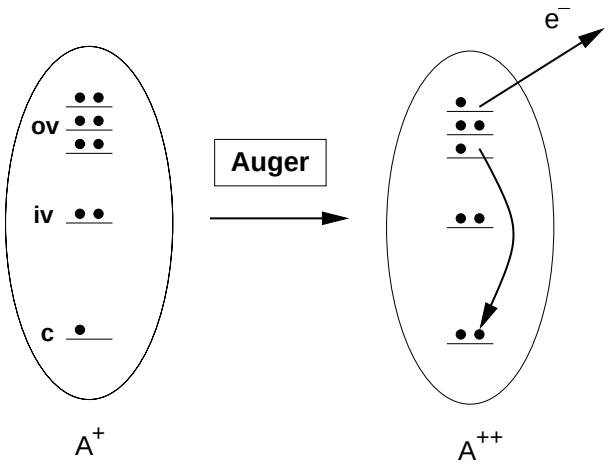


**Figure 6.1.:** Principle of Auger decay in terms of Hartree-Fock orbitals. The initial core hole is filled by a valence electron. The excess energy is released by emitting a second valence electron. **A:** atom, **ov:** outer valence orbital, **iv:** inner valence orbital, **c:** core orbital.

These new channels arise because the repulsion between two holes localized on two different monomers, the so-called *two-site states*[1], is reduced in comparison to the repulsion between two holes localized on one monomer, the so-called *one-site states*[2] due to the larger spatial separation of the two final state holes for two-site states. This increased spatial separation leads to a reduction in energy for two-site states which lowers the double ionization threshold and the decay by electron emission is allowed. *Electronic decay* turns out to be very fast and dominates the decay of these kinds of resonances in comparison to other relaxation pathways.

This decay process is termed *interatomic* or *intermolecular Coulombic decay (ICD)*[3] for clusters of atoms or clusters of molecules, respectively. It was identified in several weakly bound clusters: hydrogen fluoride $(HF)_n$ cluster [26, 28, 29], neon $(Ne)_n$ cluster [8, 27] and the neon-argon dimer NeAr [9]. A schematic representation of ICD is shown in figure 6.2. The initial inner valence vacancy is filled by a valence electron of the same monomer. The excess energy is transferred to a second valence electron of a neighboring monomer which is emitted subsequently.

### 6.1.3. Electron Transfer Mediated Decay

First of all a special decay process is explained using the NeAr dimer. The ionization spectra of the two involved atoms (neon and argon) are very different. Neon has high lying *single ionization potentials* (IP) and *double ionization potentials* (DIP). In fact the inner valence Ne $2s$ IP is larger than the $Ne^{-1}Ar^{-1}$ and the $NeAr^{-2}$ DIP in the NeAr

[1] *(German)* Zweistellige Zustände.
[2] *(German)* Einstellige Zustände.
[3] *(German)* Interatomarer/intermolekularer Coulombzerfall.

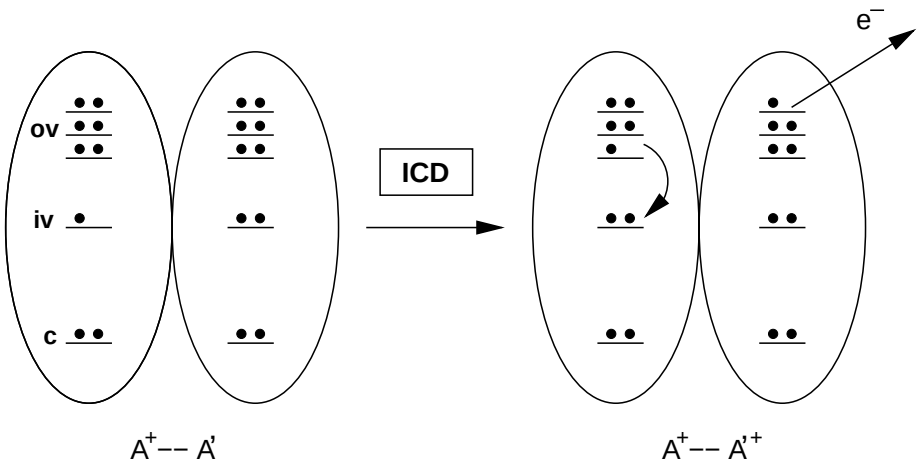


**Figure 6.2.:** Principle of interatomic or intermolecular Coulombic decay in terms of Hartree-Fock orbitals. The initial inner valence vacancy is filled by a valence electron of the same monomer. The excess energy is released by emitting a second valence electron of a neighboring monomer. **A, A′:** atoms, **ov:** outer valence orbital, **iv:** inner valence orbital, **c:** core orbital. This figure is taken from [29] (figure 1).

dimer [9] [4]. Therefore, an initial Ne $2s$ vacancy can lead to ICD.

The Ne $2s$ vacancy can decay in another way, too. A valence electron from argon may drop into the Ne $2s$ hole and the excess energy is transferred to another valence electron of argon which is emitted subsequently, leaving the dimer in a $NeAr^{-2}$ state. This process is called *electron transfer mediated decay (ETMD)*[5]. A schematic representation of the ETMD process is shown in figure 6.3.

In [9] it is shown that the contribution of ETMD to the total electronic decay width of $Ne^{-1}Ar$ is appreciably smaller compared to the contribution of ICD in NeAr. In the ETMD described, only two atoms are involved and, therefore, it is called *two-monomer ETMD*. In [9] a "*three-monomer ETMD*" is suggested for an initial $Ne^{-1}Ar_2$ state without further investigation. A schematic representation of this process is given in figure 6.4. A valence electron of the first argon atom drops into the initial Ne $2s$ hole. The excess energy is transferred to a valence electron of the second argon atom which is emitted subsequently, leaving the trimer in a $NeAr^{-1}Ar^{-1}$ state.

### 6.1.4. Terminology

The terminology introduced above is not the only one used in the literature: the interatomic processes ICD, two- and three-monomer ETMD are termed *interatomic Auger decay*Auger decay in [20]. In detail, interatomic Coulombic decay is called inter-intra decay, two- and three-monomer ETMD are called inter-inter decay. The expressions for

[4] The superscript numbers $-1$, $-2$ denote the number of electrons missing on the atom written to its left (compared to the isolated atom). This idealized picture assumes a strong localization of the electron vacancies on an atoms.

[5] *(German)* Elektronentransferzerfall.

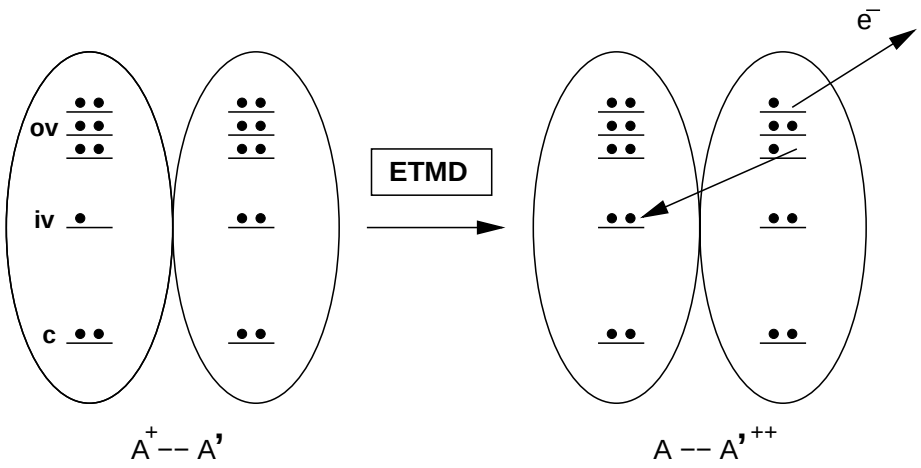


**Figure 6.3.:** Principle of two-monomer electron transfer mediated decay in terms of Hartree-Fock orbitals. A valence electron of A′ drops into the hole on A and the excess energy is transferred to another valence electron of A′ which is emitted subsequently. **A, A′:** atoms, **ov:** outer valence orbital, **iv:** inner valence orbital, **c:** core orbital. The ionization potentials of A are higher than in A′.

the interatomic decay rates derived in [20] are questioned in [21]. To call these decay processes "interatomic Auger" is misleading because Auger decay in molecules means the whole process of emitting an electron out of the molecule after an initial ionization and not only the intra-atomic process (subsections 6.1.1, 6.2.1).

## 6.2. Phenomena

The former section concentrated on the physics of the electronic decay processes in singly ionized atomic or molecular clusters. This section will summarize the phenomena observed in the Auger decay of core-ionized molecules. Furthermore a new terminology is suggested for the phenomenon that there are inner valence ionized monomers which decay electronically if they are part of a cluster.

### 6.2.1. Self Imaging and Foreign Imaging

Auger decay in *atoms* produces double vacancies in the *atomic* valence shells. Likewise Auger decay in molecules produces double vacancies in the valence molecular orbitals. The Auger spectrum of $2p$ ionized silicon atoms exhibits a three-region structure. Each region is characterized by the dicationic final states $p^{-2}$, $p^{-1}s^{-1}$ and $s^{-2}$ in the atomic valence shell [22] [6].

Core holes in singly ionized molecules or solids are strongly localized. Therefore one may assume that the Auger decay rate matrix elements are dominated by intra-atomic terms. For this reason, it was assumed that the molecular orbitals, involved in molecular Auger decay, may be approximated by the atomic orbitals of the atom, carrying the initial

[6] The notation is explained in footnote 4 on page 57.

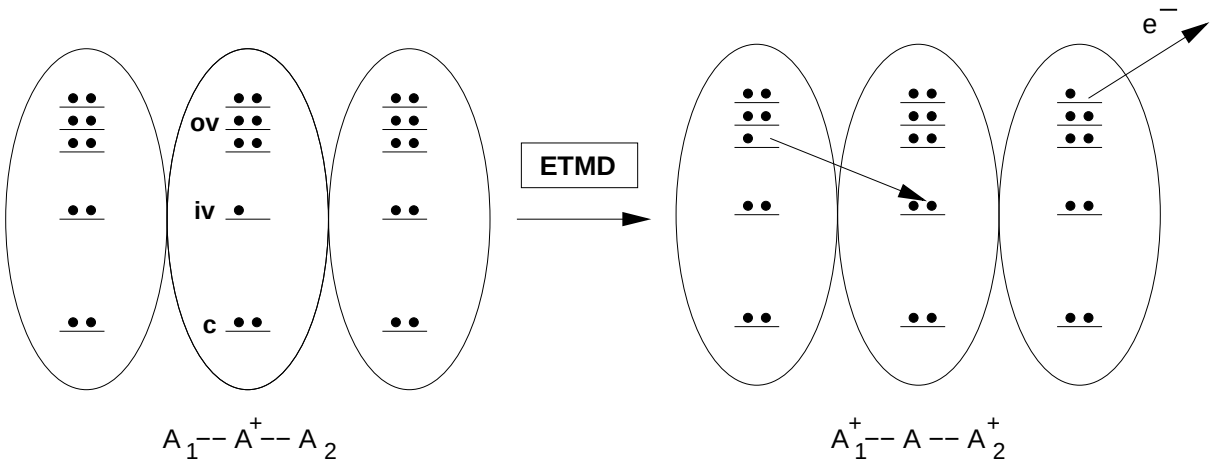


**Figure 6.4.:** Principle of three-monomer electron transfer mediated decay in terms of Hartree-Fock orbitals. A valence electron of $A_1$ drops into the hole on A and the excess energy is transferred to a valence electron of $A_2$. **A, $A_1$, $A_2$:** atoms, **ov:** outer valence orbital, **iv:** inner valence orbital, **c:** core orbital. The ionization potentials of A are higher than the ionization potentials in $A_1$, $A_2$.

vacancy. In this picture, the chemical bond is seen as small modulation. This is called the *self-imaging picture*[7] of molecular Auger decay [22] and the Auger spectrum of a molecule exhibits the structure of atomic Auger decay, described above. This picture of Auger decay in molecules is only valid if the molecular orbitals are very similar to the atomic orbitals of the initially ionized atom.

If this condition is not fulfilled the situation changes dramatically [22, 23]. A good example for this situation is silicon tetrafluoride. The bonds in $SiF_4$ are highly polarized towards the fluorine atoms, leaving the silicon atom nearly deprived of valence electrons. The Auger spectrum of Si $2p$ ionized $SiF_4$ exhibits eight, instead of three, distinct regions because of the eight possibilities to produce two holes in the valence molecular orbitals: 1. $F_1\, p^{-1}\, F_2\, p^{-1}$, 2. $F\, p^{-2}$ (triplet), 3. $F\, p^{-2}$ (singlet), 4. $F_1\, p^{-1}\, F_2\, s^{-1}$, 5. $F\, p^{-1} s^{-1}$ (triplet), 6. $F\, p^{-1} s^{-1}$ (singlet), 7. $F_1\, s^{-1}\, F_2\, s^{-1}$, 8. $F\, s^{-2}$ in increasing energetical order. This phenomenon is termed the *foreign-imaging picture*[8] of molecular Auger decay [22, 23].

The fact that the initial core hole is a Si $2p$ hole and the fact that the vast majority of final dicationic states are situated on one or two neighboring fluorine atoms suggests that ETMD is the dominant decay process because ETMD is the only process that produces final states on neighboring atoms exclusively. One may further speculate that the reason for the intra-atomic and ICD decay rates to drop below the two- and three-atomic ETMD rates is the ionic bonding in $SiF_4$ because the central silicon atom is nearly deprived of outer valence electrons. This extreme reduction in valence electron density on silicon may cause the dominance of ETMD. To prove this one has to calculate the partial decay widths of the various decay processes in $SiF_4$ which has not been done yet.

[7] *(German)* Selbstabbildung.
[8] *(German)* Fremdabbildung.

### 6.2.2. Neighbor Induced Electronic Decay

Apart from the decay processes ICD and ETMD, a new phenomenon is described in subsections 6.1.2 and 6.1.3: electronic decay of a singly ionized monomer is enabled by the presence of neighboring monomers which also participate in the decay. There is no possibility, for the isolated ionized monomer, to decay by the intra-atomic decay of subsection 6.1.1. It is highly desirable to keep the decay process and the phenomenon, causing the decay, well separated. Therefore, I would like to call the phenomenon *neighbor induced electronic decay (NIED)*[9] with the addition *in weakly bound clusters* where appropriate.

## 6.3. Decay Widths

The calculation of electronic decay widths for core holes is difficult because the standard techniques for inner valence holes, see section 2.3 and chapter 3, are not applicable due to the bad representation of the decay electron in the Gaussian basis sets which are used in the numerical calculation. Nevertheless one can analyze the decay channels using some sort of Wigner-Weisskopf theory (section 3.1).

### 6.3.1. Decay Channels

The core hole is abbreviated to "ch". If the decay produces two final state holes one must sum over all energetically accessible dicationic final states which are denoted with the single index $n$. The total decay width reads

$$\Gamma_{\mathrm{ch}} = \sum_n \Gamma_n = \Gamma_{\mathrm{One-site}} + \Gamma_{\mathrm{Two-site}} \ .$$

There are two sorts of overall decay widths. The electronic decays which produce two holes localized on one atom, the *one-site states*, and those which produce two holes localized on two atoms, the so-called *two-site states*. The one-site final states arise from intra-atomic and two-monomer ETMD decays, as shown in figures 6.1, 6.3

$$\Gamma_{\mathrm{One-site}} = \Gamma_{\mathrm{Intra-atomic}} + \Gamma_{\mathrm{ETMD,2}} \ .$$

ICD and three-monomer ETMD decays produce two-site final states, as shown in figures 6.2, 6.4

$$\Gamma_{\mathrm{Two-site}} = \Gamma_{\mathrm{ICD}} + \Gamma_{\mathrm{ETMD,3}} \ .$$

### 6.3.2. Wigner-Weisskopf Theory for Singly Ionized Molecules

The Wigner-Weisskopf theory of section 3.1 can also be applied to singly ionized molecules to calculate their electronic decay widths [8,9]. Let the initial state be a singly ionized resonance state $|\Psi_{\mathrm{I}}\rangle = |\Psi_i\rangle$. The final state is the $n$-th doubly ionized state together with the free electron resulting from the decay $|\Psi_{\mathrm{F}}\rangle = |\Psi_n^{\vec{k}}\rangle$. To calculate the decay width of this process, the matrix elements in (3.3) are needed.

[9] *(German)* Nachbarinduzierter elektronischer Zerfall.

In [8,9] the initial state is approximated by singly ionized Hartree-Fock determinant $\Phi_i$. Then the Slater-Condon rules[10] determine the possible final states. They are $|\Phi_{jl}^{\vec{k}}\rangle$ and $|\Phi_{jli}^{\vec{k}b}\rangle$. Then the initial state, final state and transition matrix elements of subsection 3.1.2 can be calculated easily.

Instead of going through all the calculations of the matrix elements again for an ionized molecule one can use a procedure to transform the equations for an excited molecule (3.7), (3.8), (3.9), (3.10), (3.11) into those of an ionized molecule. The initial state in section 3.1 is $|\Phi_i^a\rangle$. One must neglect all interactions with the electron in $\chi_a$, i.e.$\chi_a$ is treated like an unoccupied orbital. Consequently all terms in (3.7), (3.8), (3.9), (3.10), (3.11) which contain $\chi_a$ vanish. This leads to equations describing the electronic decay of an ionized molecule.

A non-vanishing contribution to the decay width of a singly ionized molecule results from equation (3.10)

$$\Gamma_{\text{doubly,3}} = 2\pi \sum_{\vec{k}} \sum_{\substack{j,l=1 \\ j,l\neq i \\ j<l}}^{N} |V_{i\vec{k}[lj]}|^2 \, \delta(\varepsilon_i - \varepsilon_j - \varepsilon_l + \varepsilon_{\vec{k}} + V_{jl[jl]} - V_{j\vec{k}[j\vec{k}]} - V_{l\vec{k}[l\vec{k}]}) \, .$$

This equation has already been derived in [8, 9] by direct evaluation of the matrix elements (equation (17)). A second contribution is given by (3.11)

$$\begin{aligned} \Gamma_{\text{triply}} \;=\; & 2\pi \sum_{\vec{k}} \sum_{b=N+1}^{K} \sum_{\substack{j,l=1 \\ j,l\neq i \\ j<l}}^{N} |V_{b\vec{k}[jl]}|^2 \, \delta(\varepsilon_b + \varepsilon_{\vec{k}} - \varepsilon_j - \varepsilon_l \\ & - V_{i\vec{k}[i\vec{k}]} - V_{j\vec{k}[j\vec{k}]} - V_{l\vec{k}[l\vec{k}]} - V_{ib[ib]} - V_{jb[jb]} - V_{lb[lb]} \\ & + V_{ij[ij]} + V_{jl[jl]} + V_{il[il]} + V_{b\vec{k}[b\vec{k}]}) \, . \end{aligned}$$

This contribution to the decay width was neglected in [8,9] due to energetic considerations.

### 6.3.3. ADC Wigner-Weisskopf Theory

A better approximation to the physical final state $|\Psi_n^{\vec{k}}\rangle$ shall be derived that also draws a connection to the ADC formalism. Dicationic states of a molecule $|\Psi_n\rangle$ can be calculated by the two-particle ADC(2) of subsection 5.3.3. These states can be approximately expanded in terms of dicationic Hartree-Fock determinants (5.21)

$$|\Psi_n\rangle = \sum_{ij} (\vec{X}_n)_{ij} \, |\Phi_{ij}\rangle \;\; . \tag{6.1}$$

The final state $|\Psi_n^{\vec{k}}\rangle$ is approximated by replacing the dicationic determinants in (6.1) by excited cationic determinants $\Phi_{ij}^{\vec{k}}$. The *sudden approximation* [85] is used here. Then the

[10] See footnote 1 on page 17.

final state and transition matrix element in (3.3) read

$$\begin{aligned} \langle \Psi_n^{\vec{k}} \,|\, \hat{H} \,|\, \Psi_n^{\vec{k}} \rangle &= \sum_{ij,pq} (\vec{X}_n^{\dagger})_{ij} (\vec{X}_n)_{pq} \langle \Phi_{ij}^{\vec{k}} \,|\, \hat{H} \,|\, \Phi_{pq}^{\vec{k}} \rangle \\ \langle \Psi_n^{\vec{k}} \,|\, \hat{H} \,|\, \Phi_l \rangle &= \sum_{ij} (\vec{X}_n^{\dagger})_{ij} \langle \Phi_{ij}^{\vec{k}} \,|\, \hat{H} \,|\, \Phi_l \rangle \,, \end{aligned} \tag{6.2}$$

with the index $ij$ denoting a $2h$ configurations. The matrix elements $\langle \Phi_{ij}^{\vec{k}} \,|\, \hat{H} \,|\, \Phi_l \rangle = -V_{\vec{k}l[ij]}$ in (6.2), formed with the help of ionized Hartree-Fock determinants, are termed *CI transition matrix elements* throughout. In addition the initial state could be expanded in terms of an one-particle ADC eigenvector (5.17). To keep things simple this is not done here. The decay rate reads, with the help of (6.2)

$$|\langle \Psi_n^{\vec{k}} \,|\, \hat{H} \,|\, \Phi_l \rangle|^2 = \sum_{ij,pq} (\vec{X}_n)_{ij} \, (\vec{X}_n^{\dagger})_{pq} \, \langle \Phi_{ij}^{\vec{k}} \,|\, \hat{H} \,|\, \Phi_l \rangle^* \, \langle \Phi_{pq}^{\vec{k}} \,|\, \hat{H} \,|\, \Phi_l \rangle \ .$$

Neglecting the cross terms in this equation and replacing the CI transition matrix elements $\langle \Phi_{ij}^{\vec{k}} \,|\, \hat{H} \,|\, \Phi_l \rangle$ by a mean one gives with (5.22)

$$\overline{|\langle \Phi_{ij}^{\vec{k}} \,|\, \hat{H} \,|\, \Phi_l \rangle|^2} \, \vec{X}_n^{\dagger} \vec{X}_n = \overline{|\langle \Phi_{ij}^{\vec{k}} \,|\, \hat{H} \,|\, \Phi_l \rangle|^2} \, \sum_{pq} Q_{pq,n} \ . \tag{6.3}$$

The approximation of the CI transition matrix element may be a satisfactory assumption for the partial widths of the four distinct decay processes of section 6.1 because in this case $\langle \Phi_{ij}^{\vec{k}} \,|\, \hat{H} \,|\, \Phi_l \rangle$ may vary not too much. For the full electronic decay width this approximation is likely not acceptable.

The CI transition matrix element can be simplified further with the help of *Rüdenberg's integral approximations* [86, 87]. The approximations yield a sum of one-center two-electron integrals with the basis set overlap matrix as expansion coefficients for a CI transition matrix element. Hence this approximation transforms the interatomic decay matrix elements to a sum of intra-atomic decay matrix elements.

# 7. Ionization Spectra of Xenon and its Fluorides

This chapter is devoted to the xenon fluorides: $XeF_2$, $XeF_4$ and $XeF_6$. Their electronic decay channels, after single ionization of the Xe $4d$ orbitals, are studied. The experimental results in table 7.1 from *photoelectron spectroscopy* of the Xe $4d$ lines inspired this work.

Figure 7.1 shows a plot of the line width for xenon and its fluorides. An increase of the mean line width for xenon with an increasing number of fluorine atoms is observed. Several experimental line widths are measured for each compound which correspond to the line width of different Xe $4d$ lines.

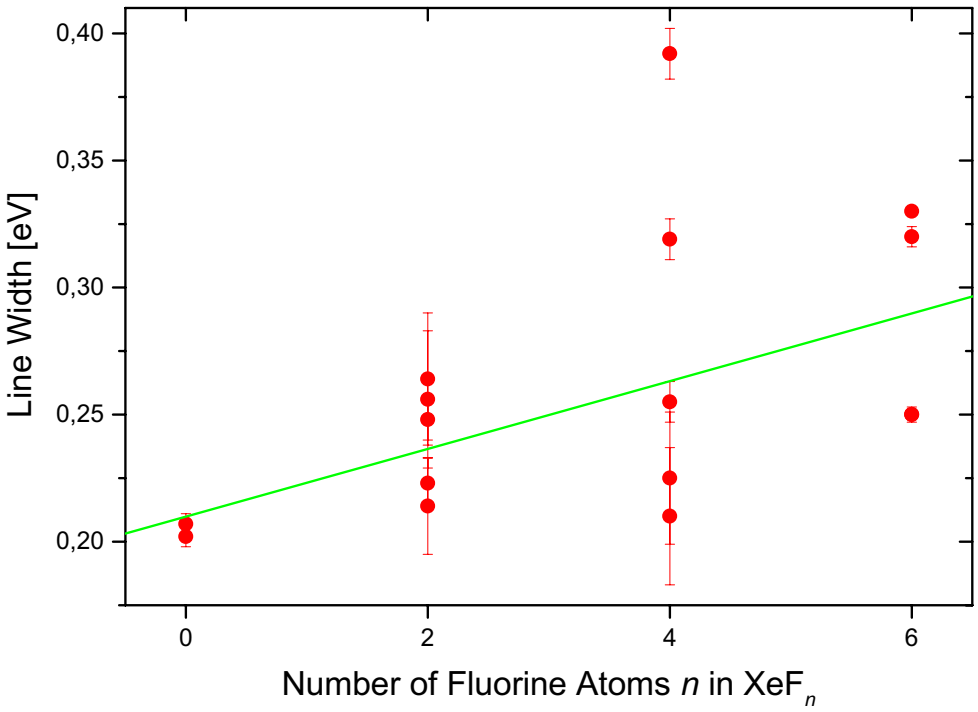


**Figure 7.1.:** (Color) Experimental widths of the Xe $4d$ lines in Xe, $XeF_2$, $XeF_4$ and $XeF_6$. The data are taken from table 7.1. The figure suggests an increase of the line width with an increasing number of fluorine atoms. According to private communication with T. Darrah Thomas.

A reason for the increase in line width may be the increase of the decay width of the initial state, with a Xe $4d$ vacancy, caused by the fluorine atoms. Another possibility is

| Cmpd. | Line | $IP_{exp}$ | $IP_{ADC}$ | $IP_{rel}$ | $\Gamma_{exp}$ |
|---|---|---|---|---|---|
| Xe | 1 | 69.525 (10) | 72.90 | 69.83 | 0.207 (4) |
| | 2 | 67.541 (9) | | | 0.202 (4) |
| $XeF_2$ | 1 | 72.568 (6) | 76.52 | 73.44 | 0.248 (8) |
| | 2 | 72.248 (6) | 76.14 | 73.06 | 0.223 (10) |
| | 3 | 70.601 (13) | 75.63 | 72.56 | 0.264 (26) |
| | 4 | 70.421 (9) | | | 0.256 (27) |
| | 5 | 70.179 (6) | | | 0.214 (19) |
| $XeF_4$ | 1 | 75.098 (6) | 79.76 | 76.68 | 0.319 (8) |
| | 2 | 74.729 (7) | 79.60 | 75.52 | 0.255 (8) |
| | 3 | 73.140 (10) | 79.01 | 75.93 | 0.392 (10) |
| | 4 | 72.816 (10) | 78.89 | 75.82 | 0.210 (27) |
| | 5 | 72.661 (5) | | | 0.225 (26) |
| $XeF_6$ | 1 | 77.462 (13) | 80.86 | 77.79 | 0.32 (4) |
| | 2 | 77.321 (11) | 80.59 | 77.51 | 0.25 (3) |
| | 3 | 75.53 | | | 0.33 |
| | 4 | 75.38 | | | 0.25 |
| | 5 | 75.25 | | | 0.25 |

**Table 7.1.:** Peak positions and widths of the Xe $4d$ lines in Xe, $XeF_2$, $XeF_4$ and $XeF_6$. *Abbreviation of labels* – Cmpd.: compound, $IP_{exp}$: experimental peak position, $IP_{ADC}$: calculated peak position, $IP_{rel}$: calculated peak position with relativistic correction, $\Gamma_{exp}$: experimental peak width. $IP_{exp}$ and $\Gamma_{exp}$ are photoelectron experimental data, reproduced from table 1 in [41]. For $XeF_6$ the data with an experimental resolution of 0.11 eV are taken. The values in brackets are the standard deviations of the peak positions and peak widths. $IP_{ADC}$ and $IP_{rel}$ are sorted descending in energy for each compound. The value of $IP_{exp}$ does not necessarily correspond to the values of $IP_{ADC}$, $IP_{rel}$ in the same row as spin-orbit splitting is neglected to obtain the latter. The $IP_{ADC}$ of $XeF_6$ are the two main peaks in figure 7.3. All data are given in electronvolt.

vibrational broadening which increases with the size of the molecule as well or a combined effect of an increase of the decay width and vibrational broadening. In the following vibrational broadening is not considered any further because the effect of electronic decay channels on the total decay with is investigated.

## 7.1. Ab Initio Calculations

The ground state geometries of $F_2$, $XeF_2$, $XeF_4$ and $XeF_6$ are taken from literature. The distance of the fluorine atoms in the *fluorine molecule* is $r(\text{F–F}) = 1.42\,\text{Å}$ from table 45 on page 446 in [88]. $F_2$ possesses $D_{\infty h}$ symmetry. *Xenon(II)-fluoride* also is a linear molecule of $D_{\infty h}$ symmetry with a Xe–F distance of 1.977 Å. *Xenon(IV)-fluoride* is square-planar ($D_{4h}$), the Xe–F distance is 1.94 Å. See chapter 12, pages 372–386 in [88] for further chemical and physical properties of the xenon fluorides. The atomic distances are given

for all molecules in the gas phase.

The ground state geometry of *xenon(VI)-fluoride* is a distorted octahedron [41,89], it can be described in $C_{3v}$ symmetry. Nevertheless, some computations were performed in $O_h$ symmetry due to computer hardware limitations. The calculations for $XeF_6$ in $C_{3v}$ symmetry, use the MP2 values for the bond length $r(\text{Xe–F1}) = 1.856\,\text{Å}$ and $r(\text{Xe–F4}) = 1.972\,\text{Å}$ which are taken from table 2 of [89] where an all-electron basis with $f$-functions is used[1]. The bond angles $\alpha = 80.8°$ and $\beta = 112.8°$ are taken from table 3 using the data of the same calculation and basis. The computations for $XeF_6$ in $O_h$ symmetry are performed using the bond length $r(\text{Xe–F}) = 1.952\,\text{Å}$ which is taken from table 1 of [89].

The ADC programs, for the calculation of single and double ionization potentials, introduced in section 5.3 rely on the molecular orbitals of a Hartree-Fock calculation, which is carried out using GAMESS-UK [16]. The employed software uses no symmetry for Xe. $D_{2h}$ symmetry is used for $F_2$, $XeF_2$ and $XeF_4$. $D_{2h}$ symmetry is also employed to calculated the double ionization potentials of $XeF_6$ in the ground state geometry of $O_h$ symmetry. The calculation of the single ionization potentials of $XeF_6$, in the ground state geometry of $C_{3v}$ symmetry, is performed in $C_s$ symmetry.

The xenon and the fluorine atoms are represented by the DZVP (DFT orbital) basis sets [46,90]. The quality of the basis sets can be estimated from table 7.2 by comparing the Hartree-Fock orbital energies of xenon, obtained by solving the Hartree-Fock equations numerically, i.e. without the help of initially given basis sets [91], with those, obtained using the DZVP (DFT orbital) basis sets. The shift of the orbitals, due to the approximation introduced by the finite basis sets, are $\Delta\varepsilon_{\text{BS}} := \varepsilon_{\text{HF, numeric}} - \varepsilon_{\text{HF, basis}}$. The shift is $\approx 0.1334\,\text{eV}$ for the Xe $4d$ orbitals and even less for the valence orbitals because basis sets are usually optimized with respect to the latter ones. This shift is neglected in the following because other errors are larger.

The ADC method and the hole population analysis of subsections 5.3.2, 5.4.1 are used to calculate the single ionization potentials. The ADC(3) matrices of $XeF_6$ can not be diagonalized fully. This means that the hole population analysis includes only the $1h$ configurations, the $2h1p$ configurations are not available, completely. The double ionization potentials are treated similarly according to the subsections 5.3.3, 5.4.2. All calculations in this section neglect relativistic effects which play an appreciable role in the xenon atom. Hence spin-orbit splitting is not considered. In section 7.2, relativistic effects and corrections for the relativistic effects are discussed in detail.

The Xe $4d$ single ionization of the xenon fluorides is a core-level ionization, with ionization potentials widely above the double ionization threshold. Therefore, not only $2h1p$ configurations but also $3h2p$ configurations are expected to have a considerable importance for the description of core-level ionization [72,83]. The ADC(3) scheme does not contain $3h2p$ configurations but the next order scheme, ADC(4), does. Hence one expects that the ADC(4) scheme gives an appreciable improvement of the core-level ionization potentials of xenon and its fluorides.

The inclusion of $3h2p$ configurations enlarges the configuration space considerably. The available single-processor computer hardware is not capable of calculating a large molecule like $XeF_6$ in an acceptable time. Therefore, the existing ADC(4) programs [72,83]

[1] The notation of figure 1a in [89] is used here.

| HF orbital | $\varepsilon_{\text{HF, basis}}$ | $\varepsilon_{\text{HF, numeric}}$ | DF orbital | $\varepsilon_{\text{DF}}$ | $\bar{\varepsilon}_{\text{DF}}$ |
|---|---|---|---|---|---|
| $4d$ | -2.78280 | -2.77788 | $4d_{3/2}$ | -2.71133 | -2.66479 |
| | | | $4d_{5/2}$ | -2.63376 | |
| $5s$ | -0.946253 | -0.944414 | $5s$ | -1.01014 | -1.01014 |
| $5p$ | -0.457894 | -0.457290 | $5p_{1/2}$ | -0.492572 | -0.457394 |
| | | | $5p_{3/2}$ | -0.439805 | |

**Table 7.2.:** Hartree-Fock (HF) and Dirac-Fock (DF) orbital energies of xenon. Hartree-Fock orbitals are given for the DZVP (DFT orbital) basis set and for the numeric solution. The Dirac-Fock orbitals were obtained numerically. All data are given in Hartree.

contain the core-valence separation approximation for core-level ionization which reduces the size of the configuration space and consequently does not calculate the ionization potentials of the valence regime. For these reasons, the ADC(4) programs are useless for the calculation of the single ionization potentials needed here. Hence all ionization spectra were calculated using the ADC(3) scheme.

## 7.2. Relativistic Effects

There are three main relativistic effects one has to take into account when examining heavy atoms like xenon. (1) The relativistic radial contraction and energetic stabilization of the $s$ and $p$ shells, (2) the spin-orbit splitting, (3) the relativistic radial expansion and the energetic destabilization of the (outer) $d$ and $f$ shells [92]. Effects (1) and (3) are termed *scalar relativistic effects*.

As the theory of chapter 5 for the calculation of ionization potentials is strictly non-relativistic one has to take into account relativistic effects by a "rule of thumb". This is done by performing Hartree-Fock and *Dirac-Fock calculations*, the relativistic counterpart to Hartree-Fock [92], for the xenon atom. Due to the spherical symmetry of atoms, the equations can be solved numerically [91, 93, 94], i.e. without fixed basis sets, to arbitrary precision. This gives exact sets of relativistic and non-relativistic orbitals in the mean field approximation.

In table 7.2, the orbitals determined in this way are listed together with Hartree-Fock orbitals obtained by a calculation employing a Gaussian basis set. By comparing the orbital energies of the two numerical solutions of the Hartree-Fock and Dirac-Fock equations, one can determine the size of relativistic effects and correct for them in non-relativistic computations of the single ionization potentials of the xenon fluorides. One has to note that the total angular momentum $j$ is the combination of the orbital angular momentum $l$ and the electron spin: $j = l \pm \frac{1}{2}$. A Dirac-Fock calculation yields two orbitals, one for $j_+ = l + \frac{1}{2}$ and one for $j_- = l - \frac{1}{2}$, for one Hartree-Fock orbital with $l \geq 1$. The $j_-$ orbital has a lower orbital energy than the $j_+$ orbital.

To compare Dirac-Fock with Hartree-Fock orbital energies, one has to calculate a weighted mean of the Dirac-Fock orbital energies which correspond to a single Hartree-

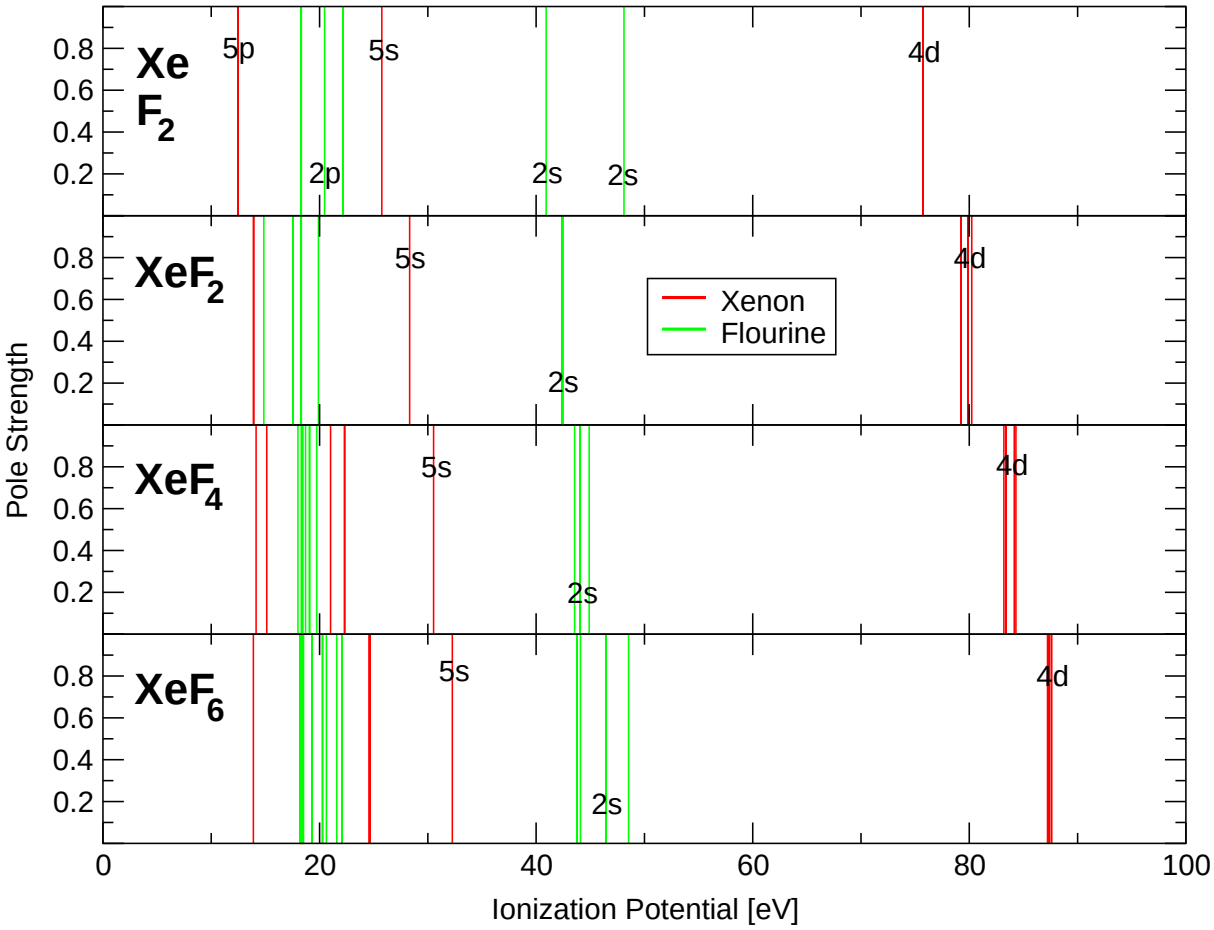


**Figure 7.2.:** (Color) Single ionization spectra of Xe, $F_2$, $XeF_2$, $XeF_4$ and $XeF_6$ calculated on Hartree-Fock level (Koopmans' theorem). The assignment of lines to being dominated by the atomic orbitals of xenon or fluorine origin is somewhat arbitrary in the valence region due to the molecular bond.

Fock orbital, with the help of

$$\bar{\varepsilon}_{\mathrm{DF}} = \frac{(2j_+ + 1)\,\varepsilon_{\mathrm{DF},+} + (2j_- + 1)\,\varepsilon_{\mathrm{DF},-}}{2j_+ + 1 + 2j_- + 1} \,.$$

The scalar relativistic shift of the non-relativistic orbitals is $\Delta\varepsilon := \bar{\varepsilon}_{\mathrm{DF}} - \varepsilon_{\mathrm{HF}}$. The shifts are 3.077 eV for the Xe $4d$, $-1.789$ eV for the Xe $5s$ and $-0.00283$ eV for the Xe $5p$ orbitals. The sign of the shift is predicted by the rules (1) and (3) in the first paragraph of this section. Due to *Koopmans' theorem* [42, 95], the ionization potentials shift by $-\Delta\varepsilon$, respectively. The shift of the Xe $5p$ orbitals is negligible and is not considered any further.

The shifts of the orbital energies of the xenon atom are used to correct the scalar relativistic effect on the Xe $4d$ orbitals. This procedure is justified by the observation that the Xe $4d$ orbitals are highly localized.

Spin-orbit splitting is not accounted for in the non-relativistic theory and is not considered any further. The spin-orbit split amounts to 2.111 eV for Xe $4d$ orbitals and 1.436 eV for Xe $5p$ orbitals (table 7.2). The amount of the split is possibly only a good approxi-

mation for Xe $4d$ orbitals because the Xe $5p$ orbitals suffer from a significant modification by the molecular bond to fluorine atoms. The experimental value for the spin-orbit split of Xe $4d$ is $1.984 \pm 0.014$ eV, it can be determined with the help of table 7.1. The theoretically and experimentally determined values are in satisfactory agreement. A good agreement is not expected because the Dirac-Fock equations are a mean field approximation and do not take electron correlation into account.

The double ionization spectra cannot be corrected as easily as the single ionization spectra because usually two states with different orbital angular momenta are involved. The situation seems to be less severe because the spectra are only accurate up to the Xe $4d$ ionization energy, so only the outer Xe $5p$ and Xe $5s$ orbitals may be involved. For the latter ones, there is no need to account for the scalar relativistic effect. Nevertheless, the amount of spin-orbit coupling cannot be estimated satisfactorily.

## 7.3. Single Ionization Potentials

### 7.3.1. One-Particle Model

#### The Spectra

Firstly, the single ionization spectra of the xenon fluorides are discussed in the one-particle model of the Hartree-Fock approximation with the help of Koopmans' theorem [42, 95]. In this model the correlation between the electrons is neglected resulting in very simple spectra which can give a hint for the interpretation of the more complex spectra which include electron correlation.

The single ionization spectra of the xenon fluorides without electron correlation are plotted in figure 7.2. The assignment of lines to being dominated by the atomic orbitals of xenon or fluorine is somewhat arbitrary in the valence region due to the molecular bond. In the lower lying molecular orbitals, this assignment is well-defined. As spin-orbit coupling is neglected, *artificial* degeneracies are introduced in the spectra of figure 7.2. This helps to understand the effect of the ligand field, caused by the fluorine atoms, on the Xe $4d$ lines.

#### Mulliken Population Analysis

The effect of adding fluorine atoms to xenon is studied by a *Mulliken population analysis* [42, 84] of the Hartree-Fock charge density in table 7.3. The Mulliken population analysis is used here, despite of its basis set dependence [42], to be consistent with the ADC population analyses of the subsections 5.4.1, 5.4.2 employed in the following sections.

One sees immediately that charge is moved from the xenon atom to the fluorine atoms: $XeF_2$: 1.1, $XeF_4$: 1.9, $XeF_6$: 2.3 electron charges. Due to the $C_{3v}$ symmetry of the ground state geometry of $XeF_6$, there are two kinds of fluorine atoms with different distances to the central xenon atom. These geometric differences are reflected in table 7.3 by the fact that the fluorine atoms which are further away from the xenon atom acquire less charge.

At first sight one may assume that this change in charge density involves only the valence electrons and has little effect on the inner molecular orbitals of the xenon fluorides.

| Compound | Atoms | Nuclear Charge | Mulliken Population | Löwdin Population |
|---|---|---|---|---|
| $XeF_2$ | Xe | 54 | 52.92 | 52.95 |
| | 2 F | 9 | 9.54 | 9.53 |
| $XeF_4$ | Xe | 54 | 52.13 | 52.12 |
| | 4 F | 9 | 9.47 | 9.47 |
| $XeF_6$ | Xe | 54 | 51.71 | 51.51 |
| | 3 F | 9 | 9.49 | 9.51 |
| | 3 F | 9 | 9.27 | 9.33 |

**Table 7.3.:** Mulliken and Löwdin population analysis of $XeF_2$, $XeF_4$ and $XeF_6$.

In the hydrogen atom, the wave functions of the higher lying shells, which are unoccupied in the ground state, have a considerable amplitude in the spatial regions of the lower lying shells of the same angular momentum [2, 3]. Although the xenon fluorides are by far not a one-electron system, this also is assumed to be true in the case of the xenon fluorides. Then a reduction of valence electron density on the xenon atom leads to a less efficient screening of its nuclear charge and consequently a lowering in energy of the low in energy lying molecular orbitals with a dominant contribution of xenon atomic orbitals.

Conversely, the increase of valence electron density on the fluorine atoms leads to a more efficient screening of their nuclear charge and consequently rises the energy of the lower lying molecular orbitals with a dominant contribution of fluorine atomic orbitals. The charge taken from the xenon atom is shared among several fluorine atoms. The net increase of charge density on each fluorine atom is $\approx 0.5$ electron charges. This value is much smaller than the loss of charge density on the xenon atom so the effect on the inner molecular orbitals of fluorine character is expected to be much smaller and most dramatic in $XeF_2$ where the fluorine atoms acquire the largest fraction.

The effects of this model can be seen in figure 7.2. The positions of the Xe $5s$ and Xe $4d$ lines shift to higher binding energies with an increasing number of fluorine atoms. The energy differences between the corresponding lines of $XeF_2$, $XeF_4$ and of $XeF_4$, $XeF_6$ are nearly equally large. The F $2p$ and F $2s$ lines also shift slightly to higher binding energies with an increasing number of fluorine atoms. This can be explained by the fact that the screening of the nuclear charge has the largest effect in $XeF_2$ and decreases in $XeF_4$ and $XeF_6$. This explanation for the shifting of the fluorine lines is supported by a comparison with $F_2$. The mean of the F $2p$ lines in $F_2$ and the mean of the F $2s$ lines in $F_2$ are higher in energy than the mean values of the corresponding lines in $XeF_2$.

### Analysis of the Ionization Potentials

The valence ionization potentials reveal a surprising feature: the first IP is nearly constant for all xenon fluorides studied. It's value is $\approx 12.5\,\mathrm{eV}$.

In the fluorine molecule, the two F $2s$ lines are split considerably due to the molecular bond. The split of the two F $2s$ lines in $XeF_2$ is tiny due to the large separation of the fluorine atoms. If one examines $F_2$, where the internuclear separation of the fluorine atoms is taken to be the separation of the fluorine atoms in $XeF_2$, then $F_2$ is not bound. In $XeF_4$

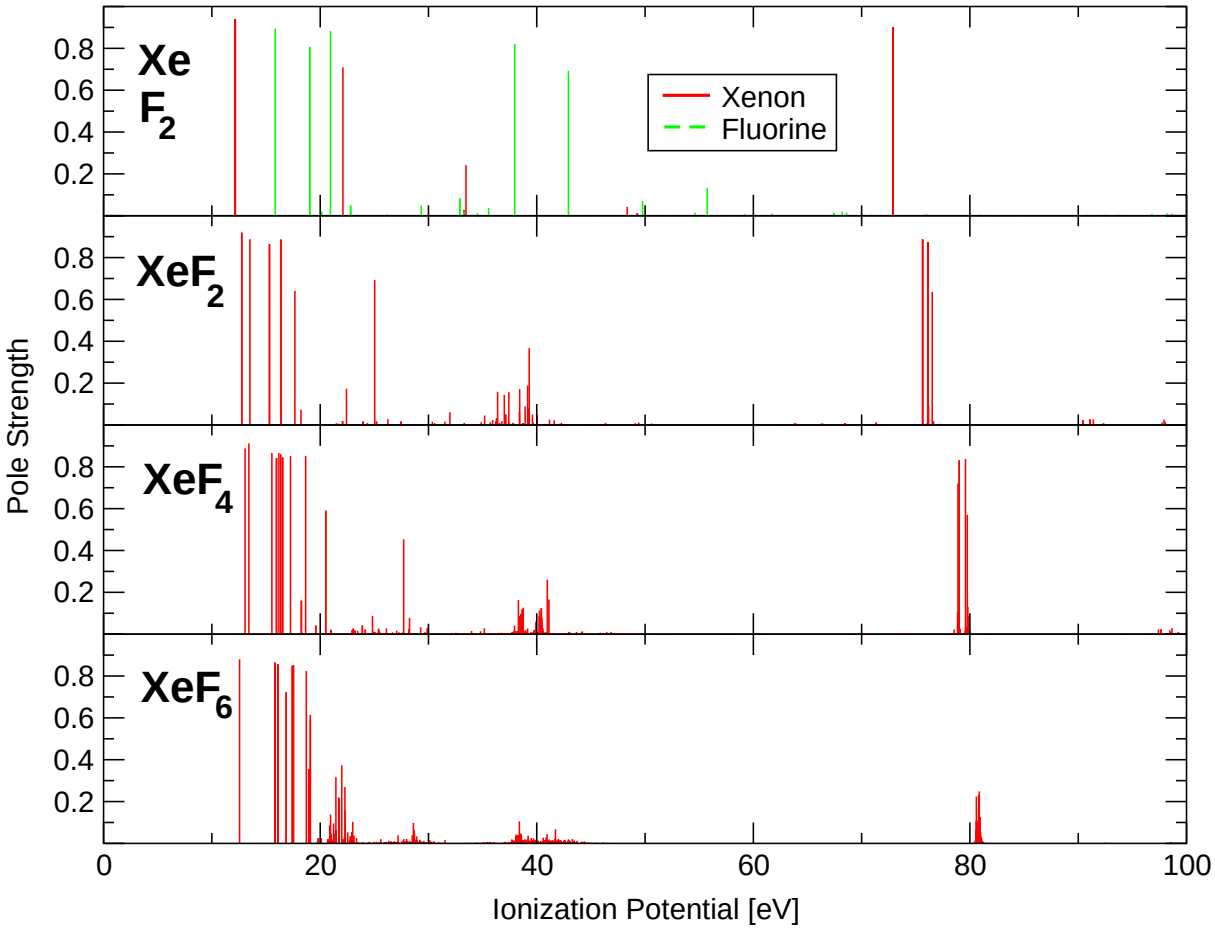


**Figure 7.3.:** (Color) Single ionization spectra of Xe, $F_2$, $XeF_2$, $XeF_4$ and $XeF_6$ calculated with the one-particle ADC(3) program (see text). The assignment of lines to being dominated by the atomic orbitals of xenon or fluorine origin is not done for $XeF_2$, $XeF_4$ and $XeF_6$.

and $XeF_6$, the fluorine atoms are closer and interact. This results in a larger split of the F $2s$ lines in comparison to the split in $XeF_2$.

The $4d$ lines are quintuply degenerate in the single ionization spectrum of the xenon atom in figure 7.2. In $XeF_2$, degeneracy is lifted by the ligand field of the fluorine atoms and three distinct lines become visible. The three lines reflect the spatial orientation of the $4d$ orbitals. Along the molecular axis, there is a ligand field. Perpendicular to the molecular axis there is no shift. Hence the former single line splits into three lines.

In $XeF_4$, there is only one dimension left that is unaffected by the ligand field: the axis perpendicular to the molecular plane. The spectrum, figure 7.2, shows that there are four distinct Xe $4d$ lines in this case. In $XeF_6$ situation changes because the fluorine atoms are grouped around the xenon in such a way that $XeF_6$ assumes nearly octahedral symmetry. This implies that the xenon atom is surrounded by charge distribution which is close to spherical symmetry. Therefore, the split of the two Xe $4d$ orbitals of $XeF_6$ in $O_h$ symmetry is only 0.1568 eV compared to the much larger splits in $XeF_2$ and $XeF_4$. $XeF_6$ in $C_{3v}$ symmetry leads to three distinct orbital energies with a total split of 0.3682 eV.

## 7.3.2. Correlation Effects

### The Spectra

Now the Hartree-Fock description of the molecules is improved by using ADC(3) to obtain the ionization potentials plotted in figure 7.3. Figure 7.2 helps to identify the one-particle origin of the states in figure 7.3. The Xe $4d$ lines are clearly separated from the outer and inner valence lines in all spectra. They are located between 72 eV and 82 eV. The F $2s$ lines show up between 35 eV and 45 eV.

### Outer Valence

Correlation effects do not change the fact that the first ionization potentials are approximately equal in all compounds. In $XeF_6$ there is a considerable breakdown in the range from 20 eV to 23 eV of valence states.

### Inner Valence

*Breakdown* of the molecular orbital picture of ionization is caused by compact $2h1p$ configurations which are close in energy to a one-particle state and contribute considerably to the description of the state. The coupling of these configurations to one-particle states leads to a broad shape of lines. Breakdown of the molecular orbital picture of ionization has been observed in the inner valence region of many molecules [59].

Due to the many-body description of a molecule, decay electrons of electronic resonances become describable. The final state of an electronic decay of a singly ionized molecule can also be approximated in terms of $2h1p$ configurations, see subsection 6.3.3. The shape of each decaying state can be identified as a thin bundle of lines which mimic a discretized Lorentzian curve [28].

Breakdown of the molecular orbital picture of ionization has to be separated clearly from a few decaying states in a small energy range where each state mimics a discretized Lorentzian curve because they are of completely different origin. Furthermore, there can be a mixing of both phenomena for a certain state but it is hard to identify a decay curve for one-particle states that suffer from breakdown.

The inner valence of the xenon fluorides comprises the Xe $5s$ and F $2s$ states. The Xe $5s$ one-particle state suffers solely from breakdown because its IP is below the double ionization threshold (see figure 7.4). In fact, the breakdown is strong, i.e. many $2h1p$ configurations contribute to the Xe $5s$ one-particle state (see figure 7.3), because the Xe $5s$ line is close to the double ionization threshold. Therefore, many $2h1p$ configurations are close in energy to this state because excited states are very dense in this energetic region.

The spectra exhibit a considerable increase of breakdown of the molecular orbital picture for the inner valence with an increasing number of fluorine atoms. Obviously, the number of possible configurations rises due to the addition of fluorine atoms. As the geometries of the xenon fluorides are very symmetric, these fluorine atoms are all equivalent, except for $XeF_6$, and the number of equivalent $2h1p$ configurations with one hole on the xenon atom doubles between $XeF_2$ and $XeF_4$. In $XeF_6$ there are even more

| Compound | 1. Experimental IP | 1. ADC IP |
|---|---|---|
| Xe | 12.129 | 12.16 |
| $XeF_2$ | 12.35 | 12.76 |
| $XeF_4$ | 13.1 | 13.07 |
| $XeF_6$ | 12.35 | 12.56 |

**Table 7.4.:** Comparison of the calculated lowest (first) ionization potentials of Xe, $XeF_2$, $XeF_4$ and $XeF_6$ with experimental results. The first IP of xenon is taken from [88]. The other first IPs are taken from [96]. All data are given in electronvolt.

such configurations than there are in $XeF_4$ but they are no longer equivalent due to the $C_{3v}$ symmetry of $XeF_6$.

Another contribution to the increase of one-particle states involved in the breakdown can be attributed to the decrease in symmetry: spherical symmetry (Xe), $D_{\infty h}$ ($XeF_2$), $D_{4h}$ ($XeF_4$), $C_{3v}$ ($XeF_6$). This decrease in symmetry leads to an increase in configurations that can couple to the respective states.

### Core

The one-particle picture is a relatively good description for the Xe $4d$ lines. $2h1p$ (and higher excited) configurations, energetically below the autoionization threshold, corresponding to spatially compact wave functions, are much lower in energy. Therefore, the mixing of $2h1p$ configurations with $1h$ configurations is weak. The splits of the Xe $4d$ lines in the xenon fluorides are of comparable size to those in figure 7.2 and the individual lines can be identified easily in all molecules but $XeF_6$.

As in all xenon fluorides the Xe $4d$ lines are above the double ionization threshold, an electronic decay of the Xe $4d$ ionized xenon fluorides is possible, see figure 7.4. The shape of the discretization of the Lorentzian curve representing a decaying state in the spectra, depends highly on the number of $2h1p$ configurations in the energy range of the decay electron. The DZVP (DFT orbital) basis used is small and contains only a few diffuse functions. Hence $XeF_6$ is the only case where the basis is sufficient to mimic the shape of Lorentzian curves well. Due to the low symmetry of $XeF_6$, the number of suitable configurations increases, too.

### Positive Electron Affinities

The charge transfer from the xenon atom to the fluorine atoms in the xenon fluorides, discussed in subsection 7.3.1, leaves a positively charged central xenon atom. Therefore, it is not surprising that $XeF_4$ and $XeF_6$ possess positive electron affinities, i.e. $(XeF_4)^-$ and $(XeF_6)^-$ are stable with respect to electron emission. In $XeF_4$ there is a doubly degenerate state at 0.6593 eV and in $XeF_6$ there are states at 1.2960 eV, 1.3078 eV, 1.8106 eV. The figures are not very accurate because the basis set is not very well suited to describe the diffuse states of electron attachment.

In $XeF_6$ the fluorine atoms form a cloud of nearly octahedral symmetry of negative charge around the central positively charged xenon atom. This potential well is similar

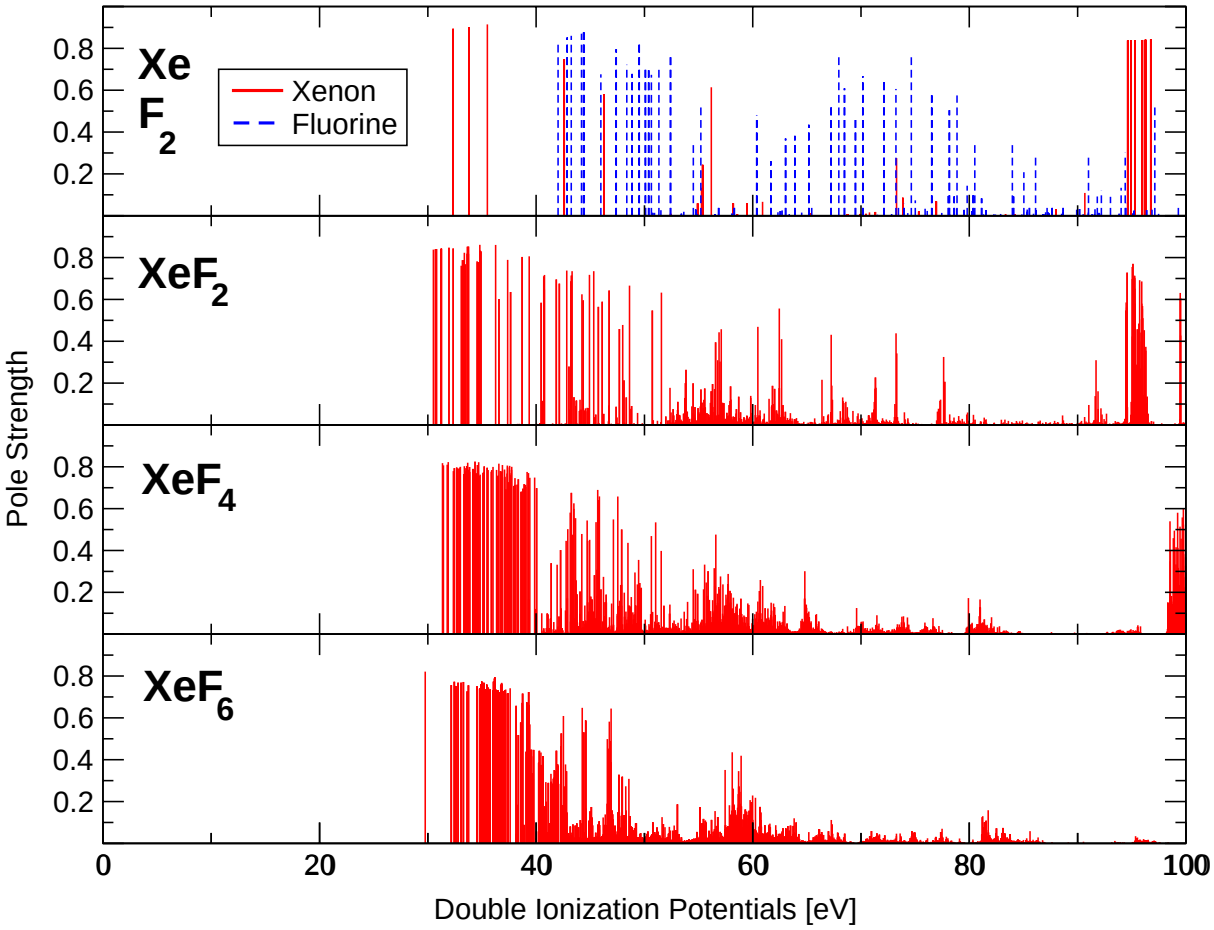


**Figure 7.4.:** (Color) Double ionization spectra of Xe, $F_2$, $XeF_2$, $XeF_4$ and $XeF_6$. The two-particle ADC(2) $2h$ pole strength is plotted on the ordinate to characterize how well the dicationic final states are described by $2h$ configurations.

to the model problem discussed in subsection 4.1.1.

### Removal of Charge

The (groups of) lines of the spectra of figure 7.3 are shifted to higher ionization potentials with an increasing number of fluorine atoms. This effect was described in subsection 7.3.1. This general trend, seen in the mean field approximation of figure 7.2, can still be identified if electron correlation is taken into account. In figure 7.3, the energy shift between the corresponding states in two compounds decreases with an increasing number of fluorine atoms, i.e. the energetic difference between the Xe $4d$ lines of $XeF_2$ and $XeF_4$ is larger than the energetic difference between the Xe $4d$ lines of $XeF_4$ and $XeF_6$. Electron correlation reduces the effect caused by charge reduction on the xenon atom.

#### Comparison with Experimental Results

The calculated non-relativistic ionization potentials are listed in table 7.1 together with the values obtained by applying the relativistic corrections of section 7.2. The number of distinct Xe $4d$ lines is smaller in the non-relativistic spectra due to a higher degeneracy caused by neglecting the spin-orbit coupling. The Xe $4d$ lines of $XeF_6$ cannot be identified clearly in figure 7.3 due to fact that the states mimic Lorentzian decay curves. One expects from subsection 7.3.1 two lines for a ground state geometry of $O_h$ symmetry and three lines for a ground state geometry of $C_{3v}$ symmetry. The two ionization potentials, in the energy range of the Xe $4d$ lines of $XeF_6$ (80–83 eV), with maximum pole strength are listed in table 7.1.

The corrected ADC(3) IPs, corresponding to the Xe $4d$ lines, differ from the experimentally obtained data in table 7.1 by 1.5–2 eV ($\approx 3\%$) which is a good agreement. The reason for the deviation is twofold. Firstly, the spin-orbit splitting is neglected which amounts to 2.111 eV for the $4d$ lines of the xenon atom, according to section 7.2. Secondly, the calculations use ADC(3) for the xenon fluorides, the $3h2p$ configurations are neglected. The inclusion of these additional configurations would shift the ionization potentials of the Xe $4d$ lines further to lower energy, due to improved hole relaxation [72], which would cause a considerable improvement.

The first ionization potentials of xenon and its fluorides are compared to the experimental results in table 7.4. The agreement of experimental IPs and calculated IPs is good.

## 7.4. Double Ionization Potentials

### 7.4.1. Spectra

The double ionization spectrum of $XeF_6$ is calculated using a ground state geometry of $O_h$ symmetry, instead of $C_{3v}$ symmetry, to make the calculation possible with the available computers. To investigate the effect of the different symmetries, the single ionization potentials are compared using Koopmans' theorem. The overall positions of the xenon lines are in good agreement in both symmetries but the split of the fluorine lines is quite different due to the increased interaction.

The double ionization spectra are shown in figure 7.4. The ADC $2h$ pole strength plotted in this figure, has the same meaning as the $1h$ pole strength for single ionization potentials: it characterizes how well the dicationic states are described by $2h$ configurations (subsection 5.4.2). The difference of the value of the $2h$ pole strength from one yields the amount of $3h1p$ configurations that contribute to the state. Analogous to the single ionization spectra, an electronically decaying state mimics a discretized Lorentzian curve in double ionization spectra [28]. Such curves may be seen above 50 eV in figure 7.4. Hence the Xe $4d$ lines in the xenon fluorides are likely above the triple ionization threshold [28].

The analysis of the double ionization potentials is more difficult than the analysis of the single ionization potentials because one has to keep in mind that there are, essentially, four contributions to a dicationic state. The dominant contribution to a state determines

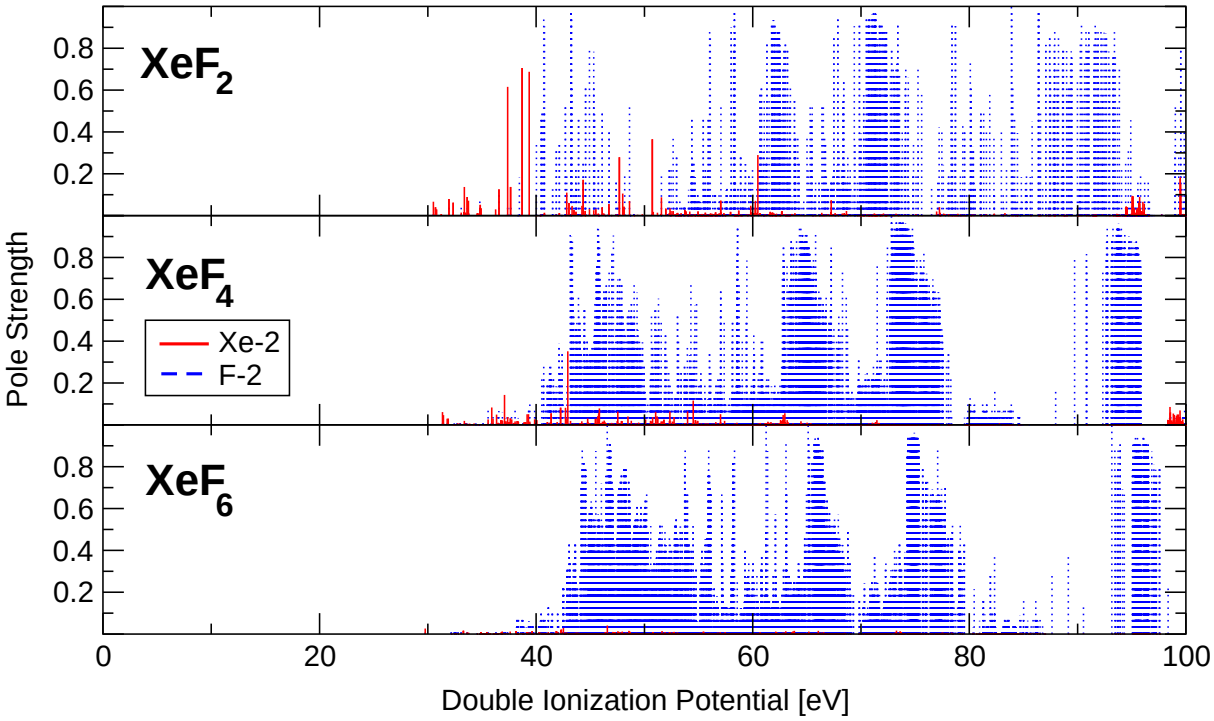


**Figure 7.5.:** (Color) One-site population of the double ionization spectra of $XeF_2$, $XeF_4$ and $XeF_6$.

its character: the one-site states have a large dicationic population number on either xenon $Xe^{-2}$ or on a single fluorine $F^{-2}$ and the two-site states are of either $Xe^{-1}F^{-1}$ or of $F1^{-1}F2^{-1}$ character[2] (subsection 5.4.2). For each dicationic state of the spectra of the xenon fluorides, the equivalent data of the population analysis are summed to yield four population numbers, one for each main contribution to a dicationic state. For example, the $Xe^{-1}F1^{-1}$, $Xe^{-1}F2^{-1}$ population numbers are added in $XeF_2$ to give a single $Xe^{-1}F^{-1}$ contribution for each dicationic state of the spectrum of $XeF_2$. The population numbers are normalized, i.e. the sum of the contributions of $Xe^{-2}$, $F^{-2}$, $Xe^{-1}F^{-1}$ and $F1^{-1}F2^{-1}$ character yields one for each state.

### 7.4.2. One-site Populations

The spectra of the one-site population numbers are plotted in figure 7.5. The first lines appear at $\approx$ 30 eV. The spectra are compared to study the effect of the increasing number of fluorine atoms for the xenon fluorides. Obviously, the density of states with a considerable $F^{-2}$ population increases due to the increasing number of fluorine atoms. The overall distribution of these states does not change much in the different compounds, certain regions are visible where the states have a high $F^{-2}$ population. These regions shift slightly to higher IPs due to the reduced excess charge that the individual fluorine atoms get from the central xenon atom.

[2]The notation is explained in footnote 4 on page 57.

Conversely, the importance of $Xe^{-2}$ contributions to the dicationic states is extremely reduced due to the reduction of the valence electron density on the xenon atom. In $XeF_6$ the contributions of $Xe^{-2}$ character have nearly vanished.

### 7.4.3. Two-site Populations

The spectra of the two-site population numbers are plotted in figure 7.6. The effect of the increasing number of fluorine atoms is seen here as well. The states with a large $F1^{-1}F2^{-1}$ population in the spectrum of $XeF_2$ are clearly separated into distinct groups of lines originating from F1 $2p^{-1}$ F2 $2p^{-1}$, F1 $2p^{-1}$ F2 $2s^{-1}$ and F1 $2s^{-1}$ F2 $2s^{-1}$ populations. This can be concluded from a simple energy summation. The single ionization potentials in figure 7.2 for ionization from molecular orbitals with F $2p$ character are located at $\approx 20\,\mathrm{eV}$, those for ionization from molecular orbitals with F $2s$ character are located at $\approx 40\,\mathrm{eV}$. In the spectrum of $XeF_2$ in figure 7.6, the groups are approximately at 40, 60 and 80 eV. Since $XeF_2$ is a linear molecule, the two fluorine atoms are separated by the central xenon atom. Such states with a large $F1^{-1}F2^{-1}$ population are termed *opposite $F1^{-1}F2^{-1}$ states*.

The situation changes in $XeF_4$ and $XeF_6$. There are *adjacent* and opposite $F1^{-1}F2^{-1}$ states and the clear separation between the groups seen in the spectrum of $XeF_2$ is removed. One reason for this effect is the interaction between adjacent fluorine atoms which is stronger than the interaction between opposite ones. This leads to a splitting of the fluorine lines which is also observed in the single ionization spectra, see subsection 7.3.1.

Furthermore, the F1–F2 distance in adjacent $F1^{-1}\,F2^{-1}$ states is considerably reduced in comparison to the F1–F2 distance in opposite states. So the hole-hole repulsion energy *varies* among those states which have a large $F1^{-1}F2^{-1}$ population that arises from the same types of orbitals. Therefore, such $F1^{-1}F2^{-1}$ states are distributed to a small region in the double ionization spectrum. The lines in $XeF_2$ mark the lower ends of such regions due to the maximum distance between the vacancies therein, in contrast to $XeF_4$ and $XeF_6$.

States with a large $Xe^{-1}F^{-1}$ population do not group like those of $F1^{-1}F2^{-1}$ character. The density of the former also increases with an increasing number of fluorine atoms but they are distributed more uniformly to the whole spectral range. In $XeF_2$ and $XeF_6$ these states are dominant and In $XeF_4$ they are comparable to the $F1^{-1}F2^{-1}$ states. The ionization potential of the $Xe^{-1}\,F^{-1}$ states is not subject to a change of the hole-hole repulsion energy in contrast to the $F1^{-1}F2^{-1}$ states because the Xe–F distance does not change within a molecule (remember that the double ionization spectrum of $XeF_6$ was calculated using octahedral symmetry).

## 7.5. Electronic Decay Processes

The electronic decay processes presented in section 6.1 are characterized according to their final state population in subsection 6.3.1. Therefore, the analysis of the final state populations can show which processes of section 6.1 are important for the electronic decay of Xe $4d$ holes in the xenon fluorides.

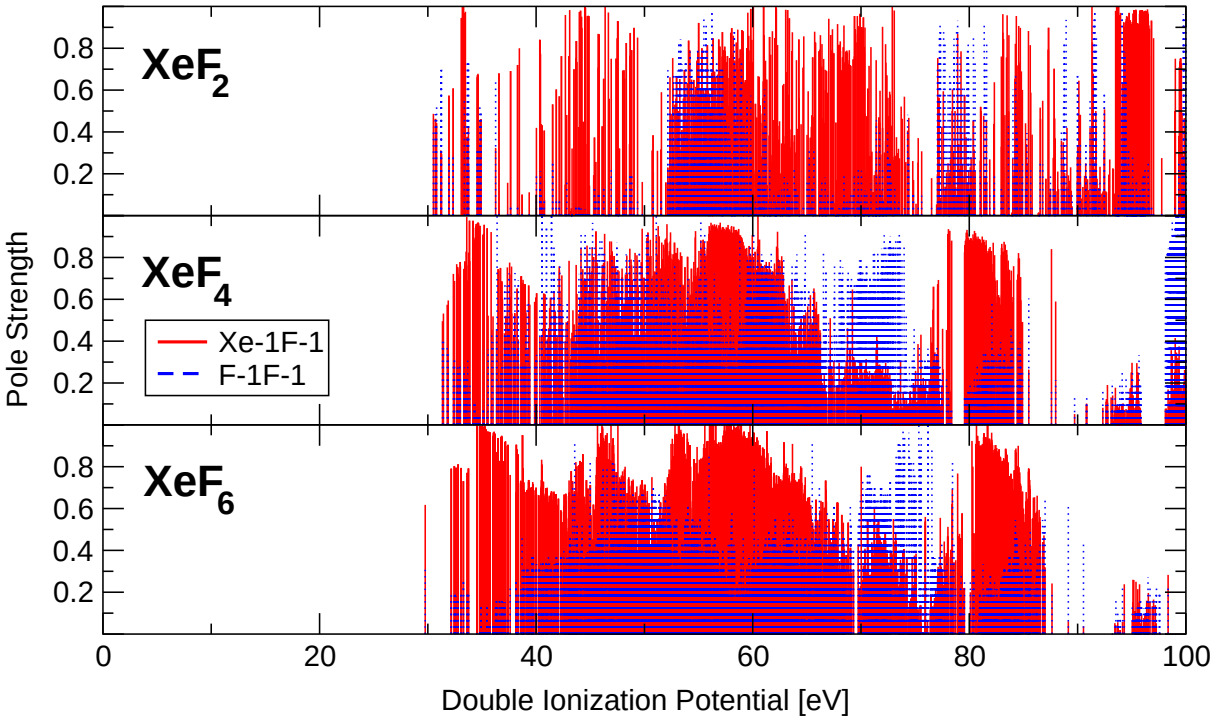


**Figure 7.6.:** (Color) Two-site population of the double ionization spectra of $XeF_2$, $XeF_4$ and $XeF_6$.

The intra-atomic decay of an initial Xe $4d$ hole produces final states of $Xe^{-2}$ type. So intra-atomic decay is suppressed (6.3), if the final states have a small $Xe^{-2}$ population. The analysis of the one-site population in figure 7.5 of subsection 7.4.2 shows that the $Xe^{-2}$ population is extremely low in the xenon fluorides, in contrast to the two-site population in figure 7.6. Therefore, one can conclude that interatomic decay processes dominate the electronic decay of Xe $4d$ holes in the xenon fluorides.

Two objections can be made: firstly, the two final state holes on the xenon atom may not be highly localized in the outer valence, in contrast to inner valence and core holes. Hence the picture of one-site and two-site holes is a crude approximation. Secondly, the intra-atomic decay matrix elements are much larger than the interatomic ones, due to the larger overlap of the involved wave functions of the initial and final states. Therefore, the suppression of intra-atomic decay by the $Xe^{-2}$ population numbers of the accessible final states may not be large enough to make interatomic decay processes comparable or even dominant (6.3). The influence of interatomic decay processes certainly increases with an increasing number of fluorine atoms due to the increasing number of accessible final states.

Now the relations among the three interatomic processes of section 6.1, ICD, two- and three-monomer ETMD, are investigated. Final states with a large $F^{-2}$ population are attributed to a two-monomer ETMD process. Final states with a large $F1^{-1}F2^{-1}$ population are attributed to a three-monomer ETMD process suggested in subsection 6.1.3. Two final state holes on a single fluorine atom may not be highly localized due to diffuse valence molecular orbitals. Therefore, a clear separation between two- and three-monomer

ETMD is difficult. As no partial decay widths for the individual processes are calculated, and three-monomer ETMD has not been studied so far, one cannot answer the question which process is more important.

ICD produces $Xe^{-1}F^{-1}$ final states. Figure 7.6 shows that the two-site final state population of ICD is comparable to that of three-monomer ETMD. This is somewhat surprising because the valence electron density on the xenon atom is considerably reduced, see subsubsection 7.3.1.

A dominance of interatomic processes implies an increase of the decay width in the xenon fluorides because the number of dicationic final states increases with the number of fluorine atoms. This is not the case for the intra-atomic decay process. This analysis suggest that the experimentally observed increase in line width is caused by an increase of the decay width. This conclusion is in contrast to conventional wisdom that the Auger decay rate in molecules is low for a low valence electron density on the atom that carries the initial vacancy [21].

The increase of the decay width in figure 7.1 is not very large. This can be attributed to the fact that the CI transition matrix element of interatomic decay processes in (6.3) is smaller than that of intra-atomic decay. As the intra-atomic decay is suppressed with an increasing number of fluorine atoms this decrease in decay width must be compensated by the increase in interatomic decay width.

# 8. Conclusion

This diploma thesis is thematically centered around the electronic decay of resonances in molecules. In this thesis, progress has been made towards an improved theoretical description of the electronic decay of excited and ionized molecules. Special emphasis is put on the decay processes, the observed phenomena due to the processes and their contribution to the decay width of excited and ionized molecules.

Perturbation theory is applied repeatedly to study electronic resonances and a major part of the present work is devoted to the elucidation of its usefulness for the calculation of their decay widths.

The application of time-dependent perturbation theory, to the calculation of the decay width of a resonance, is called Wigner-Weisskopf theory [2, 7]. It is used to study the electronic decay of a singly excited resonance state which is described by a singly excited Hartree-Fock determinant. It is shown that final states consist of singly, doubly and triply excited determinants which lead to a variety of possible decay processes that, combined, yield the electronic decay width of the initial state. Schematic representations of the individual decay channels can be drawn which help to understand their physical significance (section 3.1).

Complex absorbing potentials (CAP) transform the time-dependent decay problem into a non-Hermitian time-independent bound-state-like problem that can be treated with $\mathbb{L}^2$ techniques [17]. In the framework of CAPs, a non-Hermitian generalization of non-degenerate Rayleigh-Schrödinger perturbation theory [2] is the analogue to Wigner-Weisskopf theory. The matrix elements which occur in this theory, consist of those needed in the Wigner-Weisskopf theory of section 3.1, together with new ones originating from the CAP. In course of the derivation of this perturbation theory, more and more similarities to the time-dependent picture are revealed and finally their formal equivalence in complete basis sets is shown (section 3.2).

Both Wigner-Weisskopf theory and non-Hermitian non-degenerate Rayleigh-Schrödinger perturbation theory are single reference theories. A single Hartree-Fock determinant does not approximate a singly excited state very well. Furthermore, the single reference approaches of the former paragraphs suffer from degeneracies. To overcome this, a flexible non-Hermitian multireference perturbation theory is derived (section 3.3) on the analogy of degenerate Rayleigh-Schrödinger perturbation theory [2]. The many-body problem is described using a configuration interaction matrix including the CAP. An arbitrary set of configurations may be chosen as references. With the help of projection operators, the matrix is partitioned into a reference space, a complement space and coupling blocks. The Hamiltonian is diagonalized in the reference space to decouple the references. The problem is transformed into an effective eigenvalue problem which is solved by perturbation theory. A simple condition for the convergence of the perturbation

series is stated. The first non-vanishing term is of second order in the perturbation. It is shown that up to second order only the coupling blocks are needed for the calculation of the energy. Corrections up to fourth order in energy and up to second order in the wave function are presented. The theory reduces to the non-Hermitian Rayleigh-Schrödinger perturbation theory discussed in the previous paragraph (section 3.2) if only one reference is used.

A new theory should be tested, if possible, on a problem where the results are known beforehand. This is the case for the model problem of section 4.1.1 which possesses a (quasi)-analytic solution and was studied before [10, 11] using the CAP-method. The multireference perturbation theory is studied with respect to the accuracy of its results for a varying size of the employed reference space. The theory delivers satisfactory results with low computational effort. An integration of the multireference perturbation theory into a configuration interaction program is described.

In the following paragraphs, contributions made to the understanding of the electronic decay of singly ionized molecules, are described. Wigner-Weisskopf theory was formulated before [8,9] for ionized molecular systems and in this work a new derivation is given here that rests on the Wigner-Weisskopf theory for excited states. Excited states are more general than ionized states, so a simple transformation leads to the equations describing an ionized molecule. The Wigner-Weisskopf theory for ionized molecules is extended further to include the many-body Green's function description of dicationic states. With the help of this, a relation between the population of final states and the electronic decay width is derived (section 6.3).

Xenon fluorides ($XeF_n$, $n = 2, 4, 6$) serve as an example to study electronic decay in molecules (chapter 7). This family of compounds is chosen due to the experimental observation of an increase in line width with an increasing number of fluorine atoms. I investigate whether this effect arises due to an increase in electronic decay width. The aim is to estimate the effect on the decay width of interatomic decay processes, which are essential in the decay of weakly bound clusters [8,9,26–29] (chapter 6), in the xenon fluorides, because their partial decay width increases with an increasing number of fluorine atoms.

Xenon is a fairly heavy atom, so relativistic effects have a considerable effect on the ionization potentials of the xenon fluorides. As the theory employed here is strictly non-relativistic, a rule of thumb is devised to correct for the scalar relativistic effects, i.e. the modification of the orbital energies, by performing numeric Hartree-Fock and Dirac-Fock calculations for the xenon atom. The difference of the orbital energies is used to correct for these effects.

A Mulliken population analysis [42,84] is carried out which shows that a considerable amount of charge is moved from the central xenon atom to the fluorine atoms. The effect increases with an increasing number of fluorine atoms. This reduction of charge on the xenon atom leads to a shift of the ionization potentials of xenon in the xenon fluorides to higher energies because the nuclear charge is less effectively screened. The effect is clearly visible in the ionization spectra.

The ionization spectra are examined on the Hartree-Fock level (Koopmans' theorem) first because the mean field approximation yields clear and easy-to-understand spectra. With the help of Green's functions, ionization spectra are calculated for correlated elec-

trons. The spectra show a significant breakdown of the molecular orbital picture of ionization in the inner valence of the xenon fluorides.

The double ionization spectra are plotted in terms of the one-site populations on $Xe^{-2}$, $F^{-2}$ and two-site populations on $Xe^{-1}\,F^{-1}$, $F1^{-1}\,F2^{-1}$ of the dicationic states. Separating these two classes of contributions gives considerable insights if these states are interpreted as dicationic final states of the decay of a single Xe $4d$ vacancy. The $Xe^{-2}$ population numbers are minimal. This implies a significant contribution of interatomic decay processes because the number of dicationic states increases with the number of fluorine atoms.

The results of the analysis of the xenon fluorides have considerable impact on the understanding of molecular Auger decay. Up to now, only the phenomenon of foreign imaging [22–24] and the significance of interatomic matrix elements [20, 21] have been known but with this work a clear identification of the possible decay processes is given. It is shown that they lead to an increase of the Xe $4d$ decay width which explains the experimentally observed increase of the Xe $4d$ line width. This conclusion is in contrast to conventional wisdom that the Auger decay rate in molecules is low for a low valence electron density on the atom that carries the initial vacancy [21].

Several questions are left open and should be investigated in subsequent work. Wigner-Weisskopf theory can be improved further. Up to now, the initial and final states are described by excited Hartree-Fock determinants, which is a crude approximation. The use of states described by the Algebraic diagrammatic construction (ADC) [30–33] scheme into this theory as commenced in section 6.3 seems to be a promising approach to calculate decay widths of electronic resonances with low computational effort and a satisfactory accuracy. Intermediate state representations [79–81] can help to calculate the needed coupling matrix elements. Then the limited accuracy of the second order Wigner-Weisskopf theory can be exploited fully.

The non-Hermitian multireference perturbation theory can be used to study some electronic resonances in molecules to compare its results with existing methods. As it is a matrix perturbation theory without concrete description of the many-body system in mind, an integration into other *ab initio* methods like ADC [30–33] could be possible.

The three-monomer electron transfer mediated decay (ETMD) is suggested to be an important process to explain the foreign imaging [22–24] phenomenon (subsection 6.2.1) observed in $SiF_4$ and is addressed in the context of the xenon fluorides (chapter 7). Therefore, it is highly desirable to study this process in a cluster like $NeAr_2$ as proposed in [9]. Particularly the decay width of this process in relation to interatomic Coulombic decay and two-monomer ETMD is relevant and can have considerable impact on the understanding of interatomic decay processes and their effects.

The accurate determination of lifetimes of electronic resonances is still a problem with *ab initio* calculations. Standard Gaussian basis sets are optimized to represent compact ground state wave functions of molecules. Hence they are less suited to represent decay electrons further away from the molecule. The situation can be relieved somewhat by augmenting the basis set with a few diffuse functions, i.e. Gaussians with a small exponent. This cannot be done excessively because (near) linear dependencies and consequently numerical instabilities arise. Therefore, new types of basis functions are needed that are capable of representing decay electrons, not only in the vicinity of a molecule. A practical requirement is that it should be possible to evaluate the integrals efficiently which are

needed on Hartree-Fock calculations. Then the lifetimes of the Xe $4d$ vacancies in the xenon fluoride could be determined by purely theoretical means.

# 9. Acknowledgments

It is a pleasure for me to thank Prof. Lorenz S. Cederbaum for giving me such an intriguing project for my Diplomarbeit. He provided a lot of motivation and support to me. Special mention has to be made of Prof. Rainer Wehrse for his willingness to evaluate this thesis.

Many of the ideas developed in this thesis are grounded on previous work by Dr. Robin Santra with whom I collaborated closely. He was a constant source of ideas and inspired my work. I am also indebted to Imke Müller and Sven Feuerbacher who always supported me. T. Darrah Thomas influenced this work considerably by pointing out to me the increase of the Xe $4d$ line width observed experimentally in the xenon fluorides.

I wish to thank Prof. Francesco Tanrantelli who provided superb support for his ADC programs and Dr. Michael Hanrath for his help with his DIESEL MRCI program.

This thesis was also influenced by Dr. Thomas Sommerfeld who discussed the CAP-method and non-Hermitian perturbation theory with me and Dr. Markus Pernpointner who helped to account for relativistic effects in the xenon fluorides.

My thanks are also extended to the system administrators Bernd Schubert, Jörg Breidbach and Frank Otto for nice talks about and help with computers.

I wish to thank my room mates Simona Briganti, Andreas Markmann and Christoph Cattarius who provided a nice working atmosphere. I would like to thank Nickolay Dobrodey and Alexej Streltsov for their patience with my Russian and Dr. Mathias Nest, Dr. Detlef Pingel and Cristian Villani for the discussions which I enjoyed. I am indebted to all members of the group for the pleasant atmosphere they created.

I would like to thank explicitly some of the people who gave a talk at our group seminar. Prof. Tucker Carrington spoke about *Preconditioned iterative methods for calculating energy levels and metastable state lifetimes*. This talk told me how to compare different numerical methods. Dr. Wolfhard Koch's talk about *Diatomic Hartree-Fock-Hückel Theory of Large Molecules and Translationally Periodic Crystals* pointed out to me how two-electron integrals can be approximated.

# Bibliography


[1] V. I. Kukulin, V. M. Krasnopol'sky, and J. Horáček, *Theory of Resonances*, Kluwer, Dordrecht, 1989.

[2] J. J. Sakurai, *Modern Quantum Mechanics*, Addison-Wesley, Reading (Massachusetts), 2nd edition, 1994.

[3] F. Schwabl, *Quantenmechanik*, volume QM I, Springer, Berlin, 5th edition, 1998.

[4] B. Povh, K. Rith, C. Scholz, and F. Zetsche, *Teilchen und Kerne*, Springer, Berlin, 5th edition, 1999.

[5] C. A. Nicolaides, Time Asymmetry, Nonexponential Decay, and Complex Eigenvalues in the Theory and Computation of Resonance States, Int. J. Quantum Chem. **89**, 94–105 (2002).

[6] A. J. F. Siegert, On the Derivation of the Dispersion Formula for Nuclear Reactions, Phys. Rev. **56**, 750–752 (1939).

[7] V. F. Weisskopf and E. P. Wigner, Z. Phys. **63**, 54 (1930).

[8] R. Santra, J. Zobeley, and L. S. Cederbaum, Electronic Decay of Valence Holes in Clusters and Condensed Matter, Phys. Rev. B **64**, 245104 (2001).

[9] J. Zobeley, R. Santra, and L. S. Cederbaum, Electronic Decay in Weakly Bound Heteroclusters: Energy Transfer Versus Electron Transfer, J. Chem. Phys. **115**, 5076–5088 (2001).

[10] R. Santra, *Non-Hermitian Many-Particle Theory for Investigating Electronic Decay of Valence Holes in Clusters*, Dissertation, Ruprecht-Karls Universität Heidelberg, Theoretische Chemie, Physikalisch-Chemisches Institut, Im Neuenheimer Feld 229, 69120 Heidelberg, Germany, 2001, Published as [11].

[11] R. Santra and L. S. Cederbaum, Non-Hermitian Electronic Theory and Applications to Clusters, Phys. Rep. **368**, 1–117 (2002).

[12] H. Feshbach, Ann. Phys. (New York) **5**, 357 (1958).

[13] H. Feshbach, Ann. Phys. (New York) **19**, 287 (1962).

[14] N. Moiseyev, Quantum Theory of Resonances: Calculating Energies, Widths and Cross-Sections by Complex Scaling, Phys. Rep. **302**, 211–293 (1998).

[15] MOLCAS Version 5. Kerstin Andersson, Maria Barysz, Anders Bernhardsson, Margareta R. A. Blomberg, D. L. Cooper, Timo Fleig, Markus P. Fülscher, Coen de Graaf, Bernd A. Hess, Gunnar Karlström, Roland Lindh, Per-Åke Malmqvist, Pavel Neogrády, Jeppe Olsen, Björn O. Roos, Andrzej J. Sadlej, Martin Schütz, Bernd Schimmelpfennig, Luis Seijo, Luis Serrano-Andrés, Per E. M. Siegbahn, Jonna Stålring, Thorstein Thorsteinsson, Valera Veryazov and Per-Olof Widmark, Lund University, Sweden (2000).

[16] GAMESS-UK is a package of ab initio programs written by M. F. Guest, J. H. van Lenthe, J. Kendrick, K. Schoffel, and P. Sherwood, with contributions from R. D. Amos, R. J. Buenker, H. J. J. van Dam, M. Dupuis, N. C. Handy, I. H. Hillier, P. J. Knowles, V. Bonacic-Koutecky, W. von Niessen, R. J. Harrison, A. P. Rendell, V. R. Saunders, A. J. Stone, D. J. Tozer, and A. H. de Vries. The package is derived from the original GAMESS code due to M. Dupuis, D. Spangler and J. Wendoloski, NRCC Software Catalog, Vol. 1, Program No. QG01 (GAMESS), 1980.

[17] U. V. Riss and H.-D. Meyer, Calculation of Resonance Energies and Widths Using the Complex Absorbing Potential Method, J. Phys. B **26**, 4503–4536 (1993).

[18] H. Haken and H. C. Wolf, *Atom- und Quantenphysik*, Springer, Berlin, 7th edition, 2000.

[19] P. Auger, Compt. Rend. (Paris) **177**, 169 (1923).

[20] J. A. D. Matthew and Y. Komninos, Transition Rates for Interatomic Auger Processes, Surf. Sci. **53**, 716–725 (1975).

[21] H. Wormeester, H. J. Borg, and A. v. Silfhout, The Influence of Inter-Atomic Transitions in Auger Valence Band Spectroscopy: Oxygen on Si(001)2 $\times$ 1, Surf. Sci. **258**, 197–209 (1991).

[22] F. Tarantelli and L. S. Cederbaum, Foreign Imaging in Auger Spectroscopy: The Si $2p$ Spectrum of Silicon Tetrafluoride, Phys. Rev. Lett. **71**, 649–652 (1993).

[23] F. O. Gottfried, L. S. Cederbaum, and F. Tarantelli, Ab initio Block-Lanczos Calculation of the Auger Spectra of $SiF_4$: Strong Two-Hole Localization Effects and Foreign Imaging, Phys. Rev. A **53**, 2118–2129 (1996).

[24] T. X. Carroll, K. J. Børve, L. J. Sæthre, J. D. Bozek, E. Kukk, J. A. Hahne, and T. D. Thomas, Carbon 1$s$ Photoelectron Spectroscopy of $CF_4$ and CO: Search for Chemical Effects on the Carbon 1$s$ Hole-State Lifetime, J. Chem. Phys. **116**, 10221–10228 (2002).

[25] Science **271**, 920 (1996), Special issue on clusters.

[26] L. S. Cederbaum, J. Zobeley, and F. Tarantelli, Giant Intermolecular Decay and Fragmentation of Clusters, Phys. Rev. Lett. **79**, 4778–4781 (1997).

[27] R. Santra, J. Zobeley, L. S. Cederbaum, and N. Moiseyev, Interatomic Coulombic Decay in van der Waals Clusters and Impact of Nuclear Motion, Phys. Rev. Lett. **85**, 4490–4493 (2000).

[28] J. Zobeley, L. S. Cederbaum, and F. Tarantelli, Highly Excited Electronic States of Molecular Clusters and their Decay, J. Chem. Phys. **108**, 9737–9750 (1998).

[29] R. Santra, J. Zobeley, L. S. Cederbaum, and F. Tarantelli, Intermolecular Coulombic Decay of Clusters, J. Electron Spectrosc. Relat. Phenom. **114-116**, 41–47 (2001).

[30] J. Schirmer, L. S. Cederbaum, and O. Walter, New Approach to the One-Particle Green's Function for Finite Fermi Systems, Phys. Rev. A **28**, 1237–1259 (1983).

[31] J. Schirmer and G. Angonoa, On Green's Function Calculations of the Static Self-Energy Part, the Ground State Energy and Expectation Values, J. Chem. Phys. **91**, 1754–1761 (1989).

[32] J. Schirmer and A. Barth, Higher-Order Approximations for the Particle-Particle Propagator, Z. Phys. A **317**, 267–279 (1984).

[33] A. Tarantelli and L. S. Cederbaum, Particle-Particle Propagator in the Algebraic Diagrammatic Construction Scheme at Third Order, Phys. Rev. A **39**, 1656–1664 (1989).

[34] J. Zobeley, L. S. Cederbaum, and F. Tarantelli, Intermolecular Coulombic Decay of Molecular Clusters: Identification of the Decay Mechanism Using a New Hole-Population Analysis, J. Phys. Chem. A **103**, 11145–11160 (1999).

[35] F. Tarantelli, A. Sgamellotti, and L. S. Cederbaum, Many Dicationic States and Two-hole Population Analysis as a Bridge to Auger Spectra: Strong Localization Phenomena in $BF_3$, J. Chem. Phys. **94**, 523–532 (1991).

[36] F. Tarantelli, A. Sgamellotti, and L. S. Cederbaum, Recent Developments in the Calculation of Molecular Auger Spectra, in *Applied Many-Body Methods in Spectroscopy and Electronic Structure*, edited by D. Mukherjee, pages 57–104, Plenum Press, New York, 1992.

[37] R. Santra, L. S. Cederbaum, and H.-D. Meyer, Electronic Decay of Molecular Clusters: Non-Stationary States Computed by Standard Quantum Chemistry Methods, Chem. Phys. Lett. **303**, 413–419 (1999).

[38] T. Sommerfeld and R. Santra, Efficient Method to Perform CAP/CI Calculations for Temporary Anions, Int. J. Quantum Chem. **82**, 218–226 (2001).

[39] R. Santra and L. S. Cederbaum, An Efficient Combination of Computational Techniques for Investigating Electronic Resonance States in Molecules, J. Chem. Phys. **115**, 6853–6861 (2001).

[40] U. Hergenhahn, A. Kolmakov, M. Riedler, A. R. B. de Castro, O. Löfken, and T. Möller, Observation of Excitonic Satellites in the Photoelectron Spectra of Ne and Ar Clusters, Chem. Phys. Lett. **351**, 235–241 (2002).

[41] J. N. Cutler, G. N. Bancroft, J. D. Bozek, K. H. Tan, and G. J. Schrobilgen, Ligand Field Splitting on the Xe $4d$ Core Levels in $XeF_x$ (x = 2, 4, 6) Compounds from High-Resolution Gas-Phase Photoelectron Spectra: The Structure of $XeF_6$, J. Am. Chem. Soc. **113**, 9125–9131 (1991).

[42] A. Szabo and N. S. Ostlund, *Modern Quantum Chemistry: Introduction to Advanced Electronic Structure Theory*, Macmillan, New York, 1982.

[43] C. C. J. Roothaan, New Developments in Molecular Orbital Theory, Rev. Mod. Phys. **23**, 69– (1951).

[44] J. A. Pople and R. K. Nesbet, J. Chem. Phys. **22**, 571 (1954).

[45] D. Feller and E. R. Davidson, Basis Sets for Ab Initio Molecular Orbital Calculations and Intermolecular Interactions, in *Reviews in Computational Chemistry*, edited by K. B. Lipkowitz and D. B. Boyd, volume 1, pages 1–43, VCH Publishers, New York, 1990.

[46] Basis sets were obtained from the *Extensible Computational Chemistry Environment Basis Set Database*, Version 5/22/02, as developed and distributed by the Molecular Science Computing Facility, Environmental and Molecular Sciences Laboratory which is part of the Pacific Northwest Laboratory, P.O. Box 999, Richland, Washington 99352, USA, and funded by the U.S. Department of Energy. The Pacific Northwest Laboratory is a multi-program laboratory operated by Battelle Memorial Institute for the U.S. Department of Energy under contract DE-AC06-76RLO 1830. Contact David Feller or Karen Schuchardt for further information.

[47] V. R. Saunders and J. H. van Lenthe, The Direct CI Method. A Detailed Analysis., Mol. Phys. **100**, 167–187 (2002).

[48] I. B. Müller, Elektronischer Zerfall nach einer Valenzionisierung molekularer Anionen, Diplomarbeit, Ruprecht-Karls Universität Heidelberg, Theoretische Chemie, Physikalisch-Chemisches Institut, Im Neuenheimer Feld 229, 69120 Heidelberg, Germany, 2001.

[49] T. Sommerfeld and F. Tarantelli, Subspace Iteration Techniques for the Calculation of Resonances Using Complex Symmetric Hamiltonians, J. Chem. Phys. **112**, 2106–2110 (2000).

[50] E. R. Davidson, The Iterative Calculation of a Few of the Lowest Eigenvalues and Corresponding Eigenvectors of Large Real-Symmetric Matrices, J. Comp. Phys. **17**, 87–94 (1975).

[51] J. K. Cullum and R. A. Willoughby, *Lanczos Algorithms for Large Symmetric Eigenvalue Computations*, Birkhäuser, Boston, 1985, two volumes.

[52] R. J. Buenker and S. D. Peyerimhoff, Energy Extrapolation in CI Calculations, Theoret. Chim. Acta (Berl.) **39**, 217–228 (1975).

[53] R. J. Buenker and S. D. Peyerimhoff, Individualized Configuration Selection in CI Calculations with Subsequent Energy Extrapolation, Theoret. Chim. Acta (Berl.) **35**, 33–58 (1974).

[54] R. Santra, J. Breidbach, J. Zobeley, and L. S. Cederbaum, Parallel Filter Diagonalization: A Novel Method to Resolve Quantum States in Dense Spectral Regions, J. Chem. Phys. **112**, 9243–9252 (2000).

[55] F. Chen, E. R. Davidson, and S. Iwata, New Time-Independent Perturbation Theory for the Multireference Problem, Int. J. Quantum Chem. **86**, 256–264 (2002).

[56] C. Møller and M. S. Plesset, Note on an Approximation Treatment for Many-Electron Systems, Phys. Rev. **46**, 618–622 (1934).

[57] P. S. Epstein, The Stark Effect from the Point of View of Schroedinger's Quantum Theory, Phys. Rev. **28**, 695–710 (1926).

[58] R. D. Nesbet, Proc. Roy. Soc. London **A230**, 312 (1955).

[59] L. S. Cederbaum, W. Domcke, J. Schirmer, and W. von Niessen, Correlation Effects in the Ionization of Molecules: Breakdown of the Molecular Orbital Picture, volume 65 of *Advances in Chemical Physics*, pages 115–159, Wiley, 1986.

[60] G. Hose, Multi-Reference Rayleigh-Schrödinger Perturbation Theory, in *Many-Body Methods in Quantum Chemistry*, edited by U. Kaldor, pages 43–64, Springer, Berlin, 1988.

[61] G. H. Golub and C. F. van Loan, *Matrix Computations*, John Hopkins University Press, Baltimore, 2nd edition, 1989.

[62] M. Metcalf and J. Reid, *FORTRAN 90/95 explained*, Oxford University Press, Oxford, New York, 1996.

[63] E. Anderson, Z. Bai, C. Bischof, S. Blackford, J. Demmel, J. Dongarra, J. Du Croz, A. Greenbaum, S. Hammarling, A. McKenney, and D. Sorensen, *LAPACK Users' Guide*, Society for Industrial and Applied Mathematics (SIAM), Philadelphia, 3rd edition, 1999.

[64] M. Hanrath, *Ein individuell selektierendes intern-extern-separiertes Multireferenz-Konfigurationswechselwirkungsverfahren*, Dissertation, Rheinische Friedrich-Wilhelms Universität zu Bonn, Institut für Physikalische und Theoretische Chemie, Wegeler Straße 12, 53115 Bonn, Germany, 1999.

[65] M. Hanrath, *User's Guide* DIESEL-MR-CI, Universität Bonn, Institut für Physikalische und Theoretische Chemie, Wegeler Straße 12, 53115 Bonn, Germany,`www.thch.uni-bonn.de/tc/people/hanrath.michael`, April 2000, Version 1.11.

[66] M. Hanrath and B. Engels, New Algorithms for an Individually Selecting MR-CI Program, Chem. Phys. **225**, 197–202 (1997), Citation for [65].

[67] R. D. Mattuck, *A Guide to Feynman Diagrams in the Many-Body Problem*, McGraw-Hill, New York, 2nd edition, 1976.

[68] A. L. Fetter and J. D. Walecka, *Quantum Theory of Many-Particle Systems*, International Series in Pure and Applied Physics, edited by Leonard I. Schiff, McGraw-Hill, New York, 1971.

[69] L. S. Cederbaum and W. Domcke, Theoretical Aspects of Ionization Potentials and Photoelectron Spectroscopy: A Green's Function Approach, volume 36 of *Adv. Chem. Phys.*, pages 205–344, Wiley, New York, 1977.

[70] J. Schirmer, Beyond the Random-phase Approximation: A New Approximation Scheme for the Polarization Propagator, Phys. Rev. A **26**, 2395–2416 (1982).

[71] H.-G. Weikert, H.-D. Meyer, L. S. Cederbaum, and F. Tarantelli, Block Lanczos and Many-body Theory: Application to the One-particle Green's Function, J. Chem. Phys. **104**, 7122–7138 (1996).

[72] G. Angonoa, O. Walter, and J. Schirmer, Theoretical K-Shell Ionization Spectra of $N_2$ and CO by a Fourth-Order Green's Function Method, J. Chem. Phys. **87**, 6789–6801 (1987).

[73] J. Schirmer, A. B. Trofimov, and G. Stelter, A Non-Dyson Third-Order Approximation Scheme for the Electron Propagator, J. Chem. Phys. **109**, 4734–4744 (1998).

[74] J. Brand and L. S. Cederbaum, Extended Two-Particle Green's Functions and Optical Potentials for Two-Particle Scattering by Many-Body Targets, Ann. Phys. (New York) **252**, 276–299 (1996).

[75] A. B. Trofimov, G. Stelter, and J. Schirmer, A Consistent Third-order Propagator Method for Electronic Excitation, J. Chem. Phys. **111**, 9982–9999 (1999).

[76] A. B. Trofimov and J. Schirmer, An Efficient Polarization Propagator Approach to Valence Electron Excitation Spectra, J. Phys. B **28**, 2299–2324 (1995).

[77] A. Tarantelli and L. S. Cederbaum, Approximation Scheme for the Three-Particle Propagator, Phys. Rev. A **46**, 81–94 (1992).

[78] R. Santa and L. S. Cederbaum, Complex absorbing potentials in the framework of electron propagator theory. I. General formalism, J. Chem. Phys. **117**, 5511–5521 (2002).

[79] J. Schirmer, Closed-Form Intermediate Representations of Many-Body Propagators and Resolvent Matrices, Phys. Rev. A **43**, 4647–4659 (1991).

[80] F. Mertins and J. Schirmer, Algebraic Propagator Approaches and Intermediate-state Representations. I. The Biorthogonal and Unitary Coupled-Cluster Methods, Phys. Rev. A **53**, 2140–2152 (1996).

[81] F. Mertins, J. Schirmer, and A. Tarantelli, Algebraic Propagator Approaches and Intermediate-State Representations. II. The Equation-of-Motion Methods for $N$, $N \pm 1$, and $N \pm 2$ Electrons, Phys. Rev. A **53**, 2153–2168 (1996).

[82] J. Schirmer and F. Mertins, Size Consistency of an Algebraic Propagator Approach, Int. J. Quantum Chem. **58**, 329–339 (1996).

[83] J. Schirmer and A. Thiel, An Intermediate State Representation Approach to K-Shell Ionization in Molecules. I. Theory, J. Chem. Phys. **115**, 10621–10635 (2001).

[84] R. S. Mulliken, J. Chem. Phys. **23**, 1833 (1955).

[85] L. Hedin and J. D. Lee, Sudden Approximation in Photoemission and Beyond, J. Electron Spectrosc. Relat. Phenom. **124**, 289–315 (2002).

[86] W. Koch, On Rüdenbergs Integral Approximations and Their Unrestricted and Combined Use in Molecular Orbital Theories of Hartree-Fock Type, Int. J. Quantum Chem. **76**, 148–160 (2000).

[87] K. Rüdenberg, On the Three- and Four-Center Integrals in Molecular Quantum Mechanics, J. Chem. Phys. **19**, 1433–1434 (1951).

[88] A. E. Holleman and N. Wiberg, *Lehrbuch der anorganischen Chemie*, de Gruyter, Berlin, 91th–100th edition, 1985.

[89] M. Kaupp, C. van Wüllen, R. Franke, F. Schmitz, and W. Kutzelnigg, The Structure of $XeF_6$ and of Compounds Isoelectronic with It. A Challenge to Computational Chemistry and to the Qualitative Theory of the Chemical Bond, J. Am. Chem. Soc. **118**, 11939–11950 (1996).

[90] N. Godbout, D. R. Salahub, J. Andzelm, and E. Wimmer, Optimization of Gaussian-Type Basis Sets for Local Spin Density Functional Calculations. I. Boron through Neon, Optimization Technique and Validation, Can. J. Chem. **70**, 560–571 (1992).

[91] C. Froese-Fischer, A General Multi-Configuration Hartree-Fock Program, Comp. Phys. Commun. **14**, 145–153 (1978).

[92] P. Pyykkö, Relativistic Effects in Structural Chemistry, Chem. Rev. **88**, 563–594 (1988).

[93] K. G. Dyall, I. P. Grant, T. Johnson, C., F. A. Parpia, and E. P. Plummer, GRASP: A General-Purpose Relativistic Atomic Structure Program, Comp. Phys. Commun. **55**, 425–256 (1989).

[94] F. A. Parpia, C. Froese-Fischer, and I. P. Grant, GRASP92: A Package for Large-Scale Relativistic Atomic Structure Calculations, Comp. Phys. Commun. **94**, 249–271 (1996).

[95] T. Koopmans, Physica **1**, 104 (1933).

[96] U. Nielsen and W. H. E. Schwarz, VUV Spectra of the Xenon Flourides, Chem. Phys. **13**, 195–202 (1976).

# Index